THE FIRST INTERNATIONAL CONFERENCE ON MARS POLAR SCIENCE AND EXPLORATION

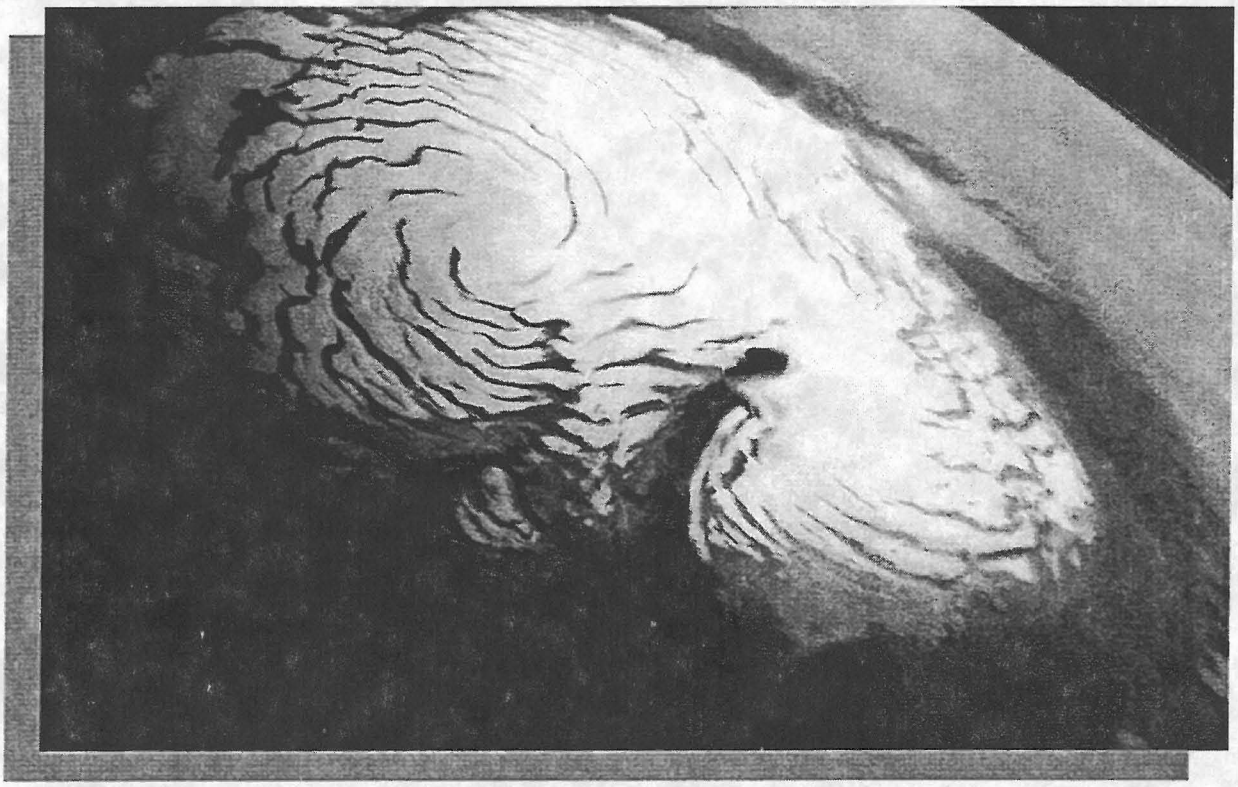

OCTOBER 18–22, 1998

FIRST INTERNATIONAL CONFERENCE ON MARS POLAR SCIENCE AND EXPLORATION

Held at

The Episcopal Conference Center at Camp Allen, Texas

Sponsored by

Geological Survey of Canada
International Glaciological Society
Lunar and Planetary Institute
National Aeronautics and Space Administration

Organizers

Stephen Clifford, Lunar and Planetary Institute
David Fisher, Geological Survey of Canada
James Rice, NASA Ames Research Center

LPI Contribution No. 953

Compiled in 1998 by
LUNAR AND PLANETARY INSTITUTE

The Institute is operated by the Universities Space Research Association under Contract No. NASW-4574 with the National Aeronautics and Space Administration.

Abstracts in this volume may be cited as

Author A. B. (1998) Title of abstract. In *First International Conference on Mars Polar Science and Exploration,* p. xx. LPI Contribution No. 953, Lunar and Planetary Institute, Houston.

This report is distributed by

ORDER DEPARTMENT
Lunar and Planetary Institute
3600 Bay Area Boulevard
Houston TX 77058-1113

Mail order requestors will be invoiced for the cost of shipping and handling.

Preface

This volume contains abstracts that have been accepted for presentation at the First International Conference on Mars Polar Science and Exploration, October 18–22, 1998. The Scientific Organizing Committee consisted of Terrestrial Members E. Blake *(Icefield Instruments)*, G. Clow *(U.S. Geological Survey, Denver)*, D. Dahl-Jensen *(University of Copenhagen)*, K. Kuivinen *(University of Nebraska)*, J. Nye *(University of Bristol)*, S. Ommaney *(International Glaciological Society)*, N. Reeh *(Danish Technical University)*, T. Sowers *(Pennsylvania State University)*, E. Mosley-Thompson *(Byrd Polar Research Center)*, L. Thompson *(Byrd Polar Research Center)*, T. Thorsteinsson *(Alfred Wegner Institute)*, E. Waddington *(University of Washington)*, and D. Wynn-Williams *(British Antarctic Survey)*. Planetary Members included G. Briggs *(NASA Ames Research Center)*, W. Calvin *(U.S. Geological Survey, Flagstaff)*, M. Carr *(U.S. Geological Survey, Menlo Park)*, D. Crisp *(Jet Propulsion Laboratory)*, J. Cutts *(Jet Propulsion Laboratory)*, W. Durham *(Lawrence Livermore National Lab)*, F. Fanale *(University of Hawai'i)*, J. Farmer *(Arizona State University)*, M. Golombek *(Jet Propulsion Laboratory)*, R. Grard *(European Space Agency/ESTEC)*, R. Haberle *(NASA Ames Research Center)*, K. Herkenhoff *(Jet Propulsion Laboratory)*, A. Howard *(University of Virginia)*, H. Kieffer *(U.S. Geological Survey, Flagstaff)*, D. McCleese *(Jet Propulsion Laboratory)*, C. McKay *(NASA Ames Research Center)*, D. Paige *(Unversity of California, Los Angeles)*, D. Smith *(NASA Goddard Spaceflight Center)*, S. Smrekar *(Jet Propulsion Laboratory)*, C. Stoker *(NASA Ames Research Center)*, P. Thomas *(Cornell University)*, and A. Zent *(NASA Ames Research Center)*.

Contents

Abstracts

CHASMA AUSTRALE, MARS: STRUCTURAL FRAMEWORK FOR A CATASTROPHIC OUTFLOW ORIGIN. F. Anguita[1], R. Babín[1], G. Benito[2], A. Collado[1], D. Gómez[1], and J. W. Rice[3], [1]Facultad de Ciencias Geológicas, Universidad Complutense, Madrid, Spain, [2]Consejo Superior de Investigaciones Científicas, Centro de Ciencias Medioambientales, Madrid, Spain, [3]NASA Ames Research Center, Moffett Field CA 94035, USA.

Chasma Australe is the most remarkable of the martian south pole erosional reentrants carved in the polar layered deposits. This chasma originates near the south pole and runs across the polar troughs over a distance of ~500 km. Its width varies between 20 and 80 km and, with a depth up to 1000 m, it reaches the bedrock. Following an idea put forward originally for Chasma Boreale [1], we propose for the genesis of Chasma Australe a mechanism of catastrophic outflow preceded by a tectonically induced powerful sapping process. A detailed geomorphological analysis of Chasma Australe shows erosional and depositional features that can be interpreted as produced by the motion of a fluid. Like other polar reentrants, Chasma Australe is clearly assymetric, with a steep eastern margin where basal and lateral erosion prevailed, and a gentler western side, where the stepped topography and bedrock spurs favored deposition. The flow also scoured the distal part of the eastern margin and spilled into marginal areas, eroding the rim of a bedrock crater. These divides and the height of the depositional area provided the lower limit for the high-water elevations used in the discharge estimates. The paleoflow reconstruction was performed on the basis of the Mars Digital Model data, and using the Manning Equation modified to take into account Mars' smaller gravity as compared to Earth's. Hydraulic parameters used in the calculations vary between 0.0013 and 0.0018 for the channel slope, and between 450 and 650 m for the water depth reached by the flow. The water velocity values range between 30 and 50 m s^{-1}, while the resulting discharge values oscillate between 7×10^8 m^3 s^{-1} and 3×10^9 m^3 s^{-1}, bracketed by values of Manning roughness coefficient from 0.030 to 0.050.

Chasma Australe follows one of the predominant strikes resulting from a tectonic study that included measuring and projecting in rose diagrams nearly 300 lineaments in a surface nearly 20 million km^2 in size centered in Mars' south pole. Of these, 85 were wrinkle ridges, and the rest were straight scarps and undefined lineations. The whole set of lineaments could be explained by a pure compression stress field N10°E in strike, in which the wrinkle ridges would correspond to reverse faults, and the other lineaments to strike-slip faults. The origin of this putative stress field is unknown, but its detection could be relevant in connecting the origin of Mars landscapes to planetary internal processes, a common relationship on Earth.

References: [1] Benito G. et al. (1997) *Icarus, 129,* 528–538.

SEPARATING THE ROLE OF REGOLITH ADSORPTION VS. POLAR CAP DEVELOPMENT AND RETREAT IN THE NORTH POLAR REGION OF MARS. D. S. Bass[1] and D. A. Paige[2], [1]Southwest Research Institute, P.O. Drawer 28510, San Antonio TX 78228-0510, USA, [2]Department of Earth and Planetary Sciences, University of California, Los Angeles, Los Angeles CA 90095-1567, USA.

Viking Infrared Thermal Mapper surface temperature (T_{20}) and Mars Atmospheric Water Detector (MAWD) atmospheric water vapor data show that although some water vapor sublimes into the atmosphere as the seasonal CO_2 cap retreated beyond the warm polar sand sea by $L_s = 81.55$, the bulk of the water vapor did not enter the atmosphere until the center of the north residual polar cap heated to beyond 200 K at approximately $L_s = 103$ (Fig. 1). We suggest the discrepancy in the timing of increasing local atmospheric water vapor may indicate the source for the additional water frost appearing on the cap; on measurable timescales, it does not appear that the water vapor is moving directly into the atmosphere from the regolith or the cap surface. If this were the case, there would be a gradual increase of water vapor in the atmosphere as the CO_2 cap sublimated. Rather, it appears that the water vapor is moving toward the cap center through its recondensation onto the cap surface along with the retreating CO_2 frost. There is a brief time lag between the darkening of the cap and the appearance of a large amount of water vapor in the atmosphere over the residual polar cap; atmospheric water vapor amounts peak at $L_s = 111$ (Fig. 1). The time lag indicates that a local temperature differential governs some water transport in the north polar region; some water is released into the atmosphere as the surface heats up.

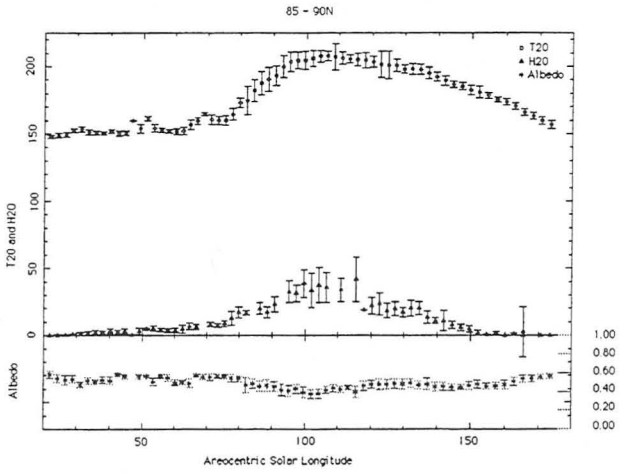

Fig. 1.

CLIMATE-ROTATION FEEDBACK ON MARS. B. G. Bills, NASA Goddard Space Flight Center, Greenbelt MD 20771, USA, and San Diego, Institute for Geophysics and Planetary Physics, Scripps Institution of Oceanography, University of California, La Jolla CA 92037, USA (bbills@igpp.ucsd.edu).

Introduction: It has long been understood that changes in the orbital and rotational geometry of Mars will influence the seasonal and latitudinal pattern of insolation [1–5], and this will likely dominate climatic fluctuations on timescales of 10^5 to 10^7 yr [6–9]. Equally important, but less widely appreciated, is the influence climatic change can have on rotational dynamics. The primary means

by which climate influences rotation is via its influence on transport of mass (volatiles and dust) into and out of the polar regions. Both the rate and direction of Mars rotation can be changed by these mass fluxes, but only the directional changes are climatically relevant.

Rotational Influence on Climate: The orientation of the rotation axis can be specified by a unit vector **s**. Changes in its orientation can be viewed in two different ways: from an external, orbit-fixed reference frame, and from an internal, body-fixed reference frame. Orientation of the orbit is characterized by two unit vectors: the orbit normal **n** determines the plane in which the orbit lies, and the apsidal vector **a** (pointing from perihelion toward the Sun) determines orientation of the orbit within that plane. Spin axis orientation is determined by projections of **s** onto **a** and **n**. Obliquity $\theta = \cos^{-1}(\mathbf{s} \cdot \mathbf{n})$ determines the amplitude of the dominant seasonal temperature cycle. The spatiotemporal pattern of obliquity-driven insolation has symmetry such that reflection in the equatorial plane and time translation by half a year are inverse operations. The relative phase of perihelion and summer solstice is determined by the angle $\varphi = \cos^{-1}(\mathbf{a} \cdot (\mathbf{s} \times \mathbf{n}))$. In the low obliquity limit, the insolation pattern due to this effect has time reflection symmetry about the solstices.

If Mars were the Sun's only planet, its orbit would remain fixed, and the spin axis **s** would precess at a uniform angular rate on a circular cone centered on **n**. Obliquity θ would remain constant, and the perihelion phase angle φ would circulate at a fixed rate. Insolation patterns would change from year to year, but would do so in a perfectly periodic fashion. However, due to gravitational interaction and angular momentum exchange with other planets, the orbit of Mars changes on a variety of time scales [10]. As a result, both the obliquity and the perihelion phase rate fluctuate considerably.

Climatic Influence on Rotation: Changes in the surface mass distribution of Mars, driven by climatic processes, can influence the rotational state.

Obliquity change. The rate of spin axis precession depends on the oblateness of the mass distribution. To the extent that climate change can modulate the gravitational oblateness, it will influence the precession. During periods of low obliquity, polar regions will be especially cold and will accumulate additional mass, in the form of H_2O and CO_2 ice plus dust. During times of intermediate obliquity, the polar volatiles will tend to disperse, and in epoch of high obliquity, there may be equatorial ice and dust accumulations [11]. Thus, it seems likely that climatic change in general, and obliquity-driven climatic change in particular, will influence oblateness. This influences the rotation in two fundamentally different ways.

The present spin axis precession rate of Mars is close to resonance with some of the orbital precession frequencies [12]. That is the basic reason why the obliquity oscillations computed for Mars are so much larger than for Earth. Even quite small changes in instantaneous spin precession rate can thus move Mars into and out of resonance, yielding significant deviations from the obliquity pattern that would be obtained for a static mass distribution.

Insolation changes determine mass fluxes, whereas torques depend on where the mass is, not how fast it is moving. As a result, mass distribution tends to lag behind the insolation pattern driving it. The torques associated with this phase lag can add a secular trend to the obliquity history [13–15].

Polar motion. If the polar mass accumulations are not symmetric about the rotation axis, they will produce polar motion. A positive mass anomaly on an otherwise featureless Mars is in rotational equilibrium only at the poles or the equator. The two polar equilibria are rotationally unstable, and the equatorial equilibrium, though rotationally stable, is thermally unstable. The amount of polar motion caused by a given mass anomaly will depend on its magnitude and location, and on the long-term mechanical response of Mars. The most effective location is at 45° latitude, north or south. The present mass distribution of Mars is well known, but there is still great uncertainty about the long-term strength. If Mars were perfectly rigid, an accumulation of ice, centered at 45°N, and equivalent in mass to a 30-m thick global layer, would move the pole by 0.2°.

Two competing effects determine the actual amount of polar motion that would be produced in a viscoelastic planet [16,17]. A positive feedback results from changes in the rotational potential induced by the initial polar motion. Under this influence alone, a positive mass anomaly placed on the surface would eventually migrate clear to the equator. A negative feedback results from isostatic compensation of the surface load. The effectiveness of a fixed surface load in exciting motion of the pole diminishes with time. The total amount of polar motion obtained from a given initial excitation depends on the competition between these two effects, but the rigid body value provides a lower bound. Plausible viscosity models yield polar motion amplitudes as much as 30× larger than the rigid response.

Temperature anomalies associated with a 1° change in obliquity and a 1° change in geographic location of the pole are similar in magnitude, but different in spatiotemporal pattern The obliquity change primarily influences the amplitude of the seasonal cycle, while the polar motion primarily changes the annual mean temperatures. The polar motion-induced temperature anomaly is such that it will act as a powerful negative feedback on ice accumulation.

References: [1] Ward W. R. (1974) *JGR, 79,* 3375–3381. [2] Ward W. R. (1979) *JGR, 84,* 237–241. [3] Bills B. G. (1990) *JGR, 95,* 14137–14153. [4] Hilton J. L. (1992) *Astron. J., 103,* 619–637. [5] Touma J. and Wisdom J. (1993) *Science, 259,* 1294–1297. [6] Pollack J. B. (1979) *Icarus, 37,* 479–553. [7] Fanale F. P. et al. (1982) *Icarus, 50,* 381–407. [8] Francois L. M. et al. (1990) *JGR, 95,* 14761–14778. [9] Clifford S. M. et al. (1988) *Eos, 69,* 1585–1596. [10] Laskar J. (1988) *Astron. Astrophys., 198,* 341–362. [11] Jakosky B. M. and Carr M. H. (1985) *Nature, 315,* 559–561. [12] Ward W. R. and Rudy D. (1991) *Icarus, 94,* 160–164. [13] Rubincam D. R. (1990) *Science, 248,* 720–721. [14] Rubincam D. R. (1993) *JGR, 98,* 10827–10832. [15] Bills B. G. (1994) *GRL, 21,* 177–180. [16] Sabadini R. et al. (1982) *JGR, 87,* 2885–2903. [17] Bills B. G. and James T. S. (1997) *JGR, 102,* 7579–7602.

GLACIOLOGY OF ICELAND: ICE, FIRE, AND WATER — PROCESSES AND LANDFORMS.

H. Björnsson, Science Institute, University of Iceland, Dunhaga 3, IS-107, Reykjavík, Iceland (hb@raunvis.hi.is).

About 11% (11,000 km^2) of Iceland is at present covered by temperate glaciers, ranging from small cirque glaciers to large ice caps [1]. These glaciers are dynamically active with large mass turnover and high production of meltwater. Lying on easily erodable beds, typical landforms are large outwash plains and moraines, as well as cirques, troughs, and U-shaped valleys. Surges and outburst floods from ice-dammed lakes are frequent.

The presence of active volcanos beneath the glaciers adds dimensions to the erosional and sedimentological processes and their

impact on landscapes. About 60% of glaciers in Iceland are underlain by the active neovolcanic zone, and outburst floods (jökulhlaups) occur regularly from subglacial lakes at geothermal areas, occasionally due to subglacial eruptions [2–4]. Their effects are seen in the transport and deposition of sediments over outwash plains and in the erosion of large canyons. Outburst floods from the subglacial lake Grímsvötn (one of the best-known localities in the ice cap Vatnajökull) have occurred at 1–10-yr intervals, with a peak discharge of 600–40,000 m^3/s at the outwash plain Skeiðarársandur, a duration of 2 days to 4 weeks and a total volume of 0.5–4.0 km^3 [3,5,6]. Typically, the outlet-river discharge during jökulhlaups rises approximately exponentially as a function of time; falling rapidly after peaking. Such a discharge pattern can be explained as a flow through a single ice tunnel at the glacier bed [7]. The flow is controlled mainly by tunnel enlargement due to melting of the walls by frictional heat generated by the flowing water. Occasionally the lake water may be above the melting point, expediating the expansion of the tunnel.

Volcanic eruptions have caused tremendous jökulhlaups with dramatic impact on landforms. The observed high rate of melting during subglacial eruptions, suggest that magma is quenched from the melting temperature to 0°C and fragmented into glass in a highly turbulent mixture with meltwater. During the initial phase of a volcanic eruption in 1996, meltwater was produced at the rate of 8000 m^3/s [8]. During the most violent eruptions, discharge of the jökuhlaups may rise in a few hours to a peak of several hundred thousand cubic meters per second [9]. Some of these floods consist of a hyperconcentrated fluid-sediment mixture [10]. Under the glaciers, volcanic eruptions produce hyaloclastite ridges and table mountains.

References: [1] Björnsson H. (1979) *Jökull, 29,* 74–80. [2] Björnsson H. (1975) *Jökull, 25,* 1–14. [3] Björnsson H. (1982) *Ann. Glaciol., 16,* 95–106. [4] Björnsson H. and Einarsson P. (1991) *Jökull, 40,* 147–168. [5] Björnsson H. (1988) *Soc. Sci. Islandica, 45.* [6] Guðmundsson M. T. et al. (1995) *J. Glaciol., 41,* 263–272. [7] Nye J. F. (1976) *J. Glaciol.* [8] Guðmundsson M. T. et al. (1997) *Nature, 389,* 954–957. [9] Thorarinsson S. (1957) *Jökull, 7,* 21–25. [10] Maizels J. K. (1989) *J. Sed. Petrol., 59,* 204–223.

GEOPHYSICAL SOUNDING. E. Blake, Icefield Instruments Inc., P.O. Box 5567, Whitehorse YT, Y1A 5H4, Canada (erik@icefield.yk.ca).

Of the many geophysical remote-sensing techniques available today, a few are suitable for the water ice-rich, layered material expected at the north martian ice cap.

Radio echo sounding has been used for several decades to determine ice thickness and internal structure. Selection of operating frequency is a tradeoff between signal attenuation (which typically increases with frequency and ice temperature) and resolution (which is proportional to wavelength). Antenna configuration and size will be additional considerations for a mission to Mars. Several configurations for ice-penetrating radar systems are discussed: these include orbiter-borne sounders, sounding antennas trailed by balloons and penetrators, and lander-borne systems. Lander-borne systems could include short-wave systems capable of resolving fine structure and layering in the upper meters beneath the lander. Spread-spectrum and deconvolution techniques can be used to increase the depth capability of a radar system. If soundings over several locations are available (e.g., with balloons, rovers, or panning short-wave systems), then it will be easier to resolve internal layering, variations in basal reflection coefficient (from which material properties may be inferred), and the geometry of nonhorizontal features.

Sonic sounding has a long history in oil and gas exploration. It is, however, unlikely that large explosive charges, or even swept-frequency techniques such as Vibroseis, would be suitable for a Polar lander — these systems are capable of penetrating several kilometers of material at frequencies of 10–200 Hz, but the energy required to generate the sound waves is large and potentially destructive. The use of audio-frequency and ultrasonic sound generated by piezoelectric crystals is discussed as a possible method to explore layering and fine features in the upper meters of the ice cap. Appropriate choice of transducer(s) will permit operation over a range of fixed or modulated frequencies.

Neutron scattering is used in soil science to assess the moisture content of soil. The technique relies on observing the effects of collisions between source neutrons and the H atoms in the material under test. Such a system may be useful in assessing ice content from within a borehole.

Sounding of a several-kilometer-deep ice cap presents some considerable obstacles. There are, however, several methods that could be used to sound the upper meters of the ice cap in considerable detail.

THE THERMAL AND EVOLVED GAS ANALYZER (TEGA) ON THE 1998 MARS POLAR LANDER. W. V. Boynton, R. D. Lorenz, S. H. Bailey, M. S. Williams, and D. K Hamara, Lunar and Planetary Laboratory, University of Arizona, Tucson AZ 85721-0092, USA.

Introduction: The Thermal and Evolved Gas Analyzer is an instrument in the MVACS (Mars Volatiles and Climate Surveyor) payload on the 1998 Mars Polar Lander (Fig. 1). It is due to reach the layered terrain at around 70°S latitude on Mars in December 1999. The instrument will heat soil samples acquired with a robotic arm to determine their volatile content with a differential scanning calorimeter (DSC) and an evolved gas analyzer (EGA).

Instrument Objectives: The instrument aims to measure the volatile content of the martian soil at depth, specifically to determine the water and CO_2 content. These greenhouse gases may be present in large quantities as ices and locked chemically in the soil, particularly at high latitudes. Understanding the martian climate history and the future resource potential of Mars requires that we measure the abundance of volatile-bearing material in the soil and the minerals with which they are associated. Secondary objectives include the identification of other minerals and the detection of oxidizing compounds in the soil.

Instrument Description: The instrument comprises a set of eight thermal analyzers, each of which will be used only once (Fig. 2). Each analyzer has two identical ovens, one for the sample and one (empty) for a reference. The DSC identifies the temperature and enthalpy of phase transitions by carefully determining the difference in the energy required to heat the reference and sample ovens at a controlled rate. The DSC digitally controls the duty cycle of the power to the ovens to maintain each of them at the programmed ramp temperature. The output of the DSC is simply the difference in power required by the two ovens.

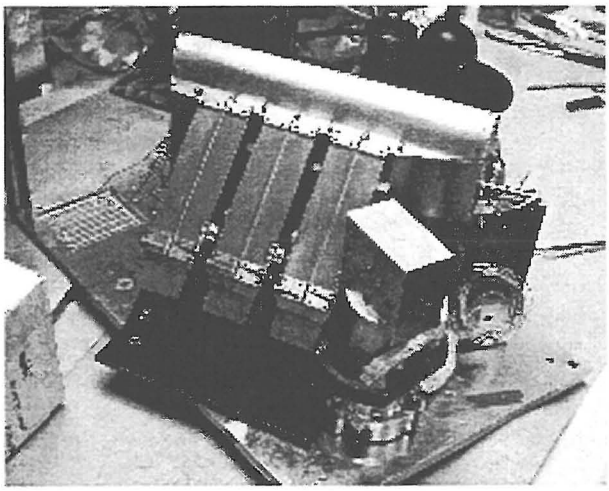

Fig. 1. The flight model TEGA instrument. The angled rectangular structures are three of the eight thermal analyzers (the remaining five are on the opposite side). Each analyzer has a sample funnel with agitator, a sample and reference oven, an oven closing mechanism, and a set of doors to prevent contamination via airborne dust or spillage from the robotic arm scoop. The box and cylinder at the right contains the Herriott gas absorption cell with the two laser diodes and detectors in the box. The section between the two banks of analyzers, with the rounded top, contains the carrier-gas and calibration-gas tanks, the gas handling manifold, and the O analysis cell.

The EGA analyzes the evolved gases as the ovens are heated to provide knowledge of correlated gas release associated with the phase transitions. The correlated gas release will aid in the identification of the phase responsible for the phase transition. The EGA will determine water and CO_2 contents via a high-resolution tunable diode laser-absorption spectrometer. The spectrometer comprises two tunable laser diodes, which are swept around a water and a CO_2 absorption line, and a small mirrored Herriott cell that provides a 1.0-m absorption pathlength in a 5-cm-long cylinder. The O analyzer uses an yttria-doped zirconia amperometric cell, the current of which is proportional to O partial pressure.

Instrument Operation: A sample of soil from depth will be acquired with a robotic arm and deposited into a hopper over the selected thermal analyzer. The sample is loaded into the sample oven from the hopper with an agitator/impeller, which prevents the sample from becoming blocked. A photodiode/LED beam-break detector provides an indication that the sample oven is full, at which point it is commanded to close.

The ovens are made from tapered nickel cylinders that seal together even in the presence of particulates. The temperature of the sample is controlled and measured by Pt windings around the oven. First the temperature will be ramped up and down around the freezing point, to detect the abundance of water ice by the influence of the ice's latent heat on the power required to heat the sample. The sample will then be heated up to around 1000°C with N carrier gas flowing over it.

The robotic arm will acquire samples from several depths, perhaps as deep as 1 m. We expect the volatile content to increase with depth, and the oxidant content may decrease with depth. The eight analyzers in TEGA will allow eight different samples to be analyzed taken from different positions and depths.

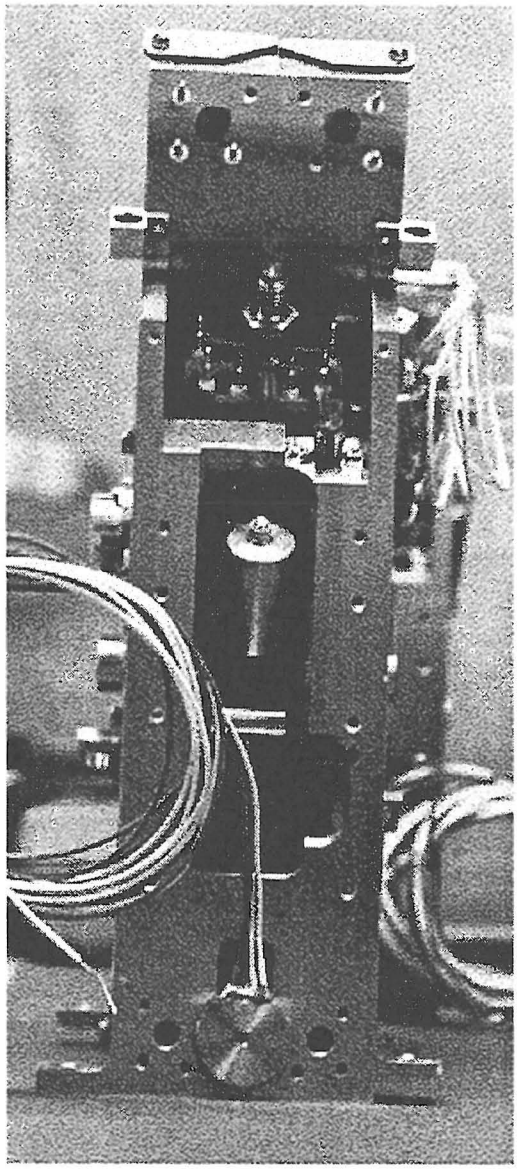

Fig. 2. One of the thermal analyzers. Uppermost is the top edge of the sample funnel doors. The threaded pipe is the outlet gas line to the O sensor and TDL; the pins surrounding it are the electrical connections to the oven windings. The cylinder at center covers a spring that closes the ovens, and the disk at the bottom is the end of a wax pellet actuator, which moves the ovens into position to be closed.

Mineral phase transformations will be calorimetrically detected, while evolution of adsorbed water and decomposition products (e.g., CO_2 from carbonates, water of crystallization from evaporite minerals, and O from peroxides) will be carried to the O sensor and finally into the TDL spectrometer.

The spectrometer will enable the quantitative determination of the volatile content of the sample, and may constrain the isotopic ratios of the evolved gases. The comparison of isotopic composition of the gases locked in the soil with that of the present atmosphere will be a valuable clue in understanding the role of the polar deposits in Mars' history.

REVIEW OF THE 1990–1997 HUBBLE SPACE TELESCOPE OBSERVATIONS OF THE MARTIAN POLAR CAPS. B. A. Cantor and P. B. James, Department of Physics and Astronomy, University of Toledo, Toledo OH 43606, USA (cantor@astrol.panet.utoledo.edu; pbj@physics.utoledo.edu).

The synoptic monitoring of Mars by the HST from December 13, 1990, through April 17, 1997, has resulted in the monitoring of five of the eight martian polar cap regressional cycles. This included parts of four consecutive north polar cap regressional cycles spanning $L_s = 335°$ to $L_s = 144°$ and part of the 1992 south polar cap regressional cycle spanning from $L_s = 259°$ to $L_s = 284°$. The HST images taken before 1994 were obtained with the Wide Field Planetary Camera 1 (WFPC1) instrument, while the ensuing observations were obtained with the improved optics of the Wide Field Planetary Camera 2 (WFPC2). The Mars observations were obtained in the spectral range from the ultraviolet (218 nm) to the near-infrared (1042 nm), which has allowed us to constrain the effects of clouds and dust particulates on cap edge measurements.

Hubble Space Telescope observations of the martian north polar cap regressions during early spring are fairly consistent from year to year with some variations possible during late winter. The 1991 observations at $L_s = 35°$ and $L_s = 59°$ in the longitude range from 270°–280°W, supporting a standstill in cap retreat at a latitude of 70°N (refer to Fig. 1). The standstill in cap retreat reported in previous years at a latitude of 67°N was not observed in the 1992–1997 data. At about $L_s = 60°$, the hexagonal asymmetry of the annual CO_2 ice is very distinct. The extent of this asymmetry, which peaked in 1991 and 1995, varies interannually. Briggs [1] suggest that the longitude dependence could be explained by topography and winds. Comparison of north polar cap regressions observed by HST with previous groundbased and spacecraft observations ([2], and references therein) suggests that interannual variations may be significant; they may be due to interannual atmospheric changes such as global dust storm activity.

The four sets of observations of the martian south polar cap retreat obtained with HST have been reevaluated using the method noted in Cantor et al. [2]. These results are consistent with those found by James et al. [5]. During late spring, the southern cap's asymmetric shape is prevalent as are the Mountains of Mitchel (Fig.2).

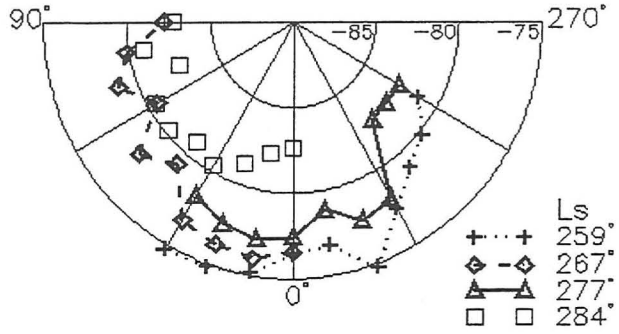

Fig. 2. 1992 south polar cap regression obtained from red filter (673 nm) HST observations.

The Lambert Albedos for the two caps were measured in the violet (410–439 nm) and red (673 nm) filters. Polar cap albedos are consistent with previous results within about 10% [2,4,6]. Both the red and violet north polar cap Lambert Albedos in Fig. 3 have a general increasing trend from $L_s = 340°$ to $L_s = 150°$ (slope = 0.0015). Scatter in the data is due to limb darkening, polar dust storms, and clouds. The red/violet Lambert Albedo ratios, which should minimize the phase effect, decrease in summer relative to spring. This could be due to dust removal from the pole by equatorward-directed surface winds [3]. This might help explain the existence of early spring polar dust storms that seem to emanate from within the polar cap [5].

Acknowledgments: This research was supported by the Space Telescope Science Institute through GO grant number 5832.

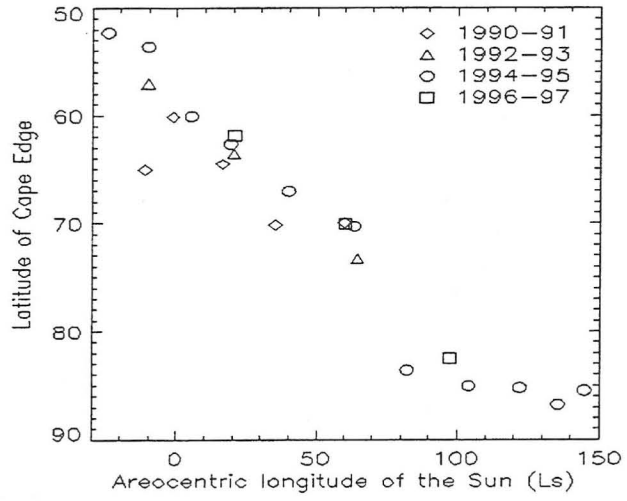

Fig. 1. North polar cap regression obtained from red filter (673 nm) HST observations in the longitude range from 270° to 280°.

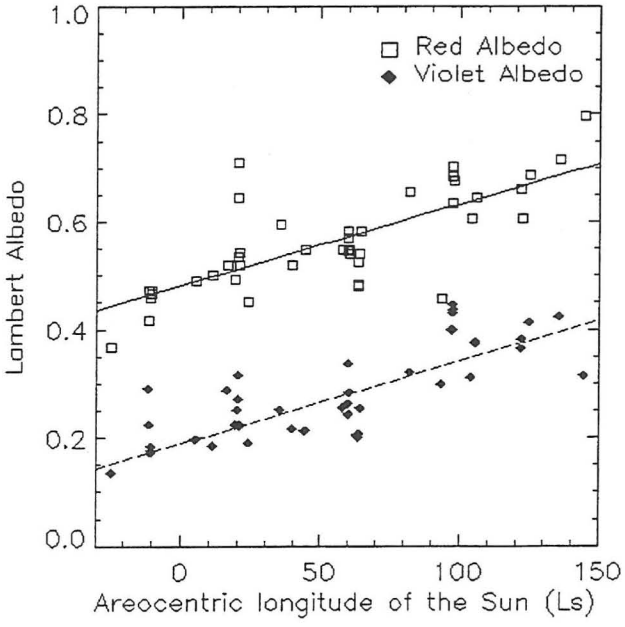

Fig. 3. North polar cap red (673 nm) and violet (410–439 nm) Lambert Albedos obtained from 1990–1997 HST observations.

References: [1] Briggs G. A. (1974) *Icarus, 23,* 167–191. [2] Cantor B. A. et al. (1998) *Icarus,* in press. [3] Haberle R. M. et al. (1979) *Icarus, 39,* 151–183. [4] James P. B. et al. (1996) *Icarus, 123,* 87–100. [5] James P. B. et al. (1998) *Icarus,* in press. [6] Paige D. A. and Ingersoll A. P. (1985) *Science, 228,* 1160–1168.

DEVELOPMENT OF AN AUDIO MICROPHONE FOR THE MARS SURVEYOR 98 LANDER. G. T. Delory[1], J. G. Luhmann[1], D. W. Curtis[1], L. D. Friedman[2], J. H. Primbsch[1], and F. S. Mozer[1], [1]Space Sciences Laboratory, University of California at Berkeley, Berkeley CA 94720, USA (gdelory@ssl.berkeley.edu), [2]The Planetary Society, 65 Catalina Avenue, Pasadena CA 91106, USA (tps.ldf@mars.planetary.org; http://sprg.ssl.berkeley.edu/marsmic).

Introduction: In December 1999, the next Mars Surveyor Lander will bring the first microphone to the surface of Mars. The Mars Microphone represents a joint effort between the Planetary Society and the University of California at Berkeley Space Sciences Laboratory and is riding on the lander as part of the LIDAR instrument package provided by the Russian Academy of Sciences in Moscow.

Instrument Objectives: The inclusion of a microphone on the Mars Surveyor Lander represents a unique opportunity to sample for the first time the acoustic environment on the surface, including both natural and lander-generated sounds. Sounds produced by martian meteorology are among the signals to be recorded, including wind and impacts of sand particles on the instrument. Photographs from the Viking orbiters as well as Pathfinder images show evidence of small tornadolike vortices that may be acoustically detected, along with noise generated by static discharges possible during sandstorms. Lander-generated sounds that will be measured include the motion and digging of the lander arm as it gathers soil samples for analysis. Along with these scientific objectives, the Mars Microphone represents a powerful tool for public outreach by providing sound samples on the Internet recorded during the mission. The addition of audio capability to the lander brings us one step closer to a true virtual presence on the Mars surface by complementing the visual capabilities of the Mars Surveyor cameras.

Instrument Description: The Mars Microphone is contained in a $5 \times 5 \times 1$ cm box, weighs less than 50 g, and uses 0.1 W of power during its most active times. The microphone used is a standard hearing-aid electret. The sound sampling and processing system relies on an RSC-164 speech processor chip, which performs 8-bit A/D sampling and sound compression. An onboard flight program enables several modes for the instrument, including varying sample ranges of 5 kHz and 20 kHz, and a selectable gain setting with 64× dynamic range. The device automatically triggers on the loudest sound during a collection period for storage in an internal flash memory. Data returned by the lander consist of a compressed time-series acoustic waveform between 2 and 10 s long, depending on the sample rate. In addition to the discrete waveform capture, the instrument continuously records the mean power in each of six frequency bands in order to provide an average characterization of the martian acoustic environment. Once the data are retrieved from the telemetry, the compressed time series is expanded into a standard PC-compatible WAV file for analysis, which will include representation in spectral format using FFTs for quantitative characterization of the sound data. The WAV files will be used to share the data with the public via the Internet. The Mars Microphone will thus fulfill a dual role on the Mars Surveyor mission, one as a possible precursor to a more sophisticated acoustic instrument on future landers and one as a mechanism to increase public awareness of efforts to explore and understand the martian climate and planetary history.

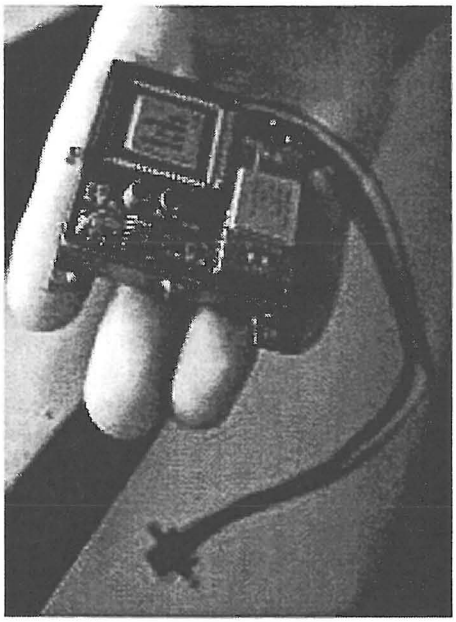

Fig. 1.

DEEPLY FROZEN LAKES IN A TERRESTRIAL PERIGLACIAL ENVIRONMENT. P. T. Doran[1] and C. H. Fritsen[2], [1]Department of Earth and Environmental Sciences, University of Illinois at Chicago, 845 West Taylor Street, Chicago IL 60607, USA (pdoran@uic.edu), [2]Biological Sciences, Desert Research Institute, P.O. Box 60220, Reno NV 89506, USA.

Introduction: Some of the largest lakes in the McMurdo Dry Valleys, Antarctica, have largely been ignored during past limnological studies because they were thought to be frozen solid. However, recent investigations have revealed the presence of saline water bodies beneath up to 19 m of permanent ice in two of these so-called "ice block" lakes (Lake Vida and Lake House). Lakes throughout the dry valleys that have been studied in detail more typically have ice covers ranging between 3 and 5 m. The existence of saline lakes with extremely thick ice covers is atypical, even among lakes in this region, which are themselves unique aquatic systems. These "deeply ice-covered" lakes are aquatic systems on the edge of cold-termination, and they warrant study as analogs of lakes purported to have existed on the surface of Mars in the past.

Radar Research: Several lakes in the McMurdo Dry Valleys were presumed in the past to be frozen solid based largely on attempts at drilling the lake ice covers [1–4]. Lake Vida has been the most intriguing because it is one of the two largest (in terms of surface area) lakes in the dry valleys, and yet it apparently contained no year-round liquid water at depth. Recently a ground-penetrating radar (GPR) survey was carried out on Lake Vida and another purported ice block

lake, Lake House [5]. In a large central portion of Lake Vida, the survey showed attenuation of the radar signal at approximately 19 m, suggesting saline water at this depth. Because GPR radar signals are absorbed by saline water, the depth of the water body (i.e., distance from the ice bottom to sediments) could not be determined. In Lake House, a similar water body was inferred at ~12 m depth.

Ice Coring and Physical Properties: Ice cores (to 14 and 15.8 m depth) extracted in 1996 from Lake Vida contained ice bubbles with unique morphologies that were atypical when compared to other vapor inclusions in 3–5 m ice covers [6]. Most of the vapor inclusions at depths greater than ~6 m contained hoar frost, which is indicative of prolonged exposure to a thermal gradient. At 15.8 m in the profile, wet saline ice was encountered at –11.6°C (logged upon collection). The brine was later determined to be NaCl with an inferred concentration of 600 ppt, or about 17× seawater. Based on the GPR survey this brine would have been 3–4 m from the ice/liquid water interface. The GPR results show parabolic reflections in the ice starting at 16 m, which we now interpret as the start of the briny ice. A meteorological station at the west end of the lake recorded a mean annual temperature at Lake Vida of –26°C. This is ~9°C colder than annual averages in Taylor and Wright Valleys during the same period [5]. The difference occurs entirely during the winter, with the summers being very similar. The reason for the cold Victoria Valley winters appears to be a lack of foehn winds. Since local topography does not seem to be blocking these winds, we suggest that a strong winter temperature inversion in the valley forces the foehn winds to stay off the valley floor. The meteorological record thus shows that the environment at Lake Vida provides greater freezing potential than the environment of other dry valley lakes.

We used these meteorological data to model the annual thermal wave in Lake Vida ice without considering the influence of the underlying water body. The modeled temperatures are compared against the actual first year's data in Fig. 1. From this comparison it is clear that the actual temperature profile gets warmer toward the bottom, suggesting a heat source at depth. There are three probable, not mutually exclusive, candidates for this heat source: (1) localized geothermal heating, (2) ice growth at the base of the ice cover with the resultant release of latent heat, and (3) additional cooling of the water column and the release of specific heat associated with ice growth and concomitant rejection of salts, which would depress the freezing temperature of the solution in front of the advancing freezing front. Another potential but less probable explanation is that the system is not in steady state and the heat is from episodic events of water inflow. We consider (2) the strongest candidate and have calculated that it would require 17.6 cm/yr of basal freezing to generate the observed heat.

Biology: Profiles of microbial biomass in the ice cores indicate that bacterial and microalgal cells (primarily filamentous cyanobacteria) are associated with sedimentary material within the ice matrices. Assays performed on ice core meltwater demonstrated that the populations of both heterotrophic and autotrophic microbes (at depths ranging from 0 to 12 m) retained metabolic potential (measured via the incorporation of radio-labeled CO_2, thymidine and leucine), which was realized upon thawing of the ice samples. This suggests that the ice-bound microbial populations are capable of growth if liquid water were to become available within the permanent ice environment [8].

Although the combination of processes that lead to the formation of active water in Lake Vida are unknown at this time, the preliminary

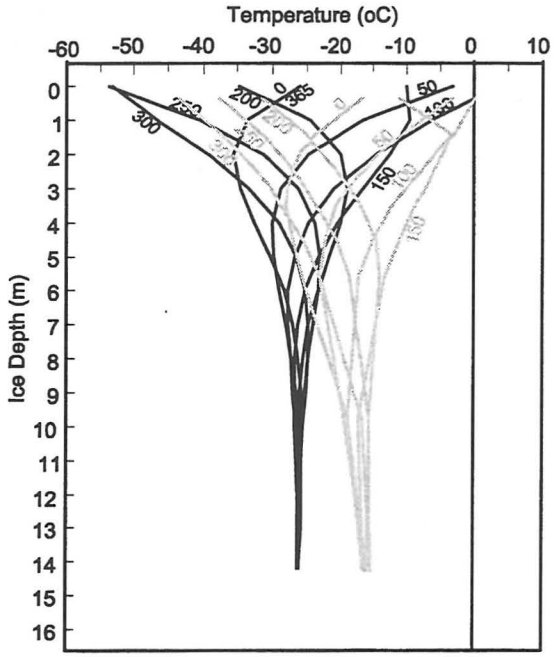

Fig. 1. Predicted ice temperature (black) vs. actual (gray) for first year of temperature measurement in Lake Vida ice. Each line is a 50-day time step from an arbitrarily filled starting point. Predicted values are based on a thermal conduction modified from [7].

temperature records and anecdotal observations [1] suggest that the upper 5 m of the approximately 20-m ice cover is an "active" zone where seasonal warming, melting, and freezing occurs. Deeper in the ice, annual temperatures remain well below 0°C. Thus, liquid water below the upper "active" layer is likely to be found only in association with the brine solution that was found at approximately 16 m.

We have no information on the geochemistry of the brine/water column beneath or within the ice cover, so we do not know if the water provides either a reducing or oxidizing environment. Therefore, we cannot yet speculate on the types of microbial consortia that may be present. Nor do we know whether the brine contains microbial cells and/or activity. The inferred below-zero temperatures (in the brine) are highly restrictive to metabolic processes and are close to the lower limits where microbial activity has been observed [9,10]. The inferred high solute concentration is likely to be an additional constraint on microbial activity. However, the water activity (~0.89) is well above the water activity of 0.62 that is believed to the limit for microbial growth [11,12]. Therefore, the inferred physical environment within the brine in the ice appears restrictive but does not preclude the possibility of active microbes. The temperature profile in the ice and the physical necessity that stratified water bodies become more dense with increasing depth suggests that the brine becomes warmer and/or saltier beneath 16 m, although how much warmer and saltier is unknown at present.

Future Research: We have proposed to return to Lakes Vida and House to carry out a comprehensive coring and water sampling program. Such a program could potentially answer several important questions: What forcing factors are needed to freeze a large Antarctic lake solid? What is the impact on microbial communities as a lake freezes? How can these types of lakes be identified in the geologic

record? Is this a phase that other Dry Valley lakes have gone through, and what does that indicate? Answers to these questions will not only be important to Antarctic science but also to the planetary science community that views dry valley lake systems as analogs for purported paleolakes on Mars and elsewhere [13,14].

References: [1] Calkin P. E. and Bull C. (1967) *J. Glaciol., 48,* 833–836. [2] Clow G., personal communication. [3] McKnight D., personal communication. [4] Priscu J. C., personal communication. [5] Unpublished data. [6] Adams E. E. et al. (1998) *Antarct. Res. Ser., 72,* 281–296. [7] Campbell G. S. (1977) *An Introduction to Environmental Biophysics,* Springer-Verlag. [8] Fritsen C. H. and Priscu J. C. (1997) *Amer. Soc. Limnol.* Oceanogr. Annual Meeting, Santa Fe. [9] Baross J. A. and Morita R. J. (1978) in *Microbial Life in Extreme Environments* (D. J. Kushner, ed.), pp. 9–71, Academic, New York. [10] Herbert R. A. (1986) in *Microbes in Extreme Environments* (R. A. Herbert and Codd, eds.), pp. 317–368, Academic, London. [11] Kushner D. J. (1978) in *Microbial Life in Extreme Environments* (D. J. Kushner, ed.), pp.317–368, Academic, New York. [12] Brown A. D. (1990) *Microbial Water Stress Physiology: Principals and Perspectives,* John Wiley and Sons, New York. [13] Doran P. T. et al. (1998) *JGR,* in press. [14] Wharton R. A. Jr. et al. (1995) *J. Paleolimnol., 13,* 267–283.

FACTORS AFFECTING THE RHEOLOGIC PROPERTIES OF MARTIAN POLAR ICE.

W. B. Durham, Lawrence Livermore National Laboratory, Livermore CA 94550, USA (durham1@llnl.gov).

Introduction: The flow of the martian polar ice caps is influenced by the martian gravity field, the physical configuration of the caps and the underlying hard terrain, and the distribution and rheology of the material in the caps. This contribution speaks to the intrinsic rheology of the material that comprises the polar caps. For a wider view of the flow of ice sheets, terrestrial and otherwise, and the role played by rheology, the reader is referred elsewhere [1,2].

The polar caps are a mixture of phases of H_2O, CO_2, and rock. There is great uncertainty in the relative proportions of these components, and there are probably differences between compositions of the north and south polar caps. Frozen CO_2 may exist as a shallow surface frost, especially on the south polar cap, but probably does not persist in rheologically important quantities [3]. A good case can be made that CO_2 is present as clathrate hydrate, and indeed, much of the material below a meter or so in the ice caps lies within the stability field of CO_2 hydrate [4]. The amount of hydrate is difficult to predict, and the ratio of dust to ice in the layered deposits is not known to within several orders of magnitude [3]. Finally, not only is the proportion of phases in the ice caps largely unknown, it is also likely to be nonuniform, as shown by layered deposits visible in sectional exposures at both poles [3].

We assume for the purposes of discussion the simplest picture of the martian ice caps as void-free, predominantly water ice I, with some clathrate hydrates and dust mixed in. The rheology of water ice is fairly well known, the rheology of hydrates is poorly known, and the dust can be safely assumed to be nondeformable in this mixture. To the extent the simple picture is incorrect (for example, if hydrates are present in very large quantities), the exercise here become less useful.

Rheology of the Polar Ice: Rheology is the relationship between stress and strain rate. Table 1 lists the some of the more important factors influencing the rheology of a mixture of water ice I, clathrate hydrate, and dust, and compares the relative importance of each. For the purposes of this comparison, Table 1 shows the effect of a roughly 10% change of each of the variables at a representative set of conditions, say, deep within the northern martian ice cap: T = 220 K, P = 10 MPa. Note the profound effect of temperature on rheology. A 10% increase in pressure causes an increase in strain rate at constant stress of about 0.7%. A 10% change in temperature, from 220 to 240 K on the other hand, causes a 20-fold increase in strain rate.

TABLE 1. Factors affecting rheology.

Variable	Function	10% Variable Change	Change in Strain Rate	Ref.
Pressure	e^{+13P}	1 MPa	0.7%	[13]
Temperature	$e^{-60000/RT}$	20 K	2000%	[13]
Grain size	$d^{1.4}$	10%	20%	[7]
Clathrate hydrate fraction	(see text)	10%	100%	[8,11]
Dust fraction	$e^{2\Phi}$	10%	20%	[13]

A dependence of strength on grain size can be expected theoretically at conditions where grain boundaries themselves play an active role in deformation, such as when they act as molecular conduits or when grains are able to slide past one another [e.g., 5]. Water ice is one of the few materials where a well-resolved grain-size dependence has actually been observed [6,7]. Goldsby and Kohlstedt [7] quantified the grain-size dependence of ice in laboratory tests at 1-atm; these measurements have recently been confirmed by us in measurements under confining pressure. Based on the Goldsby and Kohlstedt law (Table 1), a 10% decrease in grain size will cause a 20% increase in strain rate. This effect is also shown graphically in Fig. 1, which represents one of the few examples of an experimentally derived deformation map for a crystalline material. Figure 1 shows the rheology of ice I in the grain-size independent dislocation creep regime (solid lines) vs. that in the grain-size dependent regime (dashed lines) for three different grain sizes separated by an order of magnitude. The low stress sensitivity (stress exponent $n = 1.8$) causes the grain-size sensitive regime to expand to higher stresses as grain size decreases.

The strength of clathrate hydrate is being actively researched at the moment (because of recently renewed interest in terrestrial hydrate deposits). Preliminary measurements by Stern et al. [8] show complex behavior, in particular an extended dependence of strength on magnitude of strain. For the moment, it appears that methane hydrate is somewhat stronger than ice I, flowing roughly an order of magnitude more slowly than ice I at fixed stress and temperature. Methane and CO_2 hydrate have the same structure, and since the guest molecule in the hydrate structure is only weakly bonded to the lattice of water molecules [9], it can be assumed that CO_2 hydrate and methane hydrate have about the same strength. We estimate based on measurements of mixtures of ice I plus ammonia dihydrate (not a clathrate), two phases that show about the same strength contrast as clathrate hydrate and ice, that if pure ice I is mixed with 10% hydrate, strain rate will decrease by a factor of 2 [10,11]. It is important to note what is probably a much greater, albeit indirect, effect on rheology of hydrates in the martian polar ice: the effect on temperature gradient. Clathrate hydrates have a thermal conductivity roughly 1/5 that

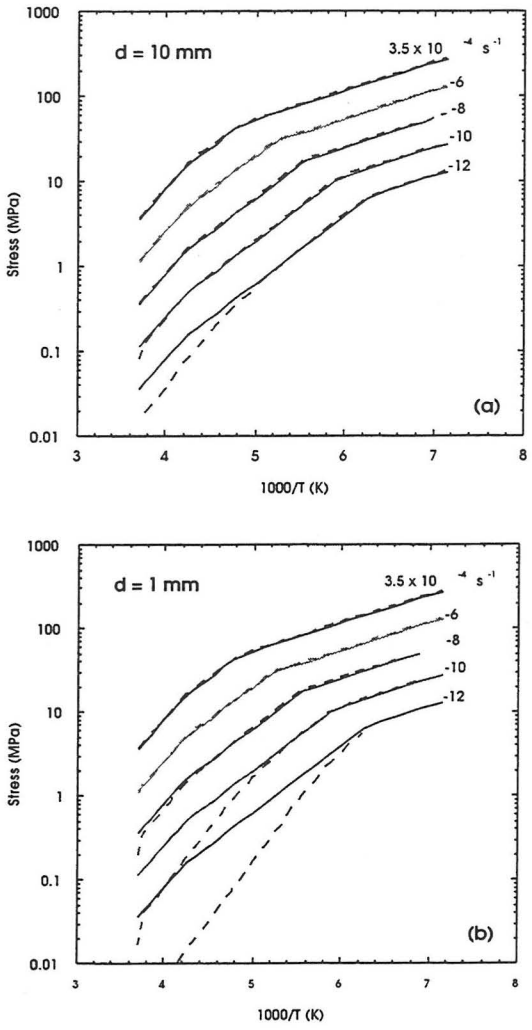

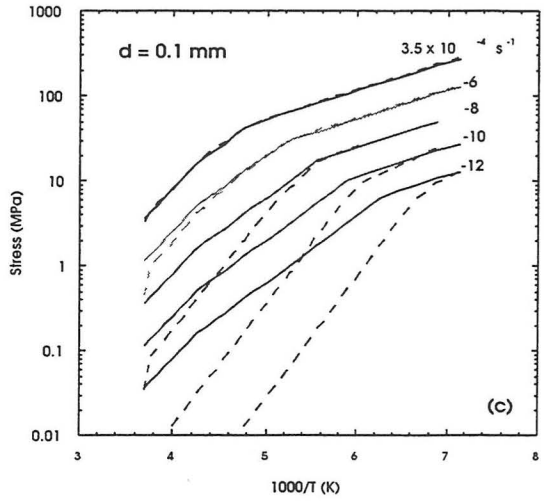

Fig. 1. Experimentally derived deformation maps for pure polycrystalline water ice I at P = 50 MPa comparing dislocation creep (solid lines) to grain-size-dependent creep (dashed lines) at three different values of grain size d of (a) 10 mm, (b) 1 mm, and (c) 0.1 mm. The solid and dashed lines are loci of strength at various fixed values of strain rate separated by two orders of magnitude, beginning with 3.5×10^{-4} s^{-1}. Solid lines are taken from [14], dashed lines from [7]. Value of stress at strain rate 3.5×10^{-8} s^{-1} and above were measured directly; values at lower strain rates are based on extrapolation. The lower stress sensitivity of grain-size-sensitive creep (evident by the more widely spaced dashed lines) cause it to dominate at low stresses.

of water ice [12]. If hydrates are present in quantities sufficient to strengthen the polar ice, they probably will warm the thermal gradient at least enough to compensate for this hardening.

The dust component in the martian polar ice can have a variety of effects, including being a barrier to flow, causing dispersion hardening, and pinning grain boundaries. The physical barrier effect [13] (Table 1) applies to volume fractions of dust up to about 0.5. Dispersion hardening (references in [13]) could cause the appearance of a threshold stress of a few tens of kPa below which no flow will occur. Grain-boundary pinning actually produces a reverse effect when it occurs in the grain-size-sensitive creep regime. Increasing the number of particles causes grain sizes to be smaller and strength to be lower [6].

Conclusion: The message of Table 1 is clear: Temperature is of overriding importance in controlling the rheology of the martian polar caps. Efforts to determine the composition, physical shape, and heterogeneous structure of the polar ice caps will bring insight into surface evolutionary processes, but nothing will tell us more about how the ice caps flow than a good determination of their temperature profile.

References: [1] Nye J. F. (1965) *J. Glaciol., 5,* 695–715. [2] Fisher D. A. (1993) *Icarus, 105,* 501–511. [3] Thomas P. et al. (1992) in *Mars* (H. H. Kieffer et al., eds.), pp. 767–795, Univ. of Arizona, Tucson. [4] Kargel J. S. and Lunine J. I. (1998) in *Solar System Ices* (B. Schmitt B. et al., eds.), pp. 97–117, Kluwer. [5] Ashby M. F. and Verrall R. A. (1973) *Acta Metal., 21,* 149–163. [6] Baker R. W. and Gerberich W. W. (1979) *J. Glaciol., 24,* 179–194. [7] Goldsby D. L. and Kohlstedt D. L. (1997) *Scripta Mater., 37,* 1399–1406. [8] Stern L. A. et al. (1996) *Science, 273,* 1843–1848. [9] Sloan E. D. (1990) *Clathrate Hydrates of Natural Gases,* Dekker, New York. [10] Durham W. B. (1993) *JGR, 98,* 17667–17682. [11] Tullis T. E. et al. (1991) *JGR, 96,* 8081–8096. [12] Cook J. G. and Leaist D. G. (1983) *GRL, 10,* 397–399. [13] Durham W. B. et al. (1992) *JGR, 97,* 20883–20897. [14] Durham W. B. et al. (1997) *JGR, 102,* 16293–16302.

PAST GLACIOLOGICAL AND HYDROLOGICAL STUDIES.

D. A. Fisher, Terrain Sciences Division, Geological Survey of Canada, 601 Booth Street, Ottawa, Ontario K1A 0E8, Canada (fisher@nrcan.gc.ca).

There are not many papers about the north cap as an ice sheet, and they often come about through people productively straying outside their fields. Budd et al. [1], Clifford [2,3], and Fisher [4] have all addressed the north cap as if it were a terrestrial ice sheet, and Clifford [2,3] has made it a key element in his model of the present martian hydrological system. The above authors postulated that the ice cap's central thickness was in the 3–6 km range and that the bed temperatures were high enough to allow plastic deformation and flow. Toon et al.'s [5] study of astronomical climate forcing looked at the surface of the north cap as a terrestrial glaciologist might.

Budd et al. [1] started with a limited dataset. They used steady state theory to derive north cap ice velocity fields from a tentative knowledge of surface elevations and temperatures provided by Mariner and Viking missions. From the ice velocity fields, the mass balance fields and age-depth profiles could be derived. Their derived accumulation rates went as high as 2 mm/yr, but were more typically a few tenths mm/yr, and their derived ablation rates averaged 0.1 mm/yr. The oldest ice at the edge of the north cap was estimated to be 100 Ma.

Clifford's work [2,3] is from the point of view of a planetary scientist whose goal was to integrate the ice cap into a model for a planet-wide ground-water system. Like Budd [1], he assumes the central thickness is in the 4–6 km range; large enough to elevate basal temperatures to the –40 to –60 range and allow flow. Following a range of thickness and bottom salt loading scenarios, he concludes the ice cap can flow and even possibly melt at the base of the ice. Even without basal melting he points out that the thick ice would elevate the melting isotherm under the ice cap and provide the recharge for the global ground-water system. He speculates that basal melt could entrap a subglacial lake that could periodically break out and produce the major reentrant valley Chasma Boreale.

Like Budd [1] and Clifford [2,3], Fisher [4] postulates ice thick enough to flow and integrates the dark scarp spirals with a theory of flow and net mass balance assuming the scarps are mobile ablation (sublimation) units. Combining the ice velocity fields with the scarp's ablation velocity toward the pole results in the spiral pattern. Since the ice flow center is offset from the pole there are regions of scarp divergence and convergence. The latter regions experience enhanced ablation producing the reentrant valleys. The model adapts the glaciological idea of mass balance to the north cap. The mobile ablation scarps continuously track poleward passing their dust load outward and downward eventually laying down their load a layer at the margin. Given flow, the temporal stratigraphy of the north cap would be laid out horizontally with the oldest at the edge and exposed in the scarp walls. A traverse gives access to this history.

Toon et al. [5] look at the energy balance at the ice caps surface including the summer radiation budget, atmospheric thermal conduction, and phase change cooling. Their solution of the heat balance equation is driven mainly by the obliquity cycle with period 1.2×10^5 yr. Using a 13° amplitude they found rather negative net mass during the high obliquity phase of the cycle. Their analysis did not however, include the possibility that the ablating dirty ice would protect itself with an ice clogged dirt layer that would constrain loss rates to those due to diffusion.

How the north cap survives high obliquity is a central problem as are the basic questions: (1) How thick is it? (2) What is the accumulation/loss rate? (3) What is the density profile? and (4) Does it flow?

References: [1] Budd W. F. et al. (1986) *Polarforsch., 56 (1/2),* 43–63. [2] Clifford S. M. (1987) *JGR, 92,* 9135–9152. [3] Clifford S. M. (1993) *JGR, 98,* 10973–11016. [4] Fisher D. A. (1993) *Icarus, 105,* 501–511. [5] Toon O. B. et al. (1980) *Icarus, 44,* 552–607.

MARTIAN GLACIAL LINEATIONS: SEDIMENTOLOGY, REMOTE SENSING, AND GEOGRAPHICAL INFORMATION SYSTEMS UNRAVEL THE PAST.

A. L. J. Ford[1] and A. Khatwa[2], [1]Department of Electronics and Computer Science, University of Southampton, Highfield, Southampton, SO17 1BJ, UK (Andrew.Ford@soton.ac.uk), [2]Department of Geography, University of Southampton, Highfield, Southampton, SO17 1BJ, UK (A.Khatwa@soton.ac.uk).

Introduction — Terrestrial Glacial Lineations: Terrestrial glacial lineations, in the form of flutes (10–10^2 m in length), drumlins and megaflutes (10^2–10^3 m in length), and megascale glacial lineations (10^3–10^4 m in length) [1], have long been the subject of study using techniques of sedimentary coring and till fabric analysis. Although this aspect of glaciological research is detailed, type sites for lineations are few and widely distributed. Conclusions drawn from such type sites can appear to conflict, as described in detail by Clark [3]. Recently there has been a move to comprehensively map glacial lineations using both optical and microwave (the latter highly sensitive to topography) remote sensing. Such mapping can reveal former ice sheet behavior by the separation of complex lineation patterns into flow sets (now associated with former ice streams [2]) using spatial analysis and Geographical Information Systems (GIS). Using additional subsurface analysis software, stratigraphic cores may then be correlated to their parent flow sets. These flow sets are then utilized as a correlation tool to link widely spaced stratigraphic sections. The result is a synoptic view of former ice sheet behavior that can finally solve conflicts in the stratigraphic evidence.

Orbital Imagery and Martian Glacial Lineations: Glacial lineations similar to those found on Earth have been recognized on orbiter imagery by Kargel and Strom [4] on the surface of Mars and form some of the strongest evidence that ice sheets were once present at the martian poles. Sufficient imagery of the planet's surface now exists for the comprehensive mapping of glacial lineations at the scale of megaflutes, drumlins, and megascale lineations. Using existing methodology and GIS, this would allow any former complex martian ice sheet behavior to be separated into flow sets. Thus former ice streams, known to be highly sensitive to climate change on present-day Earth, would become evident. Should these ice streams appear to have shifted in position and orientation of flow, shifting ice divides are the accepted explanation. As with former terrestrial ice sheets, those on Mars may then be shown to have been highly unstable with implications for equally unstable former climates.

Glacial Sedimentology — Completing the Picture: At the end of any such remote sensing and GIS study, there would remain a lack of *in situ* sedimentological evidence. Therefore any conclusions drawn from the data would be largely speculative. Such a lack of sedimentological evidence needs to be addressed, and it is the proposal of the authors that a series of future martian landers be dedicated to the supply of sedimentological data.

The largest task facing the terrestrial glaciologist is commonly the selection of lineations suitable for coring. Additionally, exploration for clear exposures free of vegetation and slumping also proves difficult on Earth. Such sites would provide excellent opportunities for the analysis and development of sedimentological facies models. Using existing imagery the former is easily accomplished for Mars, while the latter is facilitated by the lack of vegetation or significant geomorphological action.

It is proposed that landers be sent to widely distributed flow sets surrounding both martian poles so as to gain a synoptic picture of the behavior of both ice sheets. The landers must be capable of precision landings or carry rovers so as to ensure lineations are proximal and able to be cored. Having taken a core, the lander will then be able to perform sedimentological analyses before sending its data to Earth.

Sediment facies may be studied at a crude level by the use of a

stereo optical system to acquire images of the surfaces of lineations near each lander. As well as image interpretation, the geometry of facies may be quantified using existing close-range digital photogrammetric techniques.

As with current terrestrial studies, the sedimentological information can then be correlated with parent flow sets in a GIS to complete the picture of ice sheet behavior at both poles, with implications for martian climate change.

Additional Studies: Additional information regarding the velocity of former ice streams may be derived using sedimentology and fabric taken from neighboring cross-cutting lineations. As outlined by Rose [5], if the sedimentology of reworked till in one lineation is matched to that of a neighbor and the volumes of both are known, then a sediment transfer rate between the two can be derived and ice stream velocity inferred. The necessary volumes of lineations can be derived using existing optical imagery with digital photogrammetric techniques or future radar imagery with interferometric techniques. The latter would operate with near-optimal phase coherence due to the unvegetated, dry, and stable martian surface.

Another important application of combining sedimentalogical data with mapping is the location of the source of any trace minerals found within lander cores. Such work has been undertaken in Canada to aid commercial mining companies in the exploration of important minerals [6]. On Mars it may be used to improve our understanding of solid geology, presently hidden below formerly glaciated terrain.

Conclusion: By necessity any study of Mars must make use of remote sensing together with a very limited amount of *in situ* data. By using existing imagery and correlating it to a very small quantity of *in situ* data answers to two of the most important martian issues, former glaciation and climate change, may be found. Such a study will be close to optimal, creating the most results from the least quantity of data.

References: [1] Clark C. D. (1993) *Earth Surface Processes and Landforms, 18,* 1–29. [2] Clark C. D. (1994) *Sed. Geology, 91,* 253–268. [3] Clark C. D. (1997) *Quat. Sci. Rev., 16,* 1067–1092. [4] Kargel J. S. and Strom R. G. (1992) *Geology, 20,* 3–7. [5] Rose J. (1989) *Sed. Geology, 62,* 151–176. [6] Wagnar M. J. (1995) *Earth Observation Magazine, January,* 25–28.

FORMATION OF THE CARBON DIOXIDE ICE SEASONAL POLAR CAPS. F. Forget, Laboratoire de Météorologie Dynamique du Centre National de la Recherche Scientifique, BP99, Université Paris 6, 75252 Paris Cedex 05, France (forget@lmd.jussieu.fr).

One of the key processes controlling the geology of the martian polar regions is the seasonal condensation of the atmosphere into CO_2 ice caps. These polar caps mostly condense during the polar night, when surface and atmospheric temperature become cold enough to reach the frost point of CO_2. Thus, almost all that is known about the formation of the polar caps has come from the Mariner 9 and Viking infrared measurements. These observations showed that the physical processes controlling the condensation are complex, because of the unique radiative and microphysical properties of CO_2 ice condensing in a CO_2 atmosphere. For instance, the IRTM instrument observed variable structures exhibiting brightness temperatures far below the physical temperature appropriate for condensed CO_2 in vapor pressure equilibrium at the expected atmospheric pressure. A detailed analysis of the data suggests that these low brightness temperatures result from the radiative properties of the small CO_2 ice particles that condense in the atmosphere rather than directly on the surface [1]. Indeed, simulations performed with General Circulation Models have shown that a fraction of the total CO_2 condensation can take place in the atmosphere. Atmospheric condensation can result from radiative cooling on the one hand (especially when the atmosphere is dust laden) and from adiabatic cooling in upward motions on the other [2]. The resulting CO_2 snowfalls could create the observed features, because the CO_2 ice particles that condense in the atmosphere can be efficient scatterers at infrared wavelengths (whether they are airborne or have just fallen to the ground) carbon dioxide ice deposits composed of nonporous solid ice, however, having directly condensed on the ground or having undergone frost metamorphism should behave almost like blackbody emitters, or, more likely, be transparent in the infrared so that the ground beneath can radiate through. In fact, by simply parametrizing the radiative effects of the modeled CO_2 snow fall and the "snow metamorphism," it has been possible to accurately reproduce the general behavior of the features observed by Viking in the thermal infrared, and, in turn, the global CO_2 cycle [2].

By scavenging airborne dust, the snow falls may dramatically increase the dust sedimentation rate in the polar region. How much dust can be trapped in the polar deposits by such a process? To answer this question, the scavenging of dust by CO_2 has been simulated in a version of the LMD General Circulation Model that includes an interactive dust transport scheme and the CO_2 snow fall parametrization. Also, because the CO_2 clouds and snow falls strongly alter the radiative balance of the condensing polar caps, they affect the global CO_2 cycle and thus the global climate [3]. All these processes should be taken into account when studying past climates or the existence of permanent CO_2 ice deposits near the south pole.

New observations are being transmitted by Mars Global Surveyor. TES and MOLA data should greatly improve our understanding of what is really going on during the cap formation.

References: [1] Forget et al. (1995) *JGR, 100,* 21119–21234 [2] Forget et al. (1998) *Icarus, 131,* 302–316. [3] Forget and Pollack (1996) *JGR, 101, 16865–16880.*

35-GHz MEASUREMENTS OF CARBON DIOXIDE CRYSTALS. J. Foster, A. Chang, D. Hall, A. Tait, and A. Klein, Hydrological Sciences Branch, Laboratory for Hydrospheric Processes, NASA Goddard Space Flight Center, Greenbelt MD 20771, USA (jfoster@glacier.gsfc.nasa.gov).

In order to maximize our knowledge of the martian polar caps, it is important to compare and contrast the behavior of both frozen H_2O and CO_2 in different parts of the electromagnetic spectrum. Relatively little attention has been given, thus far, to observing the thermal microwave part of the spectrum. In this experiment, passive microwave radiation emanating from within a 33-cm snowpack was measured with a 35-GHz hand-held radiometer, and in addition to the natural snow measurements, the radiometer was used to measure the microwave emission and scattering from layers of manufactured CO_2 (dry ice) crystals. A 1-m^2 plate of aluminum sheet metal was positioned beneath the natural snow so that microwave emissions from the underlying soil layers would be minimized. 35 GHz measurements of this plate were made through the 33-cm snowpack. Layers

of the snow were removed and measurements were repeated for the diminishing snowpack until the bare plate was in view. Then, 9 cm of CO_2 crystals were deposited onto the sheet-metal plate, and as was the case for the natural snow, hand-held measurements were made each time the thickness of the deposit was altered. These CO_2 crystals were ~0.65 cm in diameter and were cylindrical. The temperature of the dry ice was –76°C, whereas the temperature at the top of the snowpack was –1.9°C (the air temperature was –3°C). Two additional 9-cm increments were placed on top of the existing CO_2 crystals, resulting in a total thickness of 27 cm of dry ice. After this series of measurements was made, the CO_2 crystals were then placed on top of the snowpack, and as before, measurements were made using the 35-GHz radiometer. As a final part of this experiment, soil particles were spread on top of the dry ice, and once again, microwave measurements were made with the 35-GHz radiometer.

Compared to the natural snow crystals, results for the dry ice layers exhibit lower microwave brightness temperatures for similar thicknesses, regardless of the incidence angle of the radiometer. For example, with a covering of 9 cm of snow and also for 9 cm of dry ice, the brightness temperatures at 50° H (horizontal polarization) were 89 K over the snow and 48 K over the dry ice. With a covering of 20 cm of snow and 18 cm of dry ice, the brightness temperatures were 125 K over the snow and 63 K over the dry ice. When the snow depth was 33 cm, the brightness temperature was 120 K, and when the total thickness of the dry ice was 27 cm, the brightness temperature was 72 K. The lower brightness temperatures are due to a combination of the lower physical temperature and the larger crystal sizes of the commercial CO_2 crystals compared to the snow crystals. As the crystal size approaches the size of the microwave wavelength, it scatters microwave radiation more effectively. The dry ice crystals in this experiment were about an order of magnitude larger than the snow crystals and 3 orders of magnitude larger than the CO_2 crystals produced in the cold stage of a scanning electron microscope. Adding a 2-cm layer of dry ice on top of the snowpack had little effect on further reducing the brightness temperatures, however, when the dry ice layer was increased by 18 cm, the brightness temperatures (at 50° H) dropped to 150 K. Spreading soil on the dry ice appeared to have no effect on the brightness temperatures.

MARTIAN POLAR REGION IMPACT CRATERS: GEOMETRIC PROPERTIES FROM MARS ORBITER LASER ALTIMETER (MOLA) OBSERVATIONS.

J. B. Garvin[1], S. E. H. Sakimoto[2], J. J. Frawley[3], and A. Matias[4], [1]Mail Code 921, NASA Goddard Space Flight Center, Greenbelt MD 20771, USA (garvin@denali.gsfc.nasa.gov), [2]Mail Code 921, Universities Space Research Association at NASA Goddard Space Flight Center, Greenbelt MD 20771, USA, [3]Herring Bay Geophysics and Raytheon-STX, Dunkirk MD 20754, USA, [4]University of Puerto Rico, Mayagüez, and NASA Goddard Space Flight Center, Greenbelt MD 20771, USA.

Introduction: The Mars Orbiter Laser Altimeter (MOLA) instrument onboard the Mars Global Surveyor (MGS) spacecraft [1] has so far observed approximately 100 impact landforms in the north polar latitudes (≥60°N) of Mars [see 2,6]. Correlation of the topography with Viking Orbiter images indicate that many of these are near-center profiles, and for some of the most northern craters, multiple data passes have been acquired. The northern high latitudes of Mars may contain substantial groundice [3–5] and be topped with seasonal frost (largely CO_2 with some water), forming each winter. We have analyzed various diagnostic crater topologic parameters for this high-latitude crater population with the objective of characterizing impact features in north polar terrains, and we explore whether there is evidence of interaction with ground ice, frost, dune movement, or other polar processes. We find that there are substantial topographic variations from the characteristics of midlatitude craters in the polar craters that are not readily apparent from prior images. The transition from small simple craters to large complex craters is not well defined, as was observed in the midlatitude MOLA data (transition at 7–8 km [6]). Additionally, there appear to be additional topographic complexities such as anomalously large central structures in many polar latitude impact features. It is not yet clear if these are due to target-induced differences in the formation of the crater or post-formation modifications from polar processes.

Sampled Craters: In Mars' northern high latitudes (≥60°N), MOLA sampled numerous flow-lobe impact craters, including a population of fresh-appearing "pedestal" or "pancake" features that appear as perched circular depressions at the center of a quasi-circular, positive-relief deposit [7]. MOLA also sampled some small simple craters, dust-mantled craters, several impact craters with high-albedo (frost-filled?) interior deposits (e.g., Korolev Crater, at 73.2°N, 162.8°E, A in Fig. 1), several large complex craters, and a handful of odd impact features in or on the residual polar ice cap and polar layered terrain.

Simple craters. For the *simple* polar latitude craters on Mars, (e.g., the crater at 60°N, 352°E, B in Fig. 1), a typical aspect ratio (depth/diameter, or d/D) of 0.053 is observed, with a cavity cross-sectional shape that is well approximated by a paraboloid (n = 1.95), and ejecta thickness function exponents of about –2.77. Subtle ramparts only tens of meters in relief are resolved in the MOLA profiles.

Large complex craters. For the large complex craters, a typical aspect ratio falls in the 0.023–0.029 interval. They are not abundant in Mars' northern plains, but MOLA has sampled each of the largest ones at least once so far and for Korolev and Lomonosov, half a dozen passes each sampled either the cavity, the ejecta, or both. It appears that Korolev, like its counterparts Lomonosov (C in Fig. 1) and Mie, is ~2.4 km in depth, with a 800-m rim, and interior terracing. However, given the limited MOLA crater floor coverage, it is difficult to ascertain whether the high albedo character of the crater floor is a mantling deposit that covers a central structure as is suggested for the two other high albedo craters discussed below. The Korolev ejecta blanket is well expressed topographically, with 300-m-tall ramparts, and well defined hummocks and lobes. The floors of Korolev, Lomonosov, and Mie all lie within 100–200 m of a common elevation of –6500 m, which is the lowest observed thus far on Mars. The fact that the MOLA-derived floor elevations are all within 100–200 m across thousands of kilometers may provide evidence of a widespread upper weak layer approximately 2.2–2.5 km in thickness overlying a more mechanically strong layer.

Ice-fill craters. For the craters with high-albedo interiors, there are two others in addition to Korolev outside the residual polar cap that have been sampled. One of these is a 49-km feature at 77°N, 215°E (D in Fig. 1). Viking Orbiter images show a fresh, polygonal rim, steep inner-crater cavity walls, and an indistinct ejecta blanket of highly variable albedo. The MOLA transects, on the other hand, illustrate considerable topographic complexity. The crater is 2.4 km deep from its rim crest, with an aspect ratio (d/D) of 0.052. The slope of the ejecta blanket, which is well defined topographically, is ~1.6°,

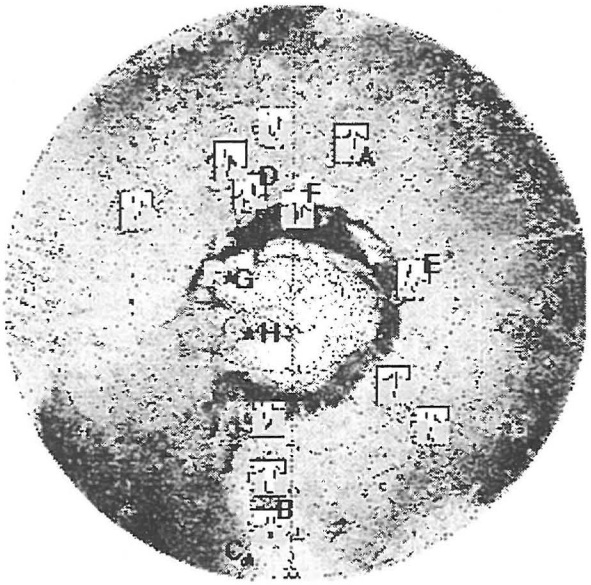

Fig. 1. Mars Polar Stereographic image from 55°N to 90°N with a dozen inset examples of MOLA crater cross sections plotted with the lower left corner at the crater center. Shaded relief base map is from the USGS 1:15,000,000 Topographic series, Map I-2160, 1991.

and the ejecta thickness function follows a –2.5 power-law, not unlike fresh lunar craters [6]. The cavity is best approximated by a polynomial with a power n of ~3. The southern ejecta ramparts have 300 m of local relief, but are less distinct to the north with <100 m of relief. An enigmatic central peak feature with D ~27 km and 670 m in relief is an inverted "U" shape, in contrast to more conical peaks in MOLA-sampled midlatitude craters [6]. The central peak volume (if axisymmetric), is ~30% of that of the cavity. The anomalous volume and topology suggests that it could represent an ice-mantled traditional central peak. It is not clear from the current image and topography coverage whether the ice deposit is a remnant of a larger ablated deposit or accumulated from deposition of ice/CO_2 atop a central deposit. The second possible ice-fill crater is at 77.3°N, 90°E (E in Fig. 1). The five available MOLA transects show a pronounced asymmetry in interior and rim elevations, a large interior deposit and the floor near the level of the surrounding terrain.

Impact features on or near residual polar ice. The first of these is an impact feature at 81.6°N, 190°E, (F in Fig. 1) that is mapped as part of the polar ice deposit outliers and is in well-developed dunes in the Utopia Planitia polar erg field. Several MOLA passes were acquired for this enigmatic crater with indistinct ejecta, which displays a d/D ratio of 0.052 and a cavity shape parameter n > 4.0, indicating it is very "U" shaped. The central deposit's volume occupies 72% of the cavity volume, which is larger than the volume of the ejecta, and 5–10× that observed for similar diameter midlatitude craters. The origin of this central deposit is unclear. It might be associated with a major deposition of ice over time or be an ablation remnant of a previously larger polar ice sheet that completely covered the crater. Its ejecta thickness function falls off much more steeply than most martian craters, and the ejecta lack either the typical polar lobate morphology or ramparts. The Viking imaging is poor, and it is possible that dune materials have encroached upon the distal ejecta.

The second impact feature is at 81.3°N, 255°E (G in Fig. 1), and is on or near the residual ice margin. The third feature is a small crater in Chasma Boreale at 83°N, 312°E (H in Fig. 1). Both of these latter features were poorly imaged by Viking, but both appear to have anomalous ejecta and cavity topography

Discussion and Conclusions: The well-defined transition from small simple to large complex craters that was observed in the midlatitudes MOLA data [1,2,6] is not observed in the polar craters. The transition may be delayed to larger crater sizes. Additionally, the complex craters have best-fitting d vs. D power law relationship ($d = kD^x$) with x = 0.79 instead of the midlatitude value of x = 0.39, which suggests that polar complex craters tend to be deeper than their midlatitude counterparts of the same diameter. However, a natural break in the topology of crater cavities is still observed at high latitudes, such that simple craters have conical to paraboloidal shapes, while complex varieties are more "U" shaped. The distribution of the ejecta thickness function exponents [see 6] for polar region craters is more variable than that reported in [6] for the midlatitude craters, with an average value near –2.2 (vs. –2.9 for midlatitudes), but a standard deviation of 3.3 and a modal value of –0.5. In general, polar region craters do not follow the simple trends that MOLA observed for nonpolar latitudes, and there often are anomalously large central structures in near polar latitude impact features. Three-dimensional polar crater ejecta blanket modeling is under way, with emphasis on polar process effects in ejecta emplacement and modification.

Acknowledgments: We gratefully acknowledge the support of the MGS Project, MOLA principal investigator D. E. Smith and deputy principal investigator M. T. Zuber. G. Neumann provided essential support.

References: [1] Smith D. E. et al. (1998) *Science, 279,* 1686–1692. [2] Garvin J. B. et al. (1998) *EOS Trans. AGU., 79,* S191. [3] Carr M. H. (1996) *Water on Mars,* Oxford Univ., New York. 229 pp. [4] Carr M. H. (1981) *The Surface of Mars,* Yale Univ., New Haven, 232 pp. [5] Thomas P. et al. (1992) in *Mars.* (H. H. Kieffer et al., eds.), Univ. Arizona, Tucson, pp. 767–795. [6] Garvin J. B. and Frawley J. J. (1998) *GRL,* submitted. [7] Head J. W. and Roth R. (1976) in *Papers Presented to Symp. on Planetary Cratering Mechanics,* pp. 50–52, LPI. [8] McGetchin T. R. (1973) *EPSL, 20,* 226–236.

DYNAMIC/THERMODYNAMIC SIMULATIONS OF THE NORTH POLAR ICE CAP OF MARS.

R. Greve, Institut für Mechanik III, Technische Universität Darmstadt, D-64289 Darmstadt, Germany (greve@mechanik.tu-darmstadt.de).

Ice Sheet Model SICOPOLIS: The present permanent north polar water ice cap of Mars is investigated with the dynamic/thermodynamic ice-sheet model SICOPOLIS (SImulation COde for POLythermal Ice Sheets), which was originally developed for and applied to terrestrial ice sheets like Greenland, Antarctica, and the glacial northern hemisphere [1–4]. The model is based on the continuum-mechanical theory of polythermal ice masses [5–7], which describes the material ice as a density-preserving, heat-conducting power-law fluid with thermomechanical coupling due to the strong temperature dependence of the ice viscosity. It is further distinguished between *cold ice* with a temperature below the pressure melting point and *temperate ice* with a temperature at the pressure melting point, the latter being considered as a binary mixture of ice

and small amounts of water. The influence of the considerable dust content of the ice cap on the mechanical properties of the ice is neglected.

The model computes three-dimensionally the temporal evolution of ice extent, thickness, temperature, water content, and age as a response to external forcing. The latter must be specified by (1) the mean annual air temperature above the ice, (2) the surface mass balance (ice accumulation minus melting and evaporation), (3) the global sea level (not relevant for martian applications), and (4) the geothermal (areothermal) heat flux from below into the ice body.

Simulation Setup: The surface topography, h, of the permanent north polar water ice cap of Mars used here is based on the map constructed by Dzurisin and Blasius [8], which was slightly filtered and digitized to a 40-km grid for this study, and complemented by the ice margin contour given by Budd et al. [9]. As for the ice thickness, H, a Gaussian distribution of

$$H = H_o e^{-r^2/r_o^2}$$

is used, where r is the distance from the position of maximum ice thickness, H_0, assumed to be at 87°N, 0°W, and $r_0 = 400$ km. Based on the horizontal extent and observed surface undulations of the ice cap, Budd et al. [9] argue that H_0 should be about 4 km. From the digitized surface topography and equation (1), an estimated digitized bedrock topography, b, follows via b = h–H. Furthermore, application of a local isostatic balance between ice load and lithosphere buoyancy yields the relaxed bedrock topography with no ice load, b_0, as

$$b_o = b + \frac{\rho}{\rho_a} H$$

where ρ is the ice density (910 kg/m³) and ρ_a the mantle density, taken as 2350 kg/m³ (terrestrial value 3300 kg/m³ times mean-density ratio Mars/Earth). The bedrock response to changing ice loads is modeled by a delayed local isostatic balance with the time lag τ_V = 3000 yr.

According to the data listed by Budd et al. [9], the mean annual air temperature above the ice, Tma, is described by a parameterization depending on elevation, h, and colatitude, $\tilde{\phi}$ ($\tilde{\phi} = 90°N - \phi$, where ϕ is the latitude),

$$T_m = T_{ma}^0 + \gamma_{ma} h + c_{ma} \tilde{\phi}$$

with $T_{ma}^0 = -90°C$, the mean lapse rate $\gamma_{ma} = -2.5°C/km$, and c_{ma} = 1.5°C/°lat. The accumulation of water ice on the surface of the ice cap is assumed to be spatially constant. Since the water vapor density in the martian atmosphere is ~1/1000th the terrestrial value, and typical accumulation rates for terrestrial ice sheets are about 300 mm WE/yr (Greenland), the order of magnitude of the accumulation rate, S, can be estimated as 0.1 . . . 1 mm WE/yr. Surface melting/evaporation is parameterized by the standard degree-day method with terrestrial (Greenland) values for the snow- and ice-melt factors, β_{snow} = 3 mm WE/(d°C) and β_{ice} = 12 mm WE/(d°C), an amplitude of the annual temperature signal of 30°C and a standard deviation of additional temperature variations of 10°C. Furthermore, the simulated ice cap is restricted to its present extent, and the areothermal heat flux is set to 33.5 mW/m² [9].

Results: A series of simulations were carried out, where the measured/estimated topography described above is used as initial condition, and the time-forward integration is conducted until the simulated ice cap is in steady state with the present climate forcing defined by the air temperature, the surface mass balance, and the areothermal heat flux. For the initial ice volume, V_{init}, the three values 2×10^6 km³, 3×10^6 km³, and 4×10^6 km³ are used, corresponding to maximum initial ice thicknesses of H_{init} = 4.26 km, 6.38 km, and 8.51 km respectively. The accumulation rate is varied such that the initial ice volume is reproduced in the steady state as accurately as possible.

TABLE 1. Results of steady-state simulation numbers 1–3 with varied ice volume.

No.	V_{init}	H_{init}	S	t_{ss}	V_{ss}	H_{ss}
1	2.00	4.26	0.04	35	2.01	3.27
2	3.00	6.38	0.4	4	3.00	4.67
3	4.00	8.51	3.0	1	3.97	6.42

V_{init}, V_{ss} in 10^6 km³, H_{init}, H_{ss} in km, S in mm WE/yr, t_{ss} in m.y. (quantities are explained in the text).

Table 1 lists V_{init}, H_{init}, S, the time required to reach the steady state, t_{ss}, and the ice volume and the maximum ice thickness in the steady state, V_{ss} and H_{ss}, for the three simulations with optimum accumulation rate to reproduce the initial volume (referred to as simulation numbers 1, 2, and 3 respectively). Evidently, the accumulation rate required to maintain the initial volume varies by 2 orders of magnitude for the three simulations, and it is within the above estimated range of 0.1 . . . 1 mm WE/yr for simulation 2, which is therefore regarded as the most realistic reference simulation. Accordingly, t_{ss} (which is also a measure for the time necessary to build up the ice cap from ice-free initial conditions) varies by 2 orders of magnitude, and it is in any case much larger than for ice sheets on Earth (~100 k.y. for Greenland, see [1]).

Even though V_{init} and V_{ss} agree very well for the three simulations, the corresponding maximum thicknesses H_{init} and H_{ss} differ by about 25%. The reason for this is that the ice flow tends to redistribute

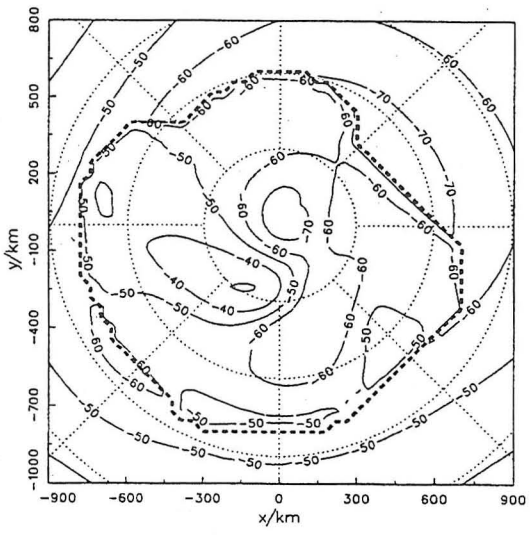

Fig. 1. Basal temperature relative to pressure melting for the steady state of simulation 2, in °C. The dashed heavy line indicates the ice margin, latitude circles are spaced by 5°, and the prime meridian 0°W points downward.

the initial (measured) surface topography with steeper gradients in the interior and flatter slopes toward the margin to a more parabolic shape with the opposite behavior. A reason for this shortcoming may be the tentative use of the terrestrial degree-day parameterization for surface melting/evaporation, which is not likely to describe the surface processes adequately under the very different martian conditions.

The ice-flow velocities are considerably smaller than for terrestrial ice sheets due to the reduced gravity acceleration and the low temperatures. For simulation 1 the maximum surface velocity in steady state is 0.058 m/yr, for simulation 2 it is 0.64 m/yr, and for simulation 3 it is 12.7 m/yr. If even smaller ice volumes/thicknesses than those of simulation 1 were assumed, virtually no ice flow would result, which is not very likely with regard to recent laser altimeter results of the Mars Global Surveyor (MGS) space probe, which have revealed that large parts of the ice cap are very smooth (MGS Press Conference, Spring Meeting of the American Geophysical Union, Boston, 1998), much like the flowing ice sheets on Earth.

It is further noticeable that for none of the three simulations does the basal temperature reach the pressure melting point. Figure 1 depicts the basal temperature (relative to pressure melting) for the reference simulation 2, with the maximum of –29.3°C being reached at 85.3°N, 30.3°W. For simulation 1, the maximum basal temperature is –46.9°C; for simulation 3 it is –4.4°C, already very close to pressure melting.

These results are strongly dependent on the applied areothermal heat flux, which is not very well known. In order to investigate under which circumstances pressure melting can be reached at the ice base, the reference simulation 2 was rerun with larger areothermal heat fluxes, namely 40, 50, 60, and 70 mW/m^2. As a consequence, the maximum basal temperatures rise to –22.4°C, –12.9°C, –4.6°C, and 0°C respectively. Hence, for 70 mW/m^2 pressure melting is reached at the ice base, with an area at pressure melting of 4784 km^2 or 0.34% of the simulated total ice-covered area, and a basal melting rate of 3.3×10^5 m^3 WE/yr.

References: [1] Greve R. (1997) *J. Climate, 10,* 901–918. [2] Greve R. (1997) *J. Glaciol., 43,* 307–310; erratum *43,* 597–600. [3] Calov R. et al. (1998) *Ann. Glaciol., 27,* in press. [4] Greve R. et al. (1998) *Ann. Glaciol., 28,* submitted. [5] Hutter K. (1982) *J. Geophys. Astrophys. Fluid Dyn., 21,* 201–224. [6] Hutter K. (1993) *J. Glaciol., 39,* 65–86. [7] Greve R. (1997) *Philos. Trans. R. Soc. Lond., A355,* 921–974. [8] Dzurisin D. and Blasius K. R. (1975) *JGR, 80,* 3286–3306. [9] Budd W. F. et al. (1986) *Polarforsch., 56,* 43–46.

RADIATIVE PROPERTIES OF THE SEASONAL CARBON DIOXIDE POLAR CAPS ON MARS.

G. B. Hansen, Hawai'i Institute of Geophysics and Planetology, School of Ocean and Earth Science and Technology, University of Hawai'i, 2525 Correa Road, Honolulu HI 96822, USA (ghansen@ pgd.hawaii.edu).

Introduction: I will present the results of two research tasks, one experimental and one theoretical. First, I will present absorption coefficients with error estimates for pure CO_2 ice in the wavelength range 0.17–1.80 μm. These are the products of an experiment where the transmission of large samples of ice with five different thicknesses was measured (preliminary results were presented in [1]). The optical constants from this work can be used in the modeling and analysis of the reflectance of the seasonal polar caps of Mars in this wavelength range. Second, I will present new results from an earlier model of the radiative and thermal properties a sheer layer CO_2 ice cap in the Mars polar night [2]. The improvements will include the use of a "rough" surface, which may serve to reduce the large amount of radiative trapping that occurs in a plane layer due to total internal reflection, and a more realistic (lower) thermal conductivity coefficient for the ice.

Absorption Coefficients of Pure Carbon Dioxide: The transmission of solid CO_2 samples from 1.6 to 107.5 mm thick and measured from $\lambda = 0.17$–1.80 μm will be combined using a technique for estimating the scattered light to estimate the linear absorption coefficients and their uncertainties. Preliminary coefficients, without uncertainties, in this wavelength range have been reported previously [1]. Other determinations of the absorption coefficients of CO_2 ice in this wavelength range include the measurement of a strong, narrow line at 1.435 μm by Fink and Sill (77K) [3] and the measurements from 1–5 μm using several different thicknesses by Quirico and Schmitt (~20 K) [4].

Experiment. The ice samples were grown from a gas at 150 K in a chamber between two CaF_2 windows separated by one of five different thicknesses between 1.6 and 107.5 μm. Their transmission was measured using a Fourier transform spectrometer (FTS, 1.2–1.8 μm) and a grating monochromator (0.17–1.80 μm). The FTS was used with a CaF_2 beamsplitter to cover the range 1.2–5 μm, and both a glow-rod and a tungsten-halogen lamp were used as sources. The monochromator was illuminated with a Xe or D arc-lamp, and the source beam was chopped for synchronous detection. The spectrometer output beams were focused through the sample chamber center using mirror optics. A reference mirror system was constructed to direct the incoming beam around the sample chamber and was used to make reference spectra with both spectrometers to account for source variations. The transmitted flux was collected by a detector, which was connected to a lock-in amplifier (monochromator) or to the FTS. Three detectors were used in the experiment: indium antimonide (0.7–5.5 μm), Si (0.2–1.1 μm), and a photomultiplier tube (0.15–0.30 μm). Three gratings and five order filters were used to cover the wavelengths 0.15–2.40 μm with the monochromator, with typical resolutions of 0.3–0.6 nm. Wavelengths were calibrated by measuring the emission lines from a Hg-A lamp. The FTS was operated with spectral resolutions as fine as 0.5 cm^{-1}. The FTS wavelengths were calibrated by observing the absorption lines from residual water vapor in the FTS enclosure.

Analysis. A technique was developed to estimate the absorption coefficient and its uncertainty using data from several (usually all five) sample thicknesses [5]. The procedure starts with an estimate of the amount of scattering extinction for each thickness, usually ~10%, which is assumed to vary smoothly with wavelength. A minimization procedure is used to refine these estimates into a solution for the absorption coefficients. This results in several solutions with nearly equal likelihood that depend on the initial values. The uncertainty from scattering is determined by varying the initial estimates of scattering over a wide range of values to determine the mean and extrema. The scattering uncertainty is negligible compared to other sources of error where the absorption coefficient exceeds 10 m^{-1}. The FTS data had to be corrected for "alias" spectra and for residual channel fringes from the polished windows of the sample chamber.

Results. Preliminary results (Fig. 1) show that the absorption between the numerous narrow absorption lines of various strengths in this region is very small (≤1 m^{-1}), and absorption even through a path of almost 110 mm of ice was undetectable in the region 0.5–

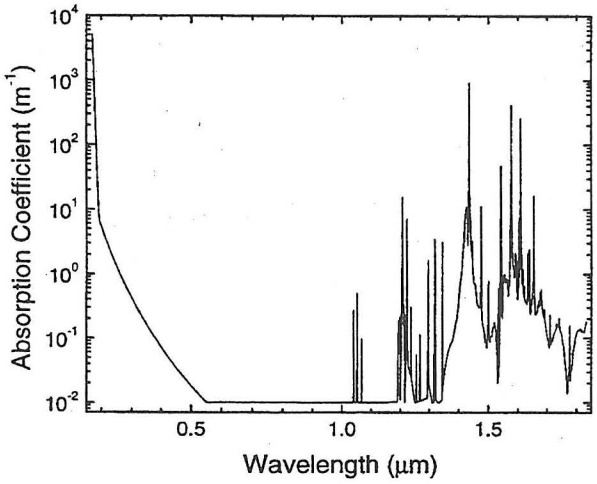

Fig. 1. Preliminary spectral absorption coefficient for pure CO_2 ice from 0.17–1.80 μm [1]. Values below about 1 m^{-1} are estimated upper limits.

1.4 μm, except for a few weak, narrow lines at 1.0–1.4 μm. A recommended (near 0.01 m^{-1}) and maximum upper limit of absorption will be reported for these regions. The ultraviolet absorption edge is smooth, starting around 0.5 μm and increasing strongly below 0.2 μm.

Thermal-Radiative Solid Carbon Dioxide Layer Model: There are many lines of evidence from previous missions, implying that the winter seasonal polar deposits of CO_2 on Mars are composed of grains with a typical size of several cm [6,7], or even a clear (in the visible) monolithic layer [8]. Such a layer would rapidly degrade by cracking into the bright, highly scattering deposits that have been observed as the cap is revealed by sunlight each spring. A model of a plane CO_2 layer was constructed based on this information to predict the polar night infrared spectrum and CO_2 layer temperature structure [2]. Since the ice is transparent in the thermal infrared in the same general regions as the atmosphere, the radiative cooling that must take place to balance the latent heat of the growing cap must predominantly occur at some depth below the surface, depending on the optical properties [5] and thermal structure. The model is iterative, wherein an initial temperature structure is used to calculate a radiative flux profile, which is then used to recalculate the temperature using a one-dimensional heat equation with distributed sources (equal to the flux divergence). The results from this model were that the subsurface cooling takes place only in the top 5–10 cm of the layer, comparable to the average e-folding absorption thickness in the 25-mm window, where a majority of the infrared flux occurs. One problem, however, was that the subsurface could only sink about 9 Wm^{-2}, about half the amount of latent heat required to make the quantity of ice in the polar caps that is consistent with the atmospheric pressure variation [9]. This discrepancy was mainly due to the trapping of all internal radiance at zenith angles more than 45° due to total internal reflection, which also requires remarkably low outgoing radiance, about half of what has been measured by many instruments (approximately a blackbody near the surface temperature). A second model with an ideal nonreflecting upper boundary resulted in an excess subsurface radiative cooling by more than 50%.

Model improvements. The model will be improved by using a rough upper surface which effectively scatters impinging radiation [e.g., 10]. A rough upper boundary of some kind should be able to achieve the required amount of subsurface radiation to space, intermediate between the plane layer and the plane layer with a nonreflecting surface. In fact, the radiative balance should not be strongly dependent on the detailed parameters of the roughness, or this model might be as unrealistic as the other models. This will involve more complicated radiative flux computations than earlier, because the radiance at each angle will not be conserved as before. The previous models also used a too-high thermal conductivity coefficient for the ice, resulting in weak thermal gradients so features in the model emitted spectrum due to the CO_2 were almost undetectable. The use of appropriate coefficients [11] that are an order of magnitude smaller should result in larger gradients and higher thermal contrast in the outgoing spectrum. This can then be compared with present and past thermal infrared measurements of the polar winter on Mars.

References: [1] Hansen G. B. (1997) *Adv. Space Res., 20,* 1613–1616. [2] Hansen G. B. (1997) *Eos Trans. AGU, 78,* F411. [3] Fink U. and Sill G. T. (1982) in *Comets* (L. L. Wilkening, ed.), pp. 164–202, Univ. of Arizona, Tucson. [4] Quirico E. and Schmitt B. (1997) *Icarus, 127,* 354–378. [5] Hansen G. B. (1997) *JGR, 102,* 21569–21587. [6] Calvin W. M. and Martin T. Z. (1994) *JGR, 99,* 21143–21152. [7] Forget F. et al. (1995) *JGR, 100,* 21219–21134. [8] Paige D. A. et al. (1995) *BAAS, 27,* 1098. [9] Wood S. E. and Paige D. A. (1992) *Icarus, 99,* 1–14. [10] Perez Quintian F. et al. (1997) *J. Mod. Optics, 44,* 447–460. [11] Cook T. and Davey G. (1976) *Cryogenics, 16,* 363–369.

EXAMINATION OF THE MOST DIAGNOSTIC SPECTRAL REGIONS FROM VISIBLE THROUGH THERMAL INFRARED FOR POLAR STUDIES OF MARS.

G. B. Hansen[1], L. E. Kirkland[2], W. M. Calvin[3], H. H. Kieffer[3], K. C. Herr[4], and P. B. Forney[5], [1]University of Hawai'i, Honolulu HI, USA (ghansen@pgd.hawaii.edu), [2]Lunar and Planetary Institute and Rice University, Houston TX 77085, USA (kirkland@lpi.jsc.nasa.gov), [3]U.S. Geological Survey, Flagstaff AZ, USA (wcalvin@flagmail.wr.usgs.gov; hkieffer@flagmail.wr.usgs.gov), [4]The Aerospace Corporation, El Segundo CA, USA, [5]Lockheed Martin Missiles and Space, Palo Alto CA, USA (paul.forney@lmco.com).

Introduction: Many outstanding polar questions can be examined using data returned by spacecraft instruments that record either multiband measurements or spectra from visible or infrared wavelengths. Here we discuss which spectral regions provide the most diagnostic information to address the following polar questions: (1) seasonal and perennial ice cap composition; (2) ice grain sizes and/or layer thicknesses; (3) fractional coverage of the ground by ice, and mixtures of ices with dust or soil; (4) radiative balance; (5) non-ice surface composition; and (6) presence and composition of clouds. To make the discussion more manageable, we divide the spectral ranges into four convenient groups: visible only; near-infrared (~0.8–5 μm); thermal infrared (~5–50 μm); and near-through-thermal infrared (~0.8–50 μm).

Datasets: Table 1 summarizes instruments that have returned spectral data from Mars. Near-infrared spectra returned by the 1969 Mariner Infrared Spectrometer (IRS) have been used to examine the composition of the southern polar cap [1], and the 1969 Mariner Infrared Radiometer (IRR) measured the cap temperature [2]. Spectra returned by the 1971 Mariner Mars Infrared Interferometer Spectrometer (IRIS) have been used to model the south residual cap in the

summer [3], and Forget et al. [4] presented a few late winter spectra of the north polar seasonal cap. Data from the two 1976 Viking Infrared Thermal Mappers (IRTM) have been extensively used for radiative balance studies in the polar night [4,5] and other polar process studies [6,7]. Spectra from the Mars Global Surveyor Thermal Emission Spectrometer (TES) are in the early stages of interpretation [8]. Both IRTM and TES have broadband (~0.3–3 μm) solar reflectance channels that can be used for radiative balance studies, but only spectra are useful for understanding the cause of broadband albedo variations.

Limitations of Previous Datasets: Each of the spectral data sets returned thus far has significant limitations. Multichannel radiometers such as IRR, IRTM, and THEMIS (Mars Surveyor 2001) cannot directly provide spectral signatures that can strongly constrain the composition of the surface or ice. For example, it is impossible to use broad-channel infrared data like that of the IRTM to distinguish variations of CO_2 particle size from dust or ice contamination. Instruments that return spectra have the potential to provide much more information. However, IRS returned spectra with very limited spatial and temporal coverage, and low spatial resolution. IRIS had a low signal to noise ratio, and also low spatial resolution. Both IRIS and TES spectra cover only the thermal infrared, and so do not measure the spectral region that is most useful for determining the composition of the surface and ice.

Information from Different Spectral Regions: *Visible (VIS).* Visible wavelength spectra can provide some constraints on the surface composition, but because ices are very transparent in this region, minerals and other opaque materials tend to dominate the reflectance. For thermal balance, VIS is only a part of the reflected energy. A significant portion of reflected or absorbed solar energy occurs in the 1–2.5 μm region, where the properties of the ices can dominate those of minerals.

1 to 5 μm (NIR). Except during the polar night, this is the most important spectral region for determining composition and grain sizes. Both water ice and CO_2 ice have rich spectral structure in this region that is diagnostic of their abundance and grain size. Strong spectral features in this region also make this an important region to use in the analysis of energy balance. For example, the absorption of water ice varies over ~6 orders of magnitude from 1 to 3 μm. Spectral resolutions as fine as ~1 cm^{-1} are needed to resolve many of the narrow CO_2 lines [9]. Paige et al. [10] used IRTM solar and thermal data to show that the autumn seasonal cap is dark and cold, while the spring seasonal cap is bright and cold, and proposed a solid, transparent layer of ice to explain the autumn results. A transparent CO_2 coating will appear strongly in the NIR due to both weak and strong absorptions that would be diagnostic of the layer thickness.

Grain sizes speak to history and age of the deposits. To the extent that age controls the average grain size by processes of sintering, any spectral data that are sensitive to ice grain size are valuable, and the greatest sensitivity is in the NIR. The regions most sensitive for water ice are 1–3(5) μm and for CO_2 ice 1–5(7) μm. Grain sizes are hard to determine from VIS since even small amounts of highly absorptive materials dominate this region, and thermal infrared measurements are also much less diagnostic.

5 to 50 μm. In the thermal infrared, water ice is hard to identify unless the effective grain size is <100 μm. Minerals such as dust tend to be almost featureless in the thermal infrared as well, unless the grain size is very small. This region, however, is the only one useful when observing in the polar night, mainly from 20 to 50 μm, where there is easily measurable flux from the polar regions, and where both CO_2 and water ice (of sufficiently small grain size) can have low emissivity. For quantitative determinations it is important to have a high enough signal-to-noise ratio to get good measurements in the 8–12 μm range, and spectral resolution ≤10 cm^{-1}.

NIR + thermal coverage. Coverage of both the near and thermal infrared can significantly improve the determination of the percent coverage of the ground by ice. For example, when making the determination from the thermal region alone, mixed surface temperatures combined with nonunit emissivity introduce uncertainty into the result. Incorporating information from the NIR should make modeling much more accurate.

TABLE 1. Comparison of Mars spectral instruments.

	1969 IRS	1969 IRR[15]	1971 IRR[16]	1971 IRIS[14]
Wavelength range μm or ch. band ctrs.	1.8–14.4	10;20	10;20	5–50
Spectral resolution	10 cm^{-1}† (1%)	370; 156 cm^{-1}	370; 156 cm^{-1}	2.4 cm^{-1} (0.24%)†
Spatial resolution (km)	130–500	>50 km	15–1000 km	125–1000
rms SNR: 2.2 μm	~190			—
rms SNR: 10 μm, 270 K	~600			~110[11]
measurements*	1340	2	2	1500
	1976 IRTM[11]	1997 TES[11]	2001 THEMIS	
Wavelength range μm or ch. band ctrs.	7;9;11;15;20	6.5–50	6.5–14	
Spectral resolution	140–1400 cm^{-1}	5 or 10 cm^{-1} (0.5 or 1%)		
Spatial resolution (km)	30–40	3		
rms SNR: 2.2 μm	—	—		
rms SNR: 10 μm, 270 K	~200	~400		
measurements*	5	286 or 143[12]	10	

* Number of measurements per spectrum, or number of channels.
† At 10 μm; SNR = signal to noise ratio; ch = channels.

TABLE 2. Information from each spectral region.

Spectral Region	Compositional Information	Mixture Information CO_2 + Water Ice + Dust	Ice History and Age from Grain Size
VIS	Can provide some constraints on dark materials	Can quantify and identify dark materials (dust, etc.)	Very large water grains detectable in silicon NIR (<1.1 μm)
NIR	Most important region except during polar night	Most important region except during polar night	Most important region except during polar night
Thermal	Weak but possible; most materials are very dark	Weak but possible; most materials are very dark (~blackbody)	For finest grain size
NIR + thermal	Thermal constraints NIR information	Thermal constraints NIR information	good
Spectral	% Coverage of Ground by Ice	CO_2 Clouds (Limb Scans)	Energy Balance
VIS	Vs. soil; water and CO_2 not distinct	Cannot tell water from CO_2 ice	some
NIR	good	4.3 mm spike (day only)	important
Thermal	good (under solar heating)	15 μm band (but atm complications)	some
NIR + thermal	best	high probability of identification	good

Carbon dioxide ice clouds may be measurable at 15 μm using limb scans, if the clouds are high enough to see them through the atmospheric 15-μm band. During daylight limb scans, the 4.3-μm reflection spike provides a unique signature of CO_2 clouds. The optical depths are probably too small to see them other than on the limb, except for thick clouds in the winter night, which tend to be indistinguishable from surface snow in the thermal infrared [4].

References: [1] Calvin W. M. and Martin T. Z., (1994) *JGR, 99,* 21143–21152. [2] Neugebauer et al. (1971) *Astron. J., 76,* 719–728. [3] Paige D. A. et al. (1990) *JGR, 95,* 1319–1335. [4] Forget F. et al. (1995) *JGR, 100,* 21219–21134. [5] Paige D. A. and Ingersoll A. P. (1985) *Science, 228,* 1160–1168. [6] Kieffer H. H. (1990) *JGR, 95,* 1481–1483. [7] Christensen P. R. and Zurek R. W. (1984) *JGR, 89,* 4587–4596. [8] Christensen P. R. et al. (1998) *Science, 279,* 1692–1698. [9] Hansen G. B. (1997) *Adv. Space Res., 20,* 1613–1616. [10] Paige D. A. et al. (1995) *BAAS, 27,* 1098. [11] Christensen P. R. (1998) *JGR, 103,* 1733. [12] Christensen P. R. et al. (1992) *JGR, 97,* 7719. [13] Erard S. (1995) *Technical Help for ISM Investigators,* unpublished. [14] Hanel R. et al. (1973) *NASA TM-X-70504.* [15] Neugebauer G. et al. (1969) *NASA SP-225,* 105. [16] Kieffer H. H. et al. (1973) *JPL Tech. Rept. 32-1550, vol. 4,* 314.

IN SITU ATMOSPHERIC PRESSURE MEASUREMENTS IN THE MARTIAN SOUTHERN POLAR REGION: MARS VOLATILES AND CLIMATE SURVEYOR METEOROLOGY PACKAGE ON THE MARS POLAR LANDER.

A.-M. Harri[1], J. Polkko[1], T. Siili[1], and D. Crisp[2], [1]Geophysical Research Division, Finnish Meteorological Institute, P.O. Box 503, FIN-00101 Helsinki, Finland, Ari-Matti.Harri@fmi.fi), [2]Jet Propulsion Laboratory, 4800 Oak Grove Drive, Pasadena CA 91109, USA.

Introduction: Pressure observations are crucial for the success of the Mars Volatiles and Climate Surveyor (MVACS) Meteorology (MET) package onboard the Mars Polar Lander (MPL), due for launch early next year. The spacecraft is expected to land in December 1999 ($L_s \approx 256°$) at a high southern latitude (74°–78°S). The nominal period of operation is 90 sols but may last up to 210 sols. The MVACS/MET experiment will provide the first *in situ* observations of atmospheric pressure, temperature, wind, and humidity in the southern hemisphere of Mars and in the polar regions.

The martian atmosphere goes through a large-scale atmospheric pressure cycle due to the annual condensation/sublimation of the atmospheric CO_2. Pressure also exhibits short period variations associated with dust storms, tides, and other atmospheric events. A series of pressure measurements can hence provide us with information on the large-scale state and dynamics of the atmosphere, including the CO_2 and dust cycles as well as local weather phenomena. The measurements can also shed light on the shorter time scale phenomena (e.g., passage of dust devils) and hence be important in contributing to our understanding of mixing and transport of heat, dust, and water vapor.

Sensors — Their Heritage and Applications: The sensing element of the MET-P will comprise four Barocap radiosonde sensors manufactured by the Vaisala Inc. These sensors were space qualified for the Mars-96 Small Stations and Penetrators. Similar sensors are currently onboard the Huygens probe as part of the atmospheric structure instrument to measure atmospheric pressure during the probe descent. Designs based on the same sensors have also been proposed for future Mars Surveyor landers as well as the European surface network mission (NetLander).

The characteristics of the seasonal and shorter-term pressure variations anticipated to take place place at the MPL landing site, the design of the MET-P instrument, and the predicted performance thereof are discussed.

GEOLOGY, COMPOSITION, AGE, AND STRATIGRAPHY OF THE POLAR LAYERED DEPOSITS ON MARS.

K. E. Herkenhoff, Astrogeology Team, U.S. Geological Survey, 2255 North Gemini Drive, Flagstaff AZ 86001, USA.

It is widely believed that the martian polar layered deposits record climate variations over at least the last 100 m.y. [1–8], but the details of the processes involved and their relative roles in layer formation and evolution remain obscure [9]. Variations in axial obliquity and orbital eccentricity are thought to influence the climates of both Earth and Mars, but are of greater amplitude in the martian case. The Earth's hydrosphere and biosphere do not have a current counterpart on Mars, so it should be simpler to determine the causes and history of climate changes on Mars. Knowledge of the geology of the martian polar deposits is essential in deducing the processes responsible for their formation and erosion and the mechanisms by which climatic variations are preserved.

A common presumption among Mars researchers is that the layered deposits are the result of variations in the proportions of dust and water ice deposited over many climate cycles [3–5], but their composition is poorly constrained in the north [10] and essentially unknown in the south. Malin (1986) estimated that the density of the northern deposits is 1 g cm^{-3}, suggesting that they are mostly ices. However, the topography and therefore volume of the north polar layered deposits is poorly known, and the uncertainty of 50% [10] allows for up to 50% dust. The lack of observed flow features in the layered deposits indicates that glacial flow has not recently occurred, implying that the layered deposits are either less than 40% water ice by volume or nearly pure water ice [11].

Calculations of the stability of water ice in the polar regions of Mars [5,11,12] indicate that interstitial ice is not currently stable at the surface of the layered deposits. The present water ice sublimation rate is high enough to erode the entire thickness of the deposits in about a million years. This result suggests that sublimation of water ice from the layered deposits results in concentration of nonvolatile material at the surface of the deposits. Such a lag deposit would insulate underlying water ice from further sublimation, stabilizing the layered deposits against rapid erosion. The existence of a stable, competent layer is indicated by slopes of up to 20° in exposures of the south polar layered deposits [13]. The color and albedo of the layered deposits suggest that bright, red dust is the major nonvolatile component of the deposits, and the association of dark saltating material indicates that there is at least a minor component of dark material in the deposits [14,15]. The albedo of the layered deposits does not necessarily indicate that an insulating dust layer is present, as the observed albedo only constrains the fraction of dust at the surface to be greater than 0.1% by mass if mixed with water ice grains that have radii of 0.1 mm or larger [16]. The existence of a lag deposit at least a few millimeters thick is more strongly supported by the low apparent thermal inertia of the surface of the south polar layered deposits [17]. However, a similar thermal-inertia mapping study of the north

polar region indicates that water ice is present near the surface of the north polar layered deposits and sublimes into the atmosphere [18]. Hence, it appears that while the present erosion rate of the south polar layered deposits is low, the north polar layered deposits (at least in some areas) are currently being eroded by ice sublimation. These inferences have important implications for the present water budget on Mars, and are consistent with estimates of the relative surface ages of the north and south polar layered deposits.

Using medium-resolution Viking imagery, Plaut et al. [8] found several craters in the southern layered deposits. In contrast, Cutts et al. [2] found no fresh impact craters larger than about 300 m in summertime images of the north polar layered deposits. Recent study of high-resolution springtime images confirms the lack of impact craters larger than 100-m diameter over most of the north polar layered terrain [19]. Clearly, the surface of the north polar layered deposits is much younger than that of the south polar layered deposits. Hence, erosional and/or depositional processes have been more active recently in the north polar region than in the south. The greater extent of eolian erosional features in the south polar layered terrain may be evidence that gradual erosive processes (such as eolian abrasion) have been more important than rapid ice sublimation in the evolution of the south polar layered deposits. Furthermore, the inferred average surface age of the south polar layered deposits (at least 10^8 yr) [8] is much longer than the timescales of theoretical orbital/axial variations (10^5–10^6 yr) [20]. At least some areas of the south polar layered terrain have therefore not been greatly modified by global climate changes over the last 100 m.y. or so.

Layering has been exposed by erosion of gently sloping trough walls in both polar regions [7,13]. It appears that erosion occurs mainly on equatorward-facing slopes of these troughs, while poleward-facing slopes are undergoing deposition aided by the presence of perennial frost [4,7]. These processes result in poleward migration of topographic troughs, as indicated by stratigraphic relations exposed in trough junctions [7]. Individual layers are visible due both to terraced topography and albedo variations caused by differential frost retention [1,13,21]. Layer thicknesses of 14–46 m have been resolved in the north polar layered deposits [21]; lower image resolution in the south polar region has allowed recognition of layer thicknesses of no less than 100 m there [13]. Angular unconformities, indicative of a complex history of erosion and deposition, have been recognized in the north polar layered deposits [2,3] but not in the south.

Howard et al. [7] found steep (20°–30°), arcuate scarps eroded into the north polar layered deposits. These scarps are a few hundred meters high and appear to be sources of the dark material that forms dunes nearby [14]. The dark material must be a minor component of the layered deposits to explain the significant difference in color and albedo between the dark dunes and the bright red layered deposits [15]. If the dark material is sand sized, it must have been transported into the polar regions by saltation, and the atmospheric circulation must have been different from that inferred from extant wind indicators [22]. Viking infrared thermal mapping (IRTM) and bistatic radar data suggest that the bulk density of the erg material is much lower than that of the average martian surface or of dark dunes at lower latitudes [23]. These data are consistent with the dark material being composed of filamentary sublimate residue (FSR) particles derived from erosion of the layered deposits. The uniqueness of the thermophysical properties of the north polar erg material may be due to a unique polar process that has created them. The visible and near-infrared spectral reflectance of the erg suggests that the dark material may be composed of low-density aggregates of basalt or ferrous clays. Dark dust may be preferentially concentrated at the surface of the layered deposits by the formation of FSR particles upon sublimation of water ice. Further weathering and erosion of these areas of exposed layered deposits may form the dark, saltating material that is found in both polar regions. The dark FSR particles could saltate for great distances before eventually breaking down into dust grains, remixing with the global dust reservoir, and being recycled into the polar layered deposits via atmospheric suspension. Although the south polar layered deposits may be the source of dark, saltating material in the southern hemisphere, the recognition of source regions is hindered by the lack of high-resolution images [14]. Steep scarps have been found in the southern layered deposits [24], but they do not currently appear to be the source of dark saltating material as in the north polar region.

Analysis of new orbital observations of the martian polar regions from the Mars Global Surveyor and surface exploration by the Mars Volatiles and Climate Surveyor will greatly enhance our understanding of the polar layered deposits and the climate changes they record.

References: [1] Murray B. C. et al. (1972) *Icarus, 17,* 328–345. [2] Cutts J. A. et al. (1976) *Science, 194,* 1329–1337. [3] Cutts J. A. et al. (1979) *JGR, 84,* 2975–2994. [4] Squyres S. W. (1979) *Icarus, 40,* 244–261. [5] Toon O. B. et al. (1980) *Icarus, 44,* 552–607. [6] Carr M. H. (1982) *Icarus, 50,* 129–139. [7] Howard A. D. et al. (1982) *Icarus, 50,* 161–215. [8] Plaut J. J. et al. (1988) *Icarus, 76,* 357–377. [9] Thomas P. et al. (1992) in *Mars,* pp. 767–795, Univ. of Arizona, Tucson. [10] Malin M. C. (1986) *GRL, 13,* 444–447. [11] Hofstadter M. D. and Murray B. C. (1990) *Icarus, 84,* 352–361. [12] Paige D. A. (1992) *Nature, 356,* 43–45. [13] Herkenhoff K. E. and Murray B. C. (1990) *JGR, 95,* 14511–14529. [14] Thomas P. C. and Weitz C.(1989) *Icarus, 81,* 185–215. [15] Herkenhoff K. E. and Murray B. C. (1990) *JGR, 95,* 1343–1358. [16] Kieffer H. H. (1990) *JGR, 95,* 1481–1493. [17] Paige D. A. and Keegan K. D. (1994) *JGR, 99,* 25993–26031.[18] Paige D. A. et al. (1994) *JGR, 99,* 25959–25991.[19] Herkenhoff K. E. et al. (1997) *LPS XXVIII,* 551–552.[20] Kieffer H. H. and Zent A. P. (1992) in *Mars,* pp. 1180–1218, Univ. of Arizona, Tucson. [21] Blasius et al. (1982) *Icarus, 50,* 140–160. [22] Thomas P. (1982) *JGR, 87,* 9999–10008. [23] Herkenhoff K. E. and Vasavada A. R. (1998) *JGR,* submitted. [24] Herkenhoff K. E. (1998) *Geologic Map of the MTM-85280 Quadrangle Planum Australe Region of Mars,* U.S. Geol. Surv. Misc. Invest. Ser. Map, in press.

THE ROLE OF EOLIAN PROCESSES IN FORMING MARTIAN POLAR TOPOGRAPHY.

A. D. Howard, Department of Environmental Sciences, University of Virginia, Charlottesville VA 22903, USA (ah6p@viriginia.edu).

Introduction: The major topographic features of the martian polar layered deposits include the conspicuous spiral troughs, subtle undulations, broad reentrants (chasma) and steep, arcuate scarps, and dune fields [1–3]. A prominent role for eolian processes in formation of all these features is suggested here.

Nature of Polar Cap Winds: The polar layered terrain underlies broad domes centered approximately at the geographic poles. Because of the domal topography and the cold surface temperatures, a stable dense surface layer probably characterizes the boundary

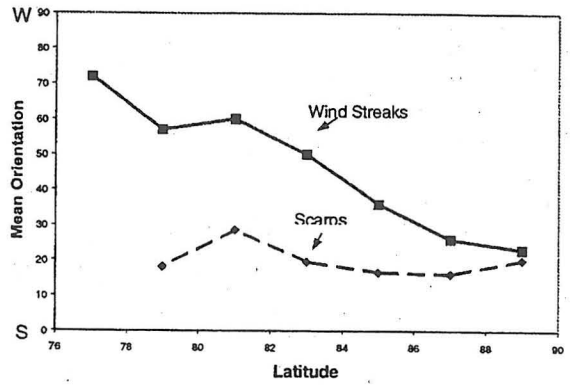

Fig. 1. Orientation of wind streaks and scarps exposing layered terrain on the martian north polar layered deposits. Scarp orientation is the azimuth of dip of the scarp, and orientations are measured as degrees west of south [4].

layer much of the time. By analogy with the terrestrial Antarctic [5–7], strong off-polar katabatic winds presumably occur at least seasonally. Such winds trend down the regional gradient but are deflected by Coriolis forces. Wind streaks mapped on the martian north polar cap follow such a pattern, with a westward deflection of about 60 degrees at 80°N latitude (Fig. 1 and [4]). Katabatic winds on the slopes of the Antarctic polar cap are capable of transporting snow, and the wind streaks on the martian caps indicate that the CO_2-H_2O seasonal frosts can likewise be transported. Maximum velocities of katabatic winds on the terrestrial polar caps are enhanced by episodic build-up and then draining of surface pools of cold air, and a similar phenomenon may occur on Mars. The following section discusses the role that these winds may play in the evolution of polar landforms.

Wavelike Undulations: Shallow wavelike undulations with wavelengths ~10 km and crest lengths commonly exceeding 50 km occur locally on the north polar cap [1,3]. Where they occur, they are conformable in orientation and phase with nearby troughs. The vertical relief of these waves is uncertain, but maximum gradients are probably less than 1°. Locally the troughs exhibit an "interference" pattern between two sets of undulations with slightly different orientations. The wavelike pattern and local interference patterns suggest that they may be due to interactions between the katabatic winds and either eolian transport of volatiles and dust (i.e., they are low relief bedforms) or are an interaction between the wind and ablational processes. The conformable direction and phasing with nearby troughs suggest two possibilities: (1) the boundary layer waves creating the undulations are set up by interaction with existing troughs, or (2) the troughs are formed when certain undulations become steep enough for differential ablation on south facing slopes [1,8].

"Spiral" Troughs: The prominent polar troughs are spaced 20 to 70 km apart and may extend hundreds of kilometers. Trough widths are ~20–30 km and maximum slope gradients are probably a few degrees[9–11]. During the summer they become defrosted on their equator-facing slopes, exposing numerous layers. Differential ablation and erosion on the Sun-facing trough margin is thought to be responsible for exposure of the layers [1,8]. Wind may play both direct and indirect roles in the creation and maintenance of the troughs. An indirect role would pertain if the wavelike undulations act as "seeds" for trough formation, as suggested above. In addition, for ablation to have persisted long enough to expose numerous layers on equator-facing slopes, the wind strength must have been great enough to remove accumulated dust released from ablation of the layered deposits. The possibility also exists that katabatic wind speeds on the equator-facing slopes become strong enough to directly entrain layered terrain materials; wind speeds on the north polar cap have been strong enough locally to cause broad-scale stripping of the layered terrain, forming "striped" terrain [1]. The orientation of troughs is intermediate between equatorward (the direction where solar radiation is maximized) and the orientation of wind streaks (Fig. 1), suggesting that both wind and ablation play roles in shaping the troughs. A suggestion that glacial flow plays a large role in creation of the troughs [12] is not concordant with either stratigraphic evidence [1] or probable ice rheology [13].

Polar Chasma: Each polar cap features one broad reentrant valley that extends several hundred kilometers into the polar cap and is about 150–200 km across. In addition, a number of shorter and shallower reentrants occur near the edges of each polar cap.

A number of formative mechanisms have been suggested for these chasma, including wind erosion [1,8] and erosion by meltwater (jokulhlaups) [14,15]. The eolian model suggests that chance irregularities attracted katabatic flows to low areas, causing enhanced erosion and further deepening, and eventually forming the chasma. Wind streaks converge into the chasma [8], and the troughs are deflected into near-parallelism with the chasma where they extend onto the laterals walls of the chasma. In addition, steep arcuate scarps of probable eolian erosion origin (see below) with associated dune fields occur in these chasma. All these features suggest that wind erosion may be a sufficient explanation for the chasma.

Steep, Arcuate Scarps: Locally near the equatorward edge of the polar deposits the slopes exposing the layered terrain have been eroded into steep scarps, generally with scooplike planforms. The gradient of these scarps may approach 30°. They are preferentially located within the chasma and other broad depressions in the layered deposits. Dune fields frequently occur just downwind of the scarps. An origin of the steep scarps by wind erosion has been suggested [1,16].

Dune Fields: The origin of the prominent band of dune fields surrounding the north polar layered deposits has remained an enigma [3, 16–20]. Seasonal wind patterns serve to constrain the dunes within their latitudinal belt [16–19]. Wind erosion of the polar layered deposits is an obvious candidate source for the dunes based upon proximity. Also suggesting an origin from erosion of the polar deposits are the dune fields within the chasma reentrants that appear to be migrating outward (equatorward) from the arcuate scarps. A potential stumbling block to this explanation is that the dunes are composed of darker material than the exposed layered deposits. However, the wind-eroded dust may become clumped into low-density, dark aggregates to form the dune field [16,19,20].

Conclusions: Eolian processes combined with differential ablation are postulated here to be sufficient explanation for the development of the major topographic features of the martian polar caps. Basal melting [21] and broad glacial flow [12,13] may limit total relief and provide a control on the large-scale form of the polar deposits, but glacial flow and meltwater are not required to explain the origin of the undulations, troughs, and chasma.

References: [1] Howard A. D. et al. (1982) *Icarus, 50,* 161–215. [2] Thomas P. et al. (1992) in *Mars,* pp. 767–795, Univ. of Arizona, Tucson. [3] Cutts J. A. et al. (1976) *Science, 194,* 1329–

1337. [4] Howard A. D. (1980) *NASA TM 82835,* 333–335. [5] Parish T. R. (1984) *Mon. Weather Rev., 112,* 545–554. [6] Parish T. R. (1988) *Rev. Geophys., 26,* 169–180. [7] Parish T. R. and Bromwich D. H. (1986) *Mon. Weather Rev., 114,* 849–860. [8] Howard A. D. (1978) *Icarus, 34,* 581–599. [9] Blasius K. R. et al., (1982) *Icarus, 50,* 140–160. [10] Howard A. D. et al. (1982) *Icarus, 50,* 245–258. [11] Herkenhoff K. E. and Murray B. C. (1990) *JGR, 95,* 14511–14529. [12] Weijermars R. (1986) *EPSL, 76,* 227–240. [13] Fisher D. A. (1993) *Icarus, 105,* 501–511. [14] Clifford S. M. (1980) *Bull. AAS, 12,* 678. [15] Benito G. et al. (1997) *Icarus, 129,* 528–538. [16] Thomas P. and Weitz C. (1989) *Icarus, 81,* 185–215. [17] Lancaster N. and Greeley R. (1990) *JGR, 95,* 10921–10927. [18] Tsoar H. et al. (1979) *JGR, 84,* 8167–8180. [19] Thomas P. C. and Gierasch P. J. (1995) *JGR, 100,* 5397–5406. [20] Herkenhoff K. E. and Vasavada A. R. (1988) *JGR,* submitted. [21] Clifford S. M. (1987) *JGR, 92,* 9135–9152.

A COMPARISON OF THE PERMANENT POLAR CAPS OF EARTH AND MARS.

A. P. Kapitsa[1], A. A. Loukashov[2], and A. G. Marchenko[2], [1]Department of Environmental Management, Faculty of Geography, Moscow State University, Vorobievy Gory, Moscow 119899, Russia (kapitsa@env.geogr.msu.su), [2]Department of Geomorphology and Paleogeography, Faculty of Geography, Moscow State University, Vorobievy Gory, Moscow 119899, Russia (root@morpho.geogr.msu.su).

Introduction: The Mars polar caps have an area comparable to that of the Earth's polar ice sheets. However, unlike the terrestrial ice caps, the martian polar caps consist of H_2O and CO_2/H_2O(?) ices on thick layered (H_2O + silt + sand) deposits [6,10]. Terrestrial and martian polar caps are significantly different in composition, stratigraphy, and age, although on both planets the volatiles originate from the atmospheres.

Age and Dynamics of the Caps: The presence of the ice sheets on Earth is a temporary event in geologic history marking the ice ages. The modern ice sheets are several million years old, and the Antarctic sheet is probably 10–20 m.y. old. In contrast, it has been suggested that the martian polar caps may be hundreds of millions years old [2, 7], or even a few billion years old [3, 4]. The dynamics of the terrestrial polar sheets is manifested by changes in their volume. On Mars, the periodic change of accumulation/ablation/erosion conditions cause the formation of layers [10].

A Terrestrial Subice Lake: Under about 3.7 km of the ice sheet of Antarctica, a large deep freshwater lake has been found [5,9]. This subice lake probably occupies a rift valley (Fig. 1). Water is 125 m or more deep, and the lake is comparable in dimensions to Lake Ontario. The residence time of the water in the lake is on the order of tens of thousands of years, and the mean age of water, since deposition as surface ice, is about 1 m.y. [5]. Steady-state theory [8,11] predicts basal melting of ~1 mm/yr for the ice sheet above this lake.

Conclusion: Geothermal basal melting has also been proposed for martian polar caps [1]. Taking into account some evidence of riftogenesis in polar regions of Mars, it is possible that similar lakes may exist here too, although they would likely consist of water and fine sediments from layered deposits.

References: [1] Clifford S. M. (1988) *NASA CP 10021,* 36–38. [2] Cutts J. A. et al. (1976) *Science, 194,* 1329–1337. [3] Fanale F. P. et al. (1982) *Icarus, 50,* 381–407. [4] Fanale F. P. et al. (1986) *Icarus, 67,* 1–18. [5] Kapitsa A. P. et al. (1996) *Nature, 381,* 684–686. [6] Malin M. C. (1986) *GRL, 13,* 444–447. [7] Pollack J. B. et al. (1979) *JGR, 84,* 2929–2945. [8] Robin G. de Q. (1955) *J. Glaciol., 2,* 523–532. [9] Robin G. de Q. et al. (1977) *Philos. Trans. R. Soc. Lond., B 179,* 185–196. [10] Thomas P. et al. (1992) in *Mars,* pp. 767–795, Univ. of Arizona, Tucson. [11] Zoticov I. A. (1961) *Academy of Sciences, USSR, Interdepartmental Comission on Antarctic Research, Commission Reports,* 22–36.

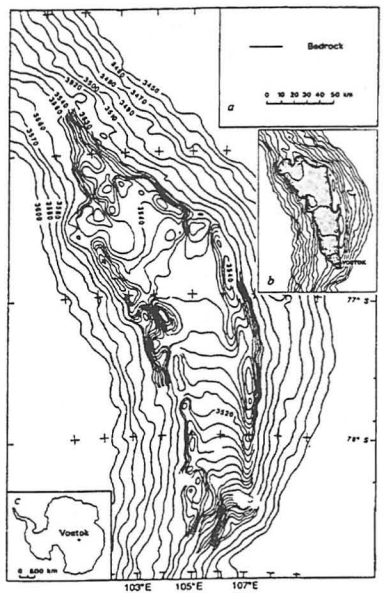

Fig. 1. (a) Surface topography, (b) the subice lake's extension, and (c) its location in Antarctica. Modified from [5].

ORIGINS AND MORPHOLOGY OF SIMILAR LANDFORMS IN TERRESTRIAL AND MARTIAN POLAR REGIONS.

A. P. Kapitsa[1], A. A. Loukashov[2], and A. G. Marchenko[2], [1]Department of Environmental Management, Faculty of Geography, Moscow State University, Vorobievy Gory, Moscow, 119899, Russia (kapitsa@ env.geogr.msu.su), [2]Department of Geomorphology and Paleogeography, Faculty of Geography, Moscow State University, Vorobievy Gory, Moscow, 119899, Russia (root@ morpho.geogr.msu.su).

Introduction: The comparison between the geology and geomorphology of terrains near the polar caps of Mars and Earth is a difficult task. The contemporaneous ice sheets and caps of Antarctica and the Arctic islands are surrounded either by water or by mountains. However, giant Pleistocene ice sheets formed the distinctive complexes of landforms and deposits over a much larger area. It is possible to find distant analogs between landforms in martian polar layered deposits and adjacent terrains, in regions of modern and relic terrestrial periglacial landforms.

Ice-rich Silt Deposits: Ice-rich silt deposits in the Arctic are widespread and form smooth plains easily eroded by water (Fig. 1). Their thickness reaches 80–100 m in northern Asia [13]. Several hypotheses (niveo-eolian, fluvial, fluvioglacial, and thermokarst)

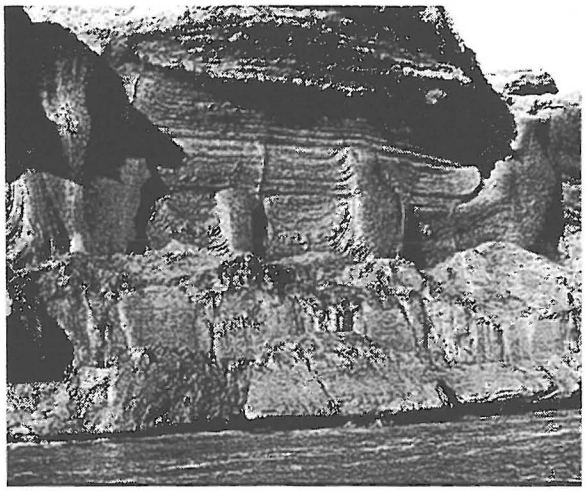

Fig. 1. The ice-rich silt deposits with ice wedges on Bolshoj Lyahovsky island (74°N, 142°E). Photo by M. Grigoriev.

have been proposed by different authors to explain the formation of these deposits. If the niveo-eolian hypothesis is correct, then these terrestrial plains could be analogous to martian terrains, which are thought to consist of layered deposits (silt + sand + ice) [6,10].

Dunes: There are landforms and deposits of a distinct niveo-eolian origin on Earth that can be compared to martian ones [4]. Large dunes of different kinds are known to consist of ice-cemented sand and snow layers on Earth. In the Antarctic dry valleys, dunes 100 m long and up to 13 m high form an erg (S. M. Myagkov, personal communication, and [12]). There are barchanoid and transverse ridges in this area. The dunes in Thelon Basin (Canada) are even taller — up to 24 m [2]. The fact that there are many ventifacts near the boundary of Antarctic ice sheet also shows that the eolian processes are active here.

Eolian dunes are much more common for the polar regions of Mars than on Earth. Studies of these reveal recent (within the past several million years) to modern eolian activity [7–9,11].

Although there is evidence of dunes forming out of material from the polar layered deposits eroded by wind [9], transverse ridges in the bell-shaped dilation of Chasma Boreale remain giant current ripples analogous to those in terrestrial catastrophic outflows, described in [1,3], only much larger. If this is the case, then it is possible that the catastrophic outflow could have been caused by sudden melting of ice (e.g., after an asteroidal impact).

Conclusion: Martian polar terrains consist of silt and sand cemented by volatiles [5,6] similar to the niveo-eolian complexes of the Arctic and Antarctic. Both are probably formed by wind action and precipitation. So such geologically young landforms as ice-rich silt plains and niveo-eolian dunes of polar regions of the Earth may be distant embrional analogs of thick martian polar complexes forming for a long time.

References: [1] Baker V. (1982) *The Channels of Mars,* Univ. of Texas, Austin, 197 pp. [2] Bird J. B. (1951) *Geog. Bull. I,* 14–29. [3] Butvilovsky V. V. (1993) *Paleogeography of the last Glaciation and Holocene of Altay (in Russian),* Tomsk Univ., Tomsk, 253 pp. [4] Cailleux A. (1972) *Cahiers Geog. Quebec 16(39),* 377–409. [5] Condit C. D. and Soderblom L. A. (1978) *USGS Map I-1076 (MC-30).* [6] Malin M. C. (1986) *GRL, 13,* 444–447. [7] Marchenko A. G. et al. (1996) *Space Planet. Sci., 14,* C792. [8] Marchenko A. G. et al. (1997) *LPS XXVIII,* 867–868. [9] Thomas P. C. (1988) *NASA Conference Publication 10021,* 32–34. [10] Thomas P. C. and Weitz C. (1989) *Icarus, 81,* 185–215. [11] Tsoar H. et al. (1979) *JGR, 84,* 8167–8180. [12] Webb P. N. and McKelvey B. D. (1959) *New Zealand J. Geol. Geophys., 2,* 120–36. [13] Yershov E. D. et al. (1987) *Petrography of Frozen Rock (in Russian),* Moscow Univ., Moscow, 311 pp.

POSSIBLE COMPOSITION OF MARTIAN POLAR CAPS AND CONTROLS ON ICE-CAP BEHAVIOR.

J. S. Kargel, U.S. Geological Survey, 2255 North Gemini Drive, Flagstaff AZ 86001, USA.

David Fisher [1] asked "if martian polar caps flow." Are martian polar caps akin to Earth's polar glacial ice sheets, or are they immobile? Though certain dynamical differences are obvious, it is unknown whether similarities in ice tectonics may also exist. The question bears not only on modern martian polar processes, but perhaps on hypothesized glacial processes elsewhere on Mars in the geologic past. The rheological properties and tectonics of martian polar caps also pertain to the possibility that liquids may have existed beneath the polar caps in the past, or even now [2], and to prospects for life in possible lakes beneath the ice caps. The cold martian polar surface temperatures and the lower martian gravity suggest a reduced propensity of martian polar ice deposits to deform under their own weight. The greater accumulation timescales of the martian polar caps [3] compared to Earth's also mean that more time has been available for accumulated deformation, possibly offsetting the effects of colder temperatures and lower gravity on Mars. Further complicating our understanding is that the martian polar caps may not be made purely of ordinary water ice — CO_2 is another possible major constituent; the rheological and melting behavior may be very different from what we are accustomed to dealing with on Earth.

Mars Global Surveyor's laser altimeter (MOLA) data for the northern polar region have imposed new constraints on physical models of the northern polar cap — chiefly that the ice thickness reaches a maximum of ~3 km (http://ltpwww.gsfc.nasa.gov/tharsis/mola.html). These new data are reassuringly similar to rougher knowledge of topography given by Viking-era data [3]. MOLA data have not been acquired over the southern polar cap, but Viking-era data suggest a comparable ice thickness. These results are used as inputs to thermal models of the martian polar caps. Four compositions are modeled, including pure H_2O, pure CO_2, CO_2 clathrate hydrate ("hydrate"), and interlayered water ice and hydrate. Hydrate is considered a likely cap-forming substance because, as widely pointed out at least for the current-epoch south polar cap [4–11], hydrate is more thermodynamically stable than water ice plus "dry ice" at prevailing south polar temperatures [12]. In the fourth (newest) model, the layering is produced by climatic oscillations due to orbital precession and cyclic variations in inclination [3,13,14]. The disparate thermal conductivities of ice and hydrate produce huge differences in the models' thermal gradients and basal temperatures [15]. These differences as well as the differing rheologies of hydrate and water ice [16] might produce distinctive tendencies for or styles of deformation. Chief new results of the models and possible tendencies (not yet modeled in detail) include the following:

Model 1. If made mainly of water ice, the polar caps are far below the pressure-melting curve of H_2O even at their bases. Their rheological stiffness might make them unlikely to have undergone significant plastic deformation, unless they are billions of years old, i.e., older than thought. If composed of water ice, the polar caps probably are static, mass-limited condensate piles subject only to sublimation and wind erosion.

Model 2. If made of CO_2 hydrate, extensive solid-state deformation is possible, and basal dissociation with local formation of two immiscible liquid phases is probable. In areas where basal melting occurs (generally where cap thickness is >2–2.5 km), regions of zero basal shear stress and almost no surface relief are expected. A state near glacial equilibrium (a balance at each point on the ice cap between accumulation and losses due to horizontal flow, basal melting and expulsion of liquid, and surface sublimation) is possible. However, the actual ice sheets, like most glaciers on Earth, may oscillate widely around equilibrium due to episodic perturbations (such as episodic liquid outflow or solid-state surge events, and changes in accumulation or sublimation).

Model 3. If made of interlayered CO_2 hydrate and water ice (for which I have a weak preference for both polar caps), a state at or approaching the melting point of water ice is expected near the base of the polar cap. Gravitationally driven solid-state deformation conceivably might occur in two greatly differing styles (or not at all) — either glacier-like transport or salt dome-type diapirism; however, the somewhat stiffer rheology of hydrate compared to water ice could hinder deformation in favor of more extensive basal melting.

Model 4. If made primarily of CO_2 ice (least favored for both polar caps), widespread basal melting is assured in areas where thickness >1 km. But the polar caps probably could not sustain the observed relief and thickness near the edges of the polar caps.

Global Surveyor images of the polar regions soon may offer new clues as to polar processes and ice composition. Possible future observations and inferences are: If no imaging evidence for either deformation or fluid outflow — favors model "1"; if large expanses of virtually no surface relief — basal lakes, models "2" or "3"; if evidence for explosive fluid outflows — models "2" or "3"; if evidence for solid-state diapirism, tectonic doming — model "3" or possibly "2"; and if evidence for extensive horizontal ice flow — model "2" or possibly "3."

Existing MOLA and Viking-era topographic data show polar caps 3 km thick, arguing against model "4," since a thick polar cap of dry ice would most likely have to contain a very deep and probably physically unstable lake of liquid CO_2; however, a possibility is that the hydraulic conductivity of the substrate allows basal flow at a rate sufficient to remove all the liquid. In any event, any liquids beneath the martian polar caps are almost certainly CO_2 rich; if aqueous, they would be solutions of carbonic acid. This possibility has implications for rock weathering (probably extensive) and biological potential. The possible periodic expulsion of basal liquids could produce eskers (glacier-deposited ridges of sand and gravel); either episodic expulsion or steady basal flow of aqueous acid solutions could have formed and transferred copious quantities of salts from polar cap areas to adjacent zones, possibly resulting in surface deposits observable by Global Surveyor. Solid-state deformation could have physically eroded rocks and deposited moraines. However, if the bases of the ice caps are not anywhere at the melting point, regardless of or because of solid-state deformation, moraines, eskers, and salt deposits would be unexpected.

Other mechanisms of volatile trapping have been considered, including occlusion of martian air and trapping of cometary/asteroidal volatiles. Both are expected to produce geochemically distinctive and scientifically valuable polar materials, but these volatiles should not be of sufficient abundance to affect the rheology and deformation of the polar caps.

References: [1] Fisher D. A. (1993) *Icarus, 105,* 501–511. [2] Clifford S. M. (1987) *JGR, 92,* 9135–9152. [3] Thomas P. et al. (1992) in *Mars* (H. H. Kieffer et al., eds.), pp. 767–798, Univ. of Arizona, Tucson. [4] Miller S. L. and Smythe W. D. (1970) *Science, 170,* 531–533. [5] Milton D. J. (1974) *Science, 183,* 654–656. [6] Dobrovolskis A. and Ingersoll A. P. (1975) *Icarus, 26,* 353–357. [7] Baker V. R. et al. (1991) *Nature, 352,* 589–594. [8] Jakosky B. M. et al. (1995) *JGR, 100,* 1579–1584. [9] Kargel J. S. et al. (1995) *JGR, 100,* 5351–5368. [10] Mellon M. T. (1996) *Icarus, 124,* 268–279. [11] Kargel J. S. and Lunine J. I. (1998) *Proc. Conf. on Solar System Ices* (de Bergh C. et al., eds.), pp. 97–117, Kluwer Academic. [12] Kieffer H. H. (1979) *JGR, 84,* 8263–8288. [13] Kieffer H. H. and Zent A. P. (1992) in *Mars* (H. H. Kieffer et al., eds.), pp. 1180–1220, Univ. of Arizona, Tucson. [14] Ward W. R. (1992) in *Mars* (H. H. Kieffer et al., eds.), pp. 298–320, Univ. of Arizona, Tucson. [15] Ross R. G. and Kargel J. S. (1998) *Proc. Conf. on Solar System Ices* (de Bergh C. et al., eds.), pp. 33–62, Kluwer Academic. [16] Stern L. A. et al. (1996) *Science, 273,* 1843–1848.

THERMAL EMISSION SPECTROMETER OBSERVATIONS OF THE SOUTH AND NORTH POLAR REGIONS DURING THE FIRST PHASE OF AEROBRAKING ORBITS.

H. H. Kieffer, T. N. Titus, and K. F. Mullins, U.S. Geological Survey, 2255 North Gemini Drive, Flagstaff AZ 86001, USA.

Repeated TES coverage of the south polar regions of Mars was obtained over much of the cap recession phase. A map has been made of the date when the last CO_2 disappeared (Fig. 1). This was defined by sliding a representative temperature vs. time curve along the observations for each location in the polar region, and picking the season of maximum temperature change rate. Regressions in the classic area "Mountains of Mitchell" are delayed significantly.

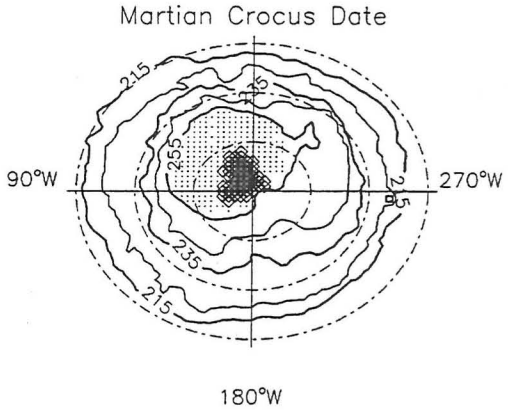

Fig. 1. Map of the aerocentric longitude of the Sun (L_s) when the last CO_2 disappeared. The dotted region indicates where the CO_2 was still present at L_s = 260. The diamonds indicate the area of the residual cap at L_s = 305.

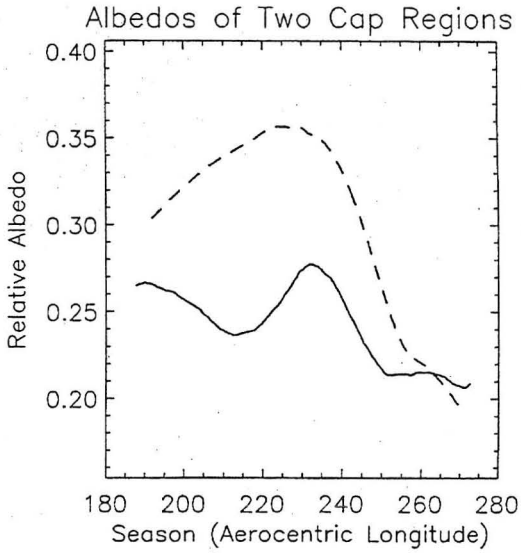

Fig. 2. Seasonal trend of albedo at two locations near the south pole. The dotted curve shows the behavior for a "normal" region near 76°S, 120°W where the last CO_2 disappeared near L_s = 247. The solid line is for the unusual region near 77°S, 210°W where the last CO_2 disappears near L_s 225 and 245 is attributed to dust scattering in the atmosphere during a regional dust storm.

One region (~ 72°–80°S, 180°–250°W) within the annual polar cap became dark long before the temperatures began to rise; in comparison with most areas that show a gradual increase in brightness until a rapid darkening as the temperature rises well above CO_2 frost values (Fig. 2). The extent of this area does not correspond to any particular surface material mapped at 1:5M scale. The cause of this unexpected behavior is under study; one working hypothesis is that as a solid CO_2 forms here nonscattering solid ice.

Observations of the north polar region in winter reveal locations where the 20-μm brightness temperature is much lower than the condensation temperature of CO_2 at Mars surface pressures similar to Viking Infrared Thermal Mapper (IRTM) observations. The TES spectra of these locations suggest that the effect is due to low emissivity temperature. The fine snow quickly metamorphoses into a coarser-grained deposit, which has emissivity closer to 1.

LUMINESCENCE DATING: A TOOL FOR MARTIAN EOLIAN GEOCHRONOLOGY.

K. Lepper[1] and S. W. S. McKeever[2], [1]Environmental Science Program, Department of Physics, 145 Physical Sciences Building, Oklahoma State University, Stillwater OK 74078, USA (Lepper@okstate.edu), [2]Department of Physics, 145 Physical Sciences Building, Oklahoma State University, Stillwater OK 74078, USA.

Introduction: The martian polar ice caps record a wealth of information about the environment and events on the surface of Mars. As on Earth, deciphering this rich record must include a sound chronology. The martian ice caps clearly exhibit stratification, one of the most critical requirements for establishing a relative chronology (Fig. 1), however, meaningful interpretation of data stored in the polar caps will require absolute dates. Stratification in the polar caps

Fig. 1. Layered deposits of the northern polar ice cap on Mars (Image 56B86, from [2]).

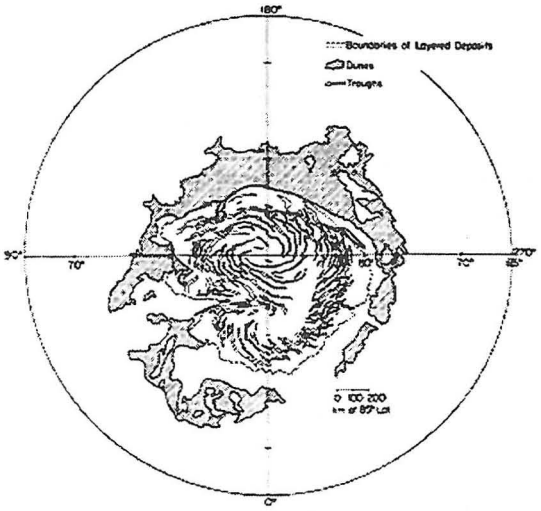

Fig. 2. Map of the northern polar region on Mars. Dune fields are shown in the hashed pattern (from [2]).

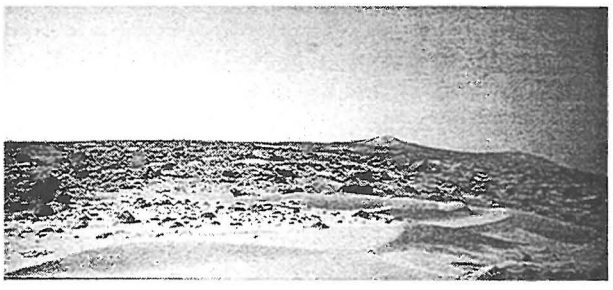

Fig. 3. Small sand dunes photographed at the Mars Pathfinder site (*Sci. Am., 279,* 45).

of Mars arises, at least in part, from the incorporation of eolian material in the ice [1]. Active eolian processes are also exhibited near the poles in the form of dune fields (Fig. 2) [2]. Eolian materials are

ideally suited for luminescence dating, and luminescence dating techniques have been used successfully to make absolute age determinations for numerous terrestrial Quaternary eolian deposits (reviewed in [3]). Luminescence dating techniques could potentially be developed to provide absolute age determinations for the eolian sediments ubiquitous on the surface of Mars, including the sediments incorporated in the martian polar ice caps, thereby affording an opportunity to correlate events recorded at the poles with the record of eolian activity across the surface of Mars.

General Principles of Luminescence Dating: Over geologic time, ionizing radiation from the decay of naturally occurring isotopes and from cosmic rays liberates charge carriers (electrons and holes) within silicate mineral grains. The charge carriers can subsequently become localized at crystal defects leading to accumulation of a "trapped" electron population. When exposed to solar radiation, the trapped charge population is depleted, thereby resetting the luminescence clock. Recombination of the charge carriers results in photon emission. In the laboratory, thermal (TL) or optical (OSL) stimulation can be employed to liberate trapped charge and initiate the luminescence measurement process. The intensity of luminescence emission from the field sample is proportional to the elapsed time since burial. The response rate of the minerals to ionizing radiation and the local ionizing radiation dose rate of the deposit must also be determined. Thorough reviews of the development of luminescence dating, and detailed discussions of procedures and limitations can be found in [3–5].

The event dated by luminescence techniques is, ideally, the last exposure of the sediment grains to solar radiation. Eolian sediments are generally well dispersed when transported, thus affording them the greatest opportunity for exposure to solar radiation and making them the best candidates for accurate luminescence age determinations.

Characteristics of Martian Eolian Sediments: Data from the Mars Pathfinder predicts martian lithologies analogous to terrestrial basalts and andesites [6]. Physical weathering alone of rock of this composition would yield sediment grains containing pyroxene, calcic plagioclase, and biotie. Spectroscopic data, however, indicates the presence of significant amounts of poorly crystalline iron oxides and clay minerals, suggesting chemically weathered surface deposits [7]. In this case, quartz would also be predicted as a chemical weathering product [8].

The morphological similarity between terrestrial and martian dunes (Fig. 3) supports the inference that the martian dunes are composed of sand-sized grains [1]. Eolian material incorporated in the polar ice caps is poorly determined at present, but is believed to be sand and smaller particles [2].

Development of Luminescence Dating for Martian Applications: Luminescence dating procedures for terrestrial quartz and feldspar are well established [4,5]. However, the applicability of luminescence dating to terrestrial pyroxenes and micas has not been investigated. Studies of the luminescence properties of pyroxenes and biotites are needed as well as dating studies of analogous terrestrial materials; sands and silts derived from highly weathered basaltic terranes.

Sands and silts are optimum grain sizes for luminescence dating [3], and recent developments make age determinations possible from extremely small samples, including single grains [9,10].

The range of ages that is accessible to luminescence dating of terrestrial materials varies with mineralogy and local ionizing radiation dose rate, but is generally considered to be from ~1 ka to ~150 ka. Pore water in terrestrial sediments attenuates the external radiation dose received by sediment grains. In effect, this extends the upper age limit recordable by the sediment grains. The attenuation effect of the water ice and CO_2 ice of the martian ice caps and the local ionizing radiation dose rates are unknown. The potential for dating events beyond 150 ka, however, is possible and should be investigated.

Terrestrial investigations should be directed toward development of preliminary dating protocols. The dating protocols could then be adapted for use with samples procured from a "sample and return" mission or in the design guidelines for a luminescence dating module for a rover-type vehicle.

Conclusion: Eolian materials, such as those incorporated in the martian polar ice caps, are ideally suited for luminescence dating. Luminescence dating techniques have been successfully applied to numerous terrestrial Quaternary eolian deposits [3]. Further research on terrestrial analogs of martian eolian materials is needed to develop luminescence dating techniques for application to martian samples. Luminescence dating holds the potential to be a valuable tool for absolute dating of the eolian sediments ubiquitous on the surface of Mars, including the sediments incorporated in the martian polar ice caps. Luminescence geochronology could provide an opportunity to correlate the timing of events recorded at the poles with the record of eolian activity across the surface of Mars.

References: [1] Greeley R. et al. (1992) in *Mars* (H. H. Kiefer et al., eds). [2] Thomas P. et al. (1992) in *Mars* (H. H. Kiefer et al., eds). [3] Huntly D. J. and Lain O.B. (1998) *Geol. Surv. Canada Bull,* in press. [4] Aitken M. J. (1985) *Thermoluminescence Dating.* [5] Wintle A. G. (1998) *Radiation Measurements,* in press. [6] Rieder R. et al. (1997) *Science, 278,* 1771–1774. [7] Soderbolm L. A. (1992) in *Mars* (H. H. Kiefer et al., eds). [8] Gooding J. L. et al. (1992) in *Mars* (H. H. Kiefer et al., eds). [9] Duller G. A. T. (1995) *Radiation Measurements, 24,* 117–145. [10] Murray A. S. et al. (1997) *Radiation Measurements, 27,* 171–184.

SMALL-SCALE TRENCH IN THE MARTIAN SOIL: CONDITIONS FOR CONDENSATION OF ATMOSPHERIC VOLATILES AT THE MARS POLAR LANDER SITE.

W. J. Markiewicz[1], K. J. Kossacki[1,2], and H. U. Keller[1], [1]Max-Planck-Institut für Aeronomie, Max-Planck-Strasse 2, D-37191 Katlenburg-Lindau, Germany (markiewicz@linmpi.mpg.de), [2]Institute of Geophysics, Warsaw University, Pasteura 7, 02-093 Warsaw, Poland.

Introduction: Mars Polar Lander (MPL) is scheduled to be launched in January 1999 and to arrive at Mars in December 1999. The MPL landing site is at the edge of the south polar cap region. The lander will be equipped with a robotic arm (RA) capable of digging a small trench. It is to be expected that the facets of such a trench will be colder then the average surrounding surface. The 2.5-dimensional thermal calculations are used to estimate the diurnal variations of the temperature within a trench. It is found that, at least on the bottom of the trench, water will condense independently of time of day. It is also found that if the thermal conductivity of the martian soil is near the minimum expected value the condensation of the atmospheric CO_2 should also be possible. Imaging of evolution of such surface frost will be possible with the camera attached to the RA.

Model: The shape of the trench will depend on the accuracy of positioning of the scoop by the RA (about 0.5 cm) and the cohesion of the soil. The trench dug during Viking mission had a roughly triangular crossection with gently sloping walls. The MPL landing site, however, is expected to be very different from that of the Viking and Pathfinder missions. At least small amounts of ground ice that should be present will strengthen the side walls of the trench. In this first study, the rectangular case is considered as an extreme, allowing for the lowest temperatures at the bottom of the trench. The trench is taken to be 0.2 m deep and 0.1 m wide.

The temperature on the inner facets of the trench are calculated as solution of two-dimensional heat transfer equations. The local energy balance at the surface outside the trench includes the absorption of the solar radiation, the IR emission and the heat transport into the soil. The energy budget for the surfaces within the trench includes also the absorption of the solar radiation scattered in the trench. The IR radiation emitted by the surfaces within the trench are treated in the same way. The multiple scattering is taken into account, assuming albedo, A = 0.5 and emissivity, e = 0.9. This three-dimensional treatment of the boundary condition together with two-dimensional heat transfer calculation within the soil makes the model 2.5-dimensional. The thermal conductivity of the soil is assumed to be constant and is a model parameter.

The diurnal variability of the position of the Sun relative to the trench is taken into account. It is assumed, that the trench is oriented east-west and the latitude is $\phi = 71°$. The absorption of radiation by an element of the internal surface of a trench is calculated assuming that the trench is long when compared to its depth and width. Thus, the radiation scattered and emitted by various points at the same depth on one side of the trench is the same.

The thermal conductivity of the martian soil can depend on its porosity, the size and shape of mineral grains, the gas pressure in the pores, the presence or absence of ice, and the soil temperature. If the ground is dry, the temperature influences only a very thin layer close to the surface, where the radiative heat transfer can become important. In the present model the ground is assumed to be dry. Thermal conductivity is therefore taken to be a function of only the density and the granulation of the soil. Various attempts have been made to estimate the thermal conductivity of such a medium.

The lowest estimate results from combining the estimates of thermal inertia of the martian ground for the latitude range 60°S to 60°N from Viking Orbiter [1] with the heat capacity of soil of 820 J kg^{-1} K^{-1} from [2]. Thermal conductivity is then 1.6 mW m^{-1} $K^{-1} < \lambda$ < 365 mW m^{-1} K^{-1}. However, the planned landing site of MPL is south of the region studied in [1]. In [3] the thermal inertia for the MPL landing region is assumed to be about 175 J m^2 $s^{1/2}$ K^{-1}. This value of the thermal inertia corresponds to λ of about 30 mW m^{-1} K^{-1}. One more estimate of the thermal conductivity comes from the experiments reported in [4], where the authors propose the formula relating thermal conductivity of the mineral powder to its density. If we assume density to be 1300 kg m^{-3}, then $\lambda = 18$ mW m^{-1} K^{-1}. Given various uncertainties in the above estimates, we will assume that the probable range of the thermal conductivity of soil at the MPL landing site is 2 mW m^{-1} $K^{-1} < \lambda < 45$ mW m^{-1} K^{-1}. For the results presented below the solar insolation corresponds to the seasonal angle $L_s = 270$ (summer solstice).

Results: Figure 1 shows results for one particular calculation with $\lambda = 42$ mW m^{-1} K^{-1}, a value near upper boundary of the likely range. Temperature on the walls and the bottom of the trench are

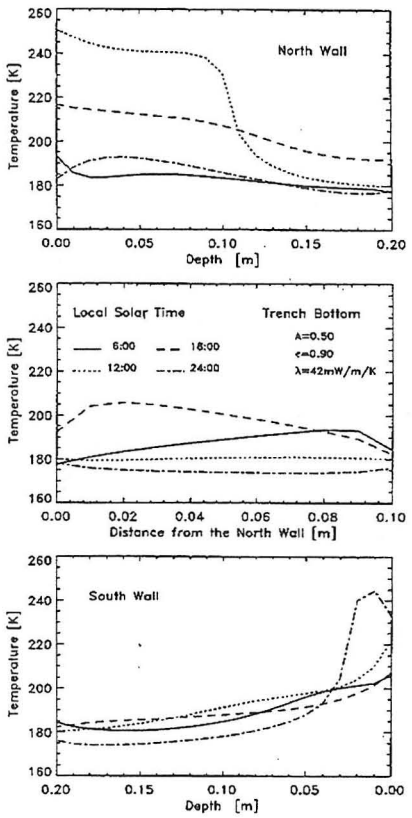

Fig. 1. Diurnal changes of the temperature distribution on the facets of rectangular trench in the martian soil.

plotted at four different times of day. The lowest values of the temperature are predicted for the bottom of the trench; however, significant fraction of the side walls have similar temperatures. The diurnal minimum of the temperature is expected around 3:00 local time. The temperature at which water may condense depends on several not precisely known atmospheric parameters but can be estimated to be about 210K. From Fig. 1 it can be seen that, with the possible exception of late afternoon, frost condensation on the bottom of the trench can be expected. Increasing the depth of the trench without changing its width does not alter these results significantly.

Once the bottom of the trench is already covered with some amount of ice, the vapor density at the surface should be near that of the phase equilibrium at the corresponding temperature. The condensation rate should be therefore controlled by the temperature within the trench and by the vapor concentration in the atmosphere. For the purpose of the present analysis, the vapor concentration in the atmosphere is assumed not to be affected by the frost formation in the trench. If the temperature is taken to be equal to 180K, the condensation flux at the bottom of the trench should be of the order of 2×10^{-4} kg m^{-2} s^{-1}. This value is equivalent to the thickening of the ice layer at a rate of about 0.5 mm/hr^{-1}. The real rate of frost formation will be somewhat lower than the above estimate due to influence of latent heat release on the local temperature. However, the progress of ice deposition should be clearly observable. Results in Fig. 1 were calculated with $\lambda = 42$ mW m^{-1} K^{-1}. If λ is near its lowest likely value of 2 mW m^{-1} K^{-1}, the temperature of the bottom of the trench may be

as low as 145K, which is just lower than the temperature of CO_2 gas-solid phase equilibrium. In this case CO_2 frost may also form.

All the above considerations do not account for the influence of the condensate on the local albedo and emissivity within the trench. When the bottom of the trench is already covered with significant amount of frost, its albedo will be higher than that of clear dust. The net effect could be further decrease of the temperature. This subject needs further consideration, however.

References: [1] Palluconi F. D. and Kieffer H. H. (1981) *Icarus, 45,* 415–426. [2] Zent A. P. et al. (1993) *JGR, 98,* 3319–3337. [3] Paige D. A. and Keegan K. D. (1994) *JGR, 99,* 25993–26013. [4] Presley M. A. and Christensen P. R. (1997) *JGR, 103,* 9221–9230.

SUBSURFACE STRUCTURE IN THE MARTIAN POLAR LAYERED DEPOSITS: THE DEEP SPACE 2 IMPACT ACCELEROMETRY EXPERIMENT.

J. E. Moersch[1] and R. D. Lorenz[2], [1]Mail Stop 239-4, NASA Ames Research Center, Moffett Field CA 94040, USA (jmoersch@mail.arc.nasa.gov), [2]Lunar and Planetary Laboratory, University of Arizona, Tucson AZ 86721, USA (rlorenz@lpl.arizona.edu).

Introduction: While primarily a technology demonstration mission, the New Millenium Mars Microprobes (also known as Deep Space 2, or simply DS2) [1] will also provide the first *in situ* science measurements of the martian subsurface. The DS2 impact accelerometry experiment will provide both engineering data about the depth of probe emplacement and science data about the physical nature of the subsurface at the probes' landing sites.

Little is known about the detailed physical properties or small-scale vertical structure of the subsurface at the DS2 landing site in the southern martian polar layered deposits. Imaging data from the Viking Orbiters (e.g., [2,3]) and Mars Global Surveyor [4] reveal alternating bands of light and dark material in this region with thicknesses at least as small as the limit of resolution, about 10 m. The overall composition of these layers is poorly constrained, but generally thought to be a mixture of dust and ice [e.g., 5,6] with the layers being caused by variations in the dust/ice ratio [7], or perhaps by dust deposits of different densities [8]. Low thermal inertias in the region [9] suggest that the top few centimeters of the surface are composed of a mantling of fine-grained dust. However, 3.5-cm radar returns indicate that the maximum depth of this dust is not greater than a few tens of centimeters [10]. Thermal models [11–13] generally agree that, while the layered deposits do provide a potential near-surface reservoir for ice, the uppermost few centimeters to meters in these regions are likely to be ice-free because of sublimation losses. Finally, while it is generally agreed that the layered deposits are the product of variations in the martian climate [8,14,15], no direct correlation has been made between band sequences and specific climate changes.

Our intention is to shed light on some of these questions about the martian polar layered deposits by using the DS2 accelerometry experiment to determine the physical nature of the layered deposits, and to detect the presence of any subsurface layering of dust, ice, and/or rock. In the process, we will also determine the final resting depth of the two microprobes, an important parameter in the interpretation of other DS2 experiments.

Experimental Technique: Penetrators similar to the DS2 microprobes have a long history of use in military applications on Earth, and their behavior upon impact has been very carefully characterized and parameterized. The canonical technique for relating impact accelerometry measurements to the physical properties of a target material is through a set of semiempirical equations developed in the Earth Penetrating Weapon program at Sandia National Laboratories [16]. In these equations, the depth of penetration for a given penetrator design and initial impact conditions is linearly related to the "penetrability parameter" (S) of the target material. S is a function of the unconfined compressive strength of the target, and the degree to which the target is affected by joints, cracks, water content, and cementation. S values have been compiled for a wide variety of target materials [16].

Conceptually, one may infer the physical nature of a homogeneous (semi-infinite) subsurface at a penetrator landing site by double-integrating accelerometry measurements during the impact event to determine the penetrator's final resting depth, converting this depth to an S value via the Sandia equations, and then comparing the result to S values measured from known materials.

A layered subsurface will be reflected in accelerometry data as changes in deceleration with depth: high S values ("soft" materials) produce lower decelerations than low S values. An accelerometry record that shows discrete steps in deceleration may be used to calculate a layered S profile as a function of depth by using the exit velocity from each overlying layer as the initial condition for impact into the next underlying layer. Once an S profile is generated, it may be related to the physical properties of the layers, as with the homogeneous case. For example, if the DS2 accelerometer detects a sudden decrease in S value from 15 to 5 at a depth several centimeters below the surface, it might be inferred that the probe had initially passed through a loose mantle of dust and then penetrated into a much harder layer of frozen soil.

Hardware: The impact accelerometer hardware in each of the two DS2 microprobes consists of a uniaxial accelerometer mounted inside the forebody of the probe, aligned with the long axis of the probe. The accelerometer is a rugged piezoresistive design (Endevco Model 7570–60K) with a measurable input range of –10,000–30,000 *g* and a precision of 10 *g*. The accelerometer is polled by the probe's advanced microcontroller at a sampling rate of 25 kHz, starting ~100 s before impact and ending when the probe forebody comes to a halt. Only the final 30 ms of accelerometer data (which will encompass the entire impact event) are stored for later transmission. Accelerometer data are sampled with 16 bits/sample, yielding a total data return from each penetrator of about 1.5 kilobytes.

Validation and Interpretation: Our plan for data validation and interpretation includes both experimental and numerical techniques, which will be used in parallel.

Experimental techniques. Proper extraction of surface properties from the accelerometer record will require an understanding of how the structural characteristics of the probes and the mounting geometry of the accelerometer affect the data. For example, we expect to see an acceleration signature from the 2.5-kHz resonant frequency of the forebody, and from both breakage of the shear pins used to hold the forebody within the aftbody and shattering of the probe's aeroshell at impact. To understand the nature of these artifacts, and to test the predictive value of the Sandia penetration equations for our particular probe design, we are making use of a low velocity airgun facility at the University of Arizona. This device, which was originally built to test prototypes of the Comet Rendez-

vous and Asteroid Flyby (CRAF) mission's penetrator experiment, is capable of accelerating a DS2 flightlike structural model to a velocity of 50 m/s. The test probes will be instrumented with flightlike accelerometers and shot with the airgun into a variety of target materials to build a database of accelerometer records that will help us interpret data returned from Mars.

The actual velocity at which the DS2 probes are expected to impact the martian surface is ~180 m/s, faster than the University of Arizona airgun is capable of providing. We also hope to test instrumented flightlike models of the probes using a higher-velocity airgun, such as the one available at the New Mexico Energetic Materials Test Center.

Numerical techniques. Two numerical codes will be used in combination to simulate impact events and accelerometer performance. These simulations will help us characterize and validate the experiment before arrival at Mars, and interpret the data returned from Mars. One code, the Integrating Mars Penetrator Accelerometer Testbed (IMPAcT), is a modified version of a code written in support of the CRAF mission. Its purpose is to simulate the performance of accelerometers on a penetrator, integrate the simulated accelerometer data, and produce a record of the derived penetrator path. IMPAcT treats six degrees of freedom (x,y,z, and yaw, pitch, and roll) and is capable of simulating errors associated with accelerometer positioning and alignment, quantization and aliasing from sampling rates, *g*-resolution, random electronic noise, and filtering in the spectral domain. Currently, IMPacT is being used to understand the uncertainties associated with the DS2 experiment. For example, experiments have shown that lateral forces on impacting penetrators can be of equal magnitude to axial loads [17]; IMPAcT will be used to assess errors associated with these lateral (and rotational) accelerations, which will go unmeasured or possibly even confound the measurements of the uniaxial DS2 accelerometer. After arrival at Mars, IMPAcT will also be used to integrate the real DS2 accelerometry records to obtain a record of velocity and path as a function of time, including error bars from the earlier simulations.

The other numerical code we will use is the Simplified Analytical Model of Penetration with Lateral Loading (SAMPLL) from Sandia National Laboratory [17]. SAMPLL uses the Sandia penetration equations to simulate penetrator performance. The code takes penetrator design parameters, initial conditions at impact, and *S* values for homogeneous or layered targets and provides predicted penetrator paths and decelerations as a function of time. Results from SAMPLL will be compared to our experimental results and used as input to test runs of IMPAcT. After arrival at Mars, SAMPLL will be run with a variety of target materials and layers in an attempt to match data from the flight instruments.

Other Applications: Deep Space 2 may only be the first of many future microprobe missions to the planets [1]. One interesting mission concept currently under discussion would send similar probes to the martian north polar cap. Whatever the target, any penetrator-style mission will certainly include impact accelerometers. It is our hope that the experience gained with the DS2 impact accelerometry experiment will have broad applicability to future missions of this type.

References: [1] Smrekar S. E. and Gavit S. A., this volume. [2] Dzurisin D. and Blasius K. R. (1975) *JGR, 82,* 4225. [3] Blasius K. R. et al. (1982) *Icarus, 50,* 140. [4] Malin M. C. et al. (1998) *Science, 279,* 1681. [5] Thomas P. T. and Weitz C. (1989) *Icarus, 81,* 185. [6] Herkenhoff K. E. and Murray B. C. (1990) *JGR, 95,* 1343. [7] Pollack J. B. et al. (1979) *JGR, 84,* 2929. [8] Cutts J. A. (1973) *JGR, 78,* 4231. [9] Paige D. A. et al. (1994) *JGR, 99,* 25993. [10] Muhleman D. O. et al. (1991) *Science, 253,* 1508. [11] Leighton R. B. and Murray B. C. (1966) *Science, 153,* 136. [12] Farmer C. B. and Doms P. E. (1979) *JGR, 84,* 2881. [13] Paige D. A. (1992) *Nature, 356,* 43. [14] Murray B. C. et al. (1972) *Icarus, 17,* 328. [15] Cutts J. A. and Lewis B. H. (1982) *Icarus, 50,* 216. [16] Young C. W. (1997) *Sandia Tech. Rep. SAND97-2426.* [17] Young C. W. (1992) *Sandia Tech. Rep. SAND91-2175.*

EVOLUTION OF THE MARS NORTHERN ICE CAP AND RESULTS FROM THE MARS ORBITER LASER ALTIMETER (MOLA).

D. O. Muhleman and A. B. Ivanov, Mail Stop 150-21, California Institute of Technology, Pasadena CA 91125, USA (dom@venus1.gps.caltech.edu).

Introduction: Martian ice caps play an extremely important role in regulating climate of Mars. It is well known that they are acting as a reservoir for CO_2 and maybe for water and dust. However, a reliable quantitative estimate of the balance or amount of volatiles inside the ice caps was never possible, because little data were available for this purpose. Here we will present initial results and analysis of topography data over the northern ice cap obtained by the Mars Orbiter Laser Altimeter (MOLA) onboard Mars Global Surveyor (MGS). We interpret the observed shape of the ice caps as created by ablation due to sublimation of water ice.

Observations: During Science Phasing Orbit (SPO), MOLA has obtained ~180 profiles across the ice cap. Due to the inclination of the MGS orbit, maximum latitude of the observations is 86.1°N. Fortunately, on several passes the spacecraft was tilted toward the north pole and MOLA was able to profile the center of the cap. (Fig. 1). The seasons varied from winter to early spring (L_s = 340° – 10°), when the perennial ice cap is believed to be at its maximum. Precision orbit determination data is not available at this time, but preliminary data reduction shows that the maximum height of the ice cap, relative to the surrounding plains is about 2.7 km. This is much less than the number previously suggested by other researchers, 5 km, [e.g., 1].

Data analysis: MOLA observations were put in a grid using hierarchical averaging algorithm ([2]) and the resulting three-dimensional structure is presented at Fig. 2. We used this representation to obtain radial profiles across the ice cap.

Modeling: Evolution of the martian northern ice cap was modeled with a very simple thermal balance approach. It simulates ablation of water from the surface. The governing equations are

$$\frac{dM}{dt} = \left(P_{sat,H_2O}(T)\right)\sqrt{\frac{2\pi kT}{m_w}}$$

$$T = \left[\frac{(1-A)^* F_s^* \cos(\theta)}{\sigma}\right]^{\frac{1}{4}}$$

where T is temperature at the surface of the cap, A is albedo (assumed to be 0.55), σ is the Stephan Boltzmann constant, F_s is the solar constant at Mars, dM/dt is H_2O loss rate, P_{sat} is the saturation pressure of water vapor over ice, θ is incidence angle of the Sun at a

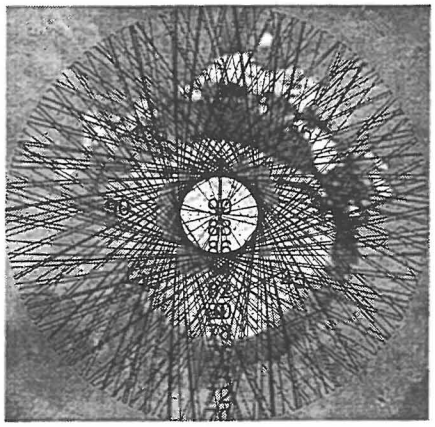

Fig. 1. MOLA groundtracks over the north pole of Mars. Data include SPO-1 and SPO-2 passes north of 70°N. Map is in polar stereographic projection.

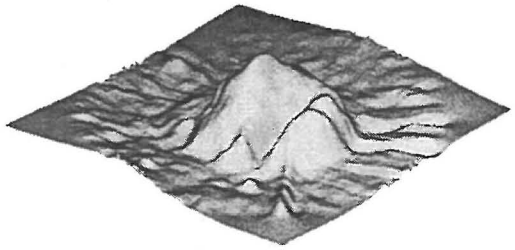

Fig. 2. Three-dimensional reconstruction of the shape of the north pole of Mars. Data is still not completely corrected for orbital errors and large deviations are clearly seen. View is from 50°W longitude. Chasma Borealis is in front. Vertical exaggeration is about 1:200.

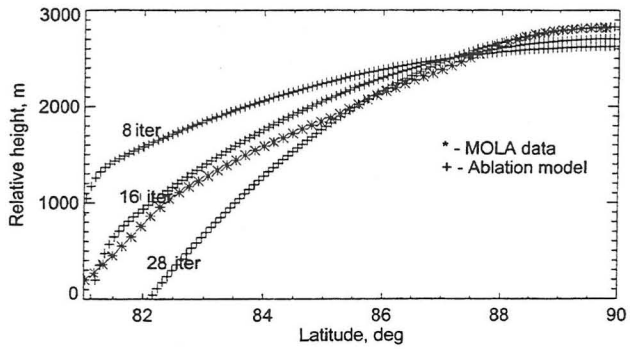

Fig. 3. Comparison of profiles obtained by MOLA and calculated from ablation model. Three model cases (8th, 16th, and 28th iterations) are shown for different ablation period lengths. One iteration is about 100,000 yr. Stars = MOLA data, plus signs = data from the model.

given point of the surface, and m_w is the molecular weight of water. The minimum ice temperature was fixed at 150 K. We assumed that the entire ice cap was a reservoir with P_{H2O} varying sinsoidally, such that it peaked at 80 pr.μm [3]. The initial conditions were a rectangular "ice poke" of ice spreading from 80°N to the pole and 2500 m thickness. The model was run for about 40 time steps. Each timestep is equivalent to about 100,000 yr.

Results: We compared a profile, taken along 180 longitude from 80°N to 90°N, with output of several iteration steps from the ablation model described above (Fig. 3). We think that agreement with 16th iteration is very good and it will get better as precision orbit determination data become available. We will also present results taken along other longitudes and cross sections across the troughs.

Conclusions: For the first time, topography data were obtained over the northern polar ice cap of Mars. Initial results suggest that the form of the ice cap can be explained by ablation of ice and the model shows good agreement with the data. Further investigation, in conjunction with the observations obtained by other MGS instruments (MOC, TES, RS) will lead to estimates of the age of the ice cap and a better understanding of the climatic history of Mars.

References: [1] Thomas P. et al. (1992) in *Mars,* Univ. of Arizona, Tucson. [2] Goetler S. J. et al. (1996) in *Computer Graphics, Annual Conference Series.* [3] Jakosky B. M. and Farmer C. B. (1982) *JGR, 87,* 2999–3019.

CARBON-ISOTOPIC DYNAMICS OF STREAMS, TAYLOR VALLEY, ANTARCTICA: BIOLOGICAL EFFECTS.

K. Neumann[1], W. B. Lyons[1], and D. J. Des Marais[2], [1]Department of Geology, University of Alabama, Tuscaloosa AL 35487-0338, USA (kneumann@wgs.geo.ua.edu; blyons@wgs.geo.ua.edu), [2]NASA Ames Research Center, Moffett Field CA 94035, USA (ddesmarais@mail.arc.nasa.gov).

Abstract: We have investigated the role of biological processes in the C-isotopic dynamics of the aquatic ecosystems in Taylor Valley, Antarctica. This cold desert ecosystem is characterized by the complete lack of vascular plants, and the presence of algal mats in ephemeral streams and perennially ice covered lakes. Streams having abundant algal mats and mosses have very low ΣCO_2 concentrations, as well as the most depleted $\delta^{13}C$ values (–4‰). Previous work by Doran et al. [1] has shown that algal mats in these streams have $\delta^{13}C$ values averaging –7.0‰. These values are similar to those observed in the algal mats in shallow areas of the lakes in Taylor Valley, where CO_2 is thought to be colimiting to growth. These low ΣCO_2 concentrations, and $\delta^{13}C$ signatures heavier than the algal mats, suggest that CO_2 may be colimiting in the streams, as well. Streams with little

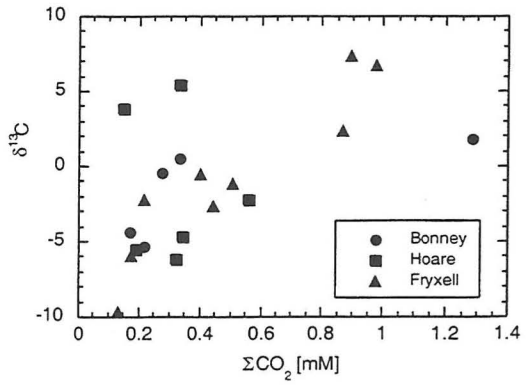

Fig. 1. ΣCO_2 vs. ΣCO_2-$\delta^{13}C$ in streams of three catchments in Taylor Valley, Antarctica. Note especially the increase in $\delta^{13}C$ with increasing ΣCO_2 in Fryxell Basin.

algal growth, especially the longer ones in Fryxell Basin, have higher ΣCO_2 concentrations and much more enriched isotopic signatures (as high as +8‰, Fig. 1). In these streams, the dissolution of isotopically enriched, cryogenic $CaCO_3$ is probably the major source of dissolved carbonate. The $\delta^{13}C$ geochemistry of Antarctic streams is radically different from the geochemistry of more temperate streams, as it is not affected by terrestrially produced, isotopically depleted ΣCO_2. These results have important implications for the understanding of "biogenic" carbonate that might have been produced from aquatic ecosystems in the past on Mars.

References: [1] Doran P. T. et al. (1998) *JGR,* in press.

MAPPING THE MARTIAN POLAR ICE CAPS: APPLICATIONS OF TERRESTRIAL OPTICAL REMOTE SENSING METHODS. A. W. Nolin, Cooperative Institute for Research in Environmental Sciences, National Snow and Ice Data Center, Campus Box 449, University of Colorado, Boulder CO 80309-0449, USA (nolin@spectra.colorado.edu).

Terrestrial Optical Remote Sensing of Snow and Ice: With improvements in both instrumentation and algorithms, methods for mapping terrestrial snow cover using optical remote sensing data have progressed significantly over the past decade. Multispectral data can now be used to determine not only the presence or absence of snow but the fraction of snow cover in a pixel [1,2]. Radiative transfer models have been used to quantify the nonlinear relationship between surface reflectance and grain size, thereby providing the basis for mapping snow grain size from surface reflectance images [3]. Because subpixel mixtures of snow and other land cover types create erroneous estimates of snow grain-size, the snow fraction information can be used in tandem with the grain size algorithm to limit its use to only those pixels that have complete snow cover. Model-derived characterization of the bidirectional reflectance distribution function (BRDF) provides the means for converting measured bidirectional reflectance to directional-hemispherical albedo. In recent work, this approach has allowed climatologists to examine the large-scale seasonal variability of albedo on the Greenland ice sheet [4,5]. This seasonal albedo variability results from increases in snow grain size and exposure of the underlying ice cap as the seasonal snow cover ablates away.

Martian Applications of Optical Remote Sensing Methods: With the current Mars Global Surveyor and future missions to Mars, it will soon be possible to apply some of these terrestrial mapping methods to learn more about martian polar caps. What is most needed for this purpose is multispectral optical imagery. The extent and variability of the ice caps and their seasonal CO_2 frost covering can be mapped with only a few spectral bands distributed through the visible and near-infrared wavelengths. For instance, just a few, well-situated bands (e.g., those used on the Landsat TM) provide sufficient spectral resolution for subpixel mapping. Imaging spectrometer data would provide the ability to quantify mineral-ice mixtures and to better characterize the martian atmosphere. These are both needed for albedo determinations while only the former is required for subpixel frost/ice mapping. Perhaps the most significant terrestrial mapping application is the potential use of the Mars Orbiter Laser Altimeter (MOLA) to map grain size on the martian polar caps. For dust concentrations less than about 1 wt%, grain size remains the dominant surface property that determines surface albedo. With its exponential response to temperature, grain size is also the physical property with the highest sensitivity to changes in the thermodynamic state of the ice. Changes in the energy balance of the surface frost regions should be reflected in changing grain size even before a change in the total frost covered area would be detected.

Distinct differences exist between Mars and Earth ice mapping conditions, including surface temperature, ice type, ice-mineral mixtures, and atmospheric properties, so a direct application of terrestrial snow and ice mapping methods may not be possible. However, expertise in mapping and interpreting terrestrial snow and ice will contribute to the inventory of techniques for mapping planetary ices. Furthermore, adaptation of terrestrial methods will provide a basis for comparison of terrestrial and planetary cryospheric components [6].

References: [1] Nolin A. W. et al. (1993) *Ann. Glaciol., 17,* 121–124. [2] Rosenthal W. and Dozier J. (1996) *Water Resour. Res., 32,* 115–130. [3] Nolin A. W. (1993) *Remote Sens. Environ., 44,* 232–238. [4] Nolin A. W. and Stroeve J. C. (1997) *Ann. Glaciol., 25,* 51–57. [5] Stroeve J. C. et al. (1997) *Remote Sens. Environ., 62,* 262–276. [6] Nolin A. W. (1998) *JGR,* in press.

MARS VOLATILES AND CLIMATE SURVEYOR (MVACS) INTEGRATED PAYLOAD FOR THE MARS POLAR LANDER MISSION. D. A. Paige[1], W. V. Boynton[2], D. Crisp[3], E. DeJong[3], A. M. Harri[4], C. J. Hansen[3], H. U. Keller[5], L. A. Leshin[1], P. H. Smith[2], and R. W. Zurek[3], [1]University of California, Los Angeles CA 90024, USA, [2]University of Arizona, Tucson AZ 87521, USA, [3]Jet Propulsion Laboratory, Pasadena CA 91109, USA, [4]Finnish Meterological Institute, Helsinki SF-00101, Finland, [5]Max-Planck-Institut für Aeronomie, Katlenburg-Lindau, Germany.

The Mars Volatiles and Climate Surveyor (MVACS) integrated payload for the Mars Polar Lander will be launched in January 1999, with a scheduled landing on Mars' south-polar layered deposits in December 1999. Over the course of its 90-day nominal mission during the martian southern spring and summer seasons, it will make *in situ* measurements that will provide new insights into the behavior and distribution of martian volatiles. MVACS consists of four major instrument systems: a surface stereo imager (SSI), which will acquire multispectral stereo images of the surface and atmosphere; a 2-m robotic arm (RA), which will dig a 0.5-m deep trench and acquire surface and subsurface samples that will be imaged by a focusable robotic arm camera (RAC), which will take close-up images of surface and subsurface samples at a spatial resolution of 21 μm; a meteorology package (MET), which will make the first measurements of surface pressure, temperature, and winds in Mars' southern hemisphere and employ a tunable diode laser (TDL) spectrometer to measure the water-vapor concentration and isotopic composition of CO_2 in the martian atmosphere; and a thermal and evolved gas analyzer (TEGA), which will use differential scanning calorimetry and TDL-evolved gas analysis to determine the concentrations of ices, adsorbed volatiles, and volatile-bearing minerals in surface and subsurface soil samples. The unique *in situ* measurements made by MVACS at its high-latitude landing site will define a number of important aspects of the physical, isotopic, and chemical nature of the martian near-surface and subsurface environment that will be valuable in better understanding Mars meteorites and returned samples, as well as in the search for martian resources that could be utilized by humans.

MARTIAN DUSTY ATMOSPHERE AS A LORENZ SYSTEM. A. A. Pankine and A. P. Ingersoll, California Institute of Technology, 1200 East California Boulevard, Pasadena CA 91125, USA.

We present a simple model of the interaction between the global circulation and dust aimed at explaining the interannual variability of martian global dust storms. The equations of the model are the Lorenz equations [1], with an additional term that represents seasonal forcing. The parameters of the model are chosen using the Mars GCM results [2]. For the range of parameter values that are suitable for Mars, the model exhibits rapid oscillations in atmospheric circulation and dust loading during early summer in both hemispheres. The oscillations repeat each year and do not reproduce the observed interannual variability. The solutions are consistent with the time of occurrence of the observed global dust storms, but contradict the occurrence of global storms only in the southern hemisphere. We suggest that physical processes not related to the global circulation are responsible for these discrepancies. These processes may include water ice condensation on the dust particles [3] or redistribution of the dust on the surface [4]. We feel that the results of our modeling are useful in distinguishing between processes that are important for the martian dust cycle and can provide guidance for the Mars GCM simulations.

References: [1] Lorenz E. N. (1963) *J. Atmos. Sci., 20,* 130–141. [2] Pollack J. B. et al. (1990) *JGR, 95,* 1473–1447. [3] Clancy R. T. et al. (1996) *Icarus, 122,* 36–62. [4] Haberle R. M. (1986) *Science, 234,* 459–461.

RECENT LIQUID WATER IN THE POLAR REGIONS OF MARS. A. V. Pathare and D. A. Paige, Department of Earth and Space Sciences, University of California, Los Angeles, 405 Hilgard Avenue, Los Angeles CA 90098-1567, USA (avp@mvacs.ess.ucla.edu; dap@mvacs.ess.ucla.edu).

The potential presence of liquid water on a planetary body during a given epoch is important to both climatology and exobiology. Our modeling of the martian surface heat balance at high latitudes and obliquities in the recent past (i.e., during the last 100 m.y.) indicates that liquid water has been stable during local spring and summer in the polar regions of Mars. Previous martian climate models concluded that liquid water would not be stable at high obliquity. However, our model differs from these previous models in three crucial respects: A more detailed atmospheric radiative transfer model is employed to assess the surface heating due to a water vapor greenhouse; the effects of atmospheric dust are incorporated; and, perhaps most importantly, idealized sublimation into a dry atmosphere is not assumed. Our results indicate that liquid water would indeed be stable at the martian poles at obliquities of 45° and higher during much of local spring and summer. Furthermore, using the best estimates of martian near-polar surface properties such as thermal inertia and albedo, we also find that such liquid water "oases" would also be stable just off of the northern polar cap at obliquities as low as 35°. The importance of such stable liquid water to climatology is twofold, as water not only influences climate but also readily erodes the surface, thereby recording past climate change. We will attempt to discuss the geologic evidence for such change in the context of new observations from Mars Global Surveyor.

THE MARS EXPRESS SUBSURFACE SOUNDING RADAR: WATER AND ICE DETECTION IN THE POLAR REGIONS. J. J. Plaut, Mail Stop 183-501, Jet Propulsion Laboratory, California Institute of Technology, 4800 Oak Grove Drive, Pasadena CA 91109, USA (plaut@jpl.nasa.gov).

Introduction: The European Space Agency (ESA) will conduct a mission to Mars during the 2003 launch opportunity, called Mars Express. Much of the payload is similar to that of the failed Mars 96 orbiter, but a completely new instrument has been selected for the payload, the Subsurface Sounding Radar/Altimeter (SSRA). The SSRA experiment is a joint project between the University of Rome, the Jet Propulsion Laboratory, and Alenia Aerospazio, Italy. This paper describes the science objectives of the experiment, the instrument characteristics, and applications of the SSRA investigation to studies of the martian polar regions.

Science Objectives: The primary objective of the SSRA experiment is to map the distribution of water, both liquid and solid, in the upper portions of the crust of Mars. Secondary objectives include subsurface geologic probing for stratigraphic and structural contacts, characterization of the surface topography, roughness and reflectivity, and ionospheric sounding. Detection of water and ice reservoirs will address many key issues in the hydrologic, geologic, climatic and possible biologic evolution of Mars, including the current and past global inventory of water, mechanisms of transport and storage of water, the role of liquid water and ice in shaping the landscape of Mars, the stability of liquid water and ice at the surface as an indication of climatic conditions, and the implications of the hydrologic history for the evolution of possible martian ecosystems. Models of the radar system performance and electromagnetic interactions with martian crustal materials indicate that aquifers of liquid water can be detected by SSRA to a depth greater than 5 km under favorable conditions of surface roughness and crustal composition. Under less favorable conditions penetration depths may be substantially smaller; in these circumstances, the distribution of ground ice and the nature of the shallow stratigraphy may nevertheless be studied.

Instrument Description: The SSRA is a multifrequency, coherent pulse, synthetic aperture radar sounder/altimeter. The instrument features flexibility in frequency selection for adaptation to the Mars environment, and a secondary, receive-only antenna and data channel to minimize the effects of surface "clutter" on subsurface feature detection. The instrument will acquire echo profiles of the subsurface of Mars at a lateral spacing of approximately 5 km and a vertical (depth) resolution of 50–100 m. Four frequency channels will be available for use: 1.9, 2.8, 3.8, and 4.8 MHz. The lower-frequency channels, which are likely to penetrate more deeply, will be used during night-side operations, when the ionospheric plasma frequency is lowest. The primary antenna consists of a simple dipole with a total length of 40 m. An impedance matching system will be used to improve antenna efficiency across the range of frequencies. The secondary antenna is designed with a null in its pattern at the spacecraft nadir, and will therefore primarily detect echoes from off-nadir surface structure (clutter). Onboard digital processing will generate echo profiles for both the primary and secondary receive streams, at two frequencies in the nominal mode. This processing greatly reduces the data volume necessary for downlink. Postprocessing on Earth will include convolution of the primary and secondary antenna profiles for surface clutter cancellation, and compilation of map products showing, for example, the depth of detected interfaces.

Applications in Polar Regions: Data from SSRA can potentially address several critical issues in Mars polar studies. Of particular interest is the depth and character of the "bed" of the polar layered deposits. If attenuation of the signal by the layered materials is not too great, it may be possible to map the base of the deposit and detect basal melting zones, should they exist. Detection of pockets of liquid water beneath the ice would be a dramatic result, with implications for possible ecosystems and regional or global hydrologic systems. Strong discontinuities in dielectric properties may also be detected within the layered deposits and may be indicative of major climate shifts. Properties of other high-latitude terrains will be studied, including the thickness of the north polar erg and possible subsurface stratigraphic contacts among sedimentary and volcanic units in both polar regions. Contacts between ice-saturated and ice-free crustal materials are likely to be detected in some regions. The thickness of the proposed low-latitude desiccation zone may be measurable. Detection of shallow (<5 km) aquifers would revolutionize our ideas on the current state of water on Mars and provide targets for future biologic searches and a possible sustained human presence.

TOPOGRAPHY OF THE SOUTH POLAR CAP AND LAYERED DEPOSITS OF MARS: VIKING STEREO GRAMMETRY AT REGIONAL AND LOCAL SCALES.

P. Schenk[1], J. Moore[2], and C. Stoker[2], Lunar and Planetary Institute, 3600 Bay Area Boulevard, Houston TX 77058, USA (schenk@lpi.jsc.nasa.gov), [2]NASA Ames Research Center, Moffett Field CA, USA.

Layered deposits and residual polar caps on Mars may record the deposition of ice and sediment modulated by periodic climate change. The 1998 Mars Polar Lander is currently targeted to land on south polar deposits between 75° and 80° latitude. Topographic information relating to layer thicknesses, erosional processes, and formation of dark spirals within these deposits has been sparce or unreliable until the arrival of MOLA in orbit in September 1997. However, MOLA will not be able to map the topography of the south polar deposits before March 1999, after the launch of the 1998 Mars Polar Lander. To assist in evaluating these terrains prior to launch and to assess formation and erosion processes in the polar deposits, we have assembled Viking stereo mosaics of the region and have produced the first reliable DEM models of the south polar deposits using automated stereogrammetry tools [1,2]. The image sequences employed cover the region from 90°S to 75°S and from 0°W to 120°W, including the Dorsa Argentea and Cavi Angusti deposits. These stereo pairs have a vertical exaggeration of 3.5, and the DEMs have a nominal contour interval of roughly 50 m. Additional stereo mapping coverage includes the original mission target longitudes for the polar lander of 200°W to 250°W, at somewhat lower resolution.

Here we report our preliminary topographic results, pending final image pointing updates. The maximum total thickness of the layered deposits in the south polar region is 2.5 km. The thick layered deposits consist of a series of megaterraces. Each terrace is several tens of kilometers wide and is flat or slopes very gently toward the pole. These terraces step downward from a central plateau near the south pole. Terraces are bounded by relatively steep scarps 100–500 m high that face toward the equator. These scarps correspond to the pattern of dark spirals observed within the residual cap in southern summer, and are interpreted as ice or frost-free surfaces warmed by solar insolation. Several tongue-shaped troughs, with rounded cirquelike heads, are observed near the margins of the deposit. These troughs are 300–600 m deep and may be similar to troughs observed in the northern polar deposit.

Mariner and Viking observations of the polar layered deposits suggested that they are composed of alternating layers of ice-rich and nonvolatile material [e.g., 3,4] possibly related to climatic change. The morphology of the deposits has been ascribed to a process of disaggregation (due to solar-insolation-driven sublimation of ice), and removal of dust by wind [e.g., 3,5], although other models have been proposed. Our results are consistent with the basic concept of sublimation-driven disaggregation and removal of dust by wind predominantly along scarp faces. The terrace floors, some of which may be sloping gently toward the pole, may be sites of net deposition in the current climate or in the recent past. These new topographic data will provide important constraints on slopes, sublimation rates [e.g., 6], and other processes operating in the polar deposits.

References [1] Schenk P. et al. (1997) *GRL, 24,* 2467–2470. [2] Schenk P. and Bulmer M. (1998) *Science, 279,* 1514–1517. [3] Sharp R. (1973) *JGR, 78,* 4222–4230. [4] Herkenhoff K. and Murray B. (1990) *JGR, 95,* 1343–1358. [5] Thomas P. and Weitz C. (1989) *Icarus, 81,* 185–215. [6] Moore J. et al. (1996) *Icarus, 122,* 63–78.

MEASURING SNOW STRUCTURE AND RESISTANCE WITH A HIGH-RESOLUTION PENETROMETER.

M. Schneebeli[1] and J. B. Johnson[2], [1]Swiss Federal Institute for Snow and Avalanche Research (SLF), CH-7260 Davos Dorf, Switzerland (schneebeli@slf.ch), [2]USA-CRREL-AK, Building 4070, P.O. Box 35170, Fort Wainwright AK 99703-0170, USA (jjohnson@crrel.usace.army.mil).

Introduction: It is possible that the polar cap of Mars is covered by CO_2 snow or ice. The measurement of mechanical properties of snow is extremely difficult because of the pronounced spatial variability and often very thin layers. In addition, the often very fragile structure makes usual mechanical tests difficult to apply. We developed a high-resolution penetrometer that measures the penetration resistance for each 4 μm. From the recorded force signal we are able to infer (1) micromechanical information about the bonding of the snow crystals, (2) microstructural information about the distance between bonds, and, indirectly, (3) the size of the snow crystals.

Construction: The penetrometer consists of a small measuring tip, 5 mm in diameter with a 60° included angle (Fig. 1). This tip is connected to a high-resolution force transducer, which is housed in a drive cone and rod 16 mm in diameter. The drive rod is geared and driven by a constant speed rotary motor [1]. The force transducer has a range from 0 to 500 N and a resolution of 0.01 N. The penetration velocity is 20 mm s^{-1}, but can be varied between about 5 and 30 mm s^{-1}. The resulting data have to be acquired at a frequency of 5000 Hz.

Measurements: We measured different snow types in the laboratory and in the field. A comparison between the tensile strength and the penetration resistance is given in [2]. We measured penetration resistance in snows ranging from very light new snow (40 kg m^{-3}) to very dense snow occurring on ski race tracks (500 kg m^{-3}). The very light new snow was at the detection limit of the force sensor, and the hard ski-track snow was difficult to penetrate.

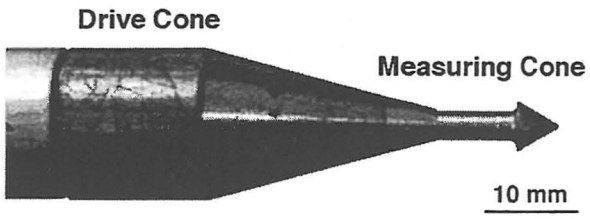

Fig. 1. Construction of the tip section of the penetrometer.

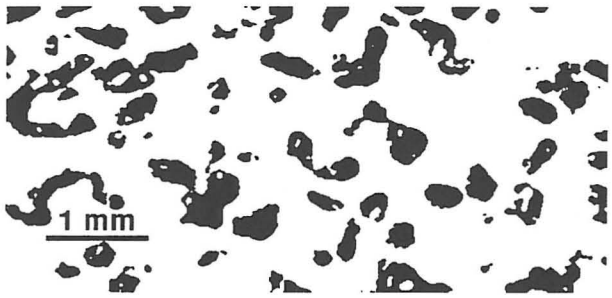

Fig. 2. Surface section of fine-grained snow.

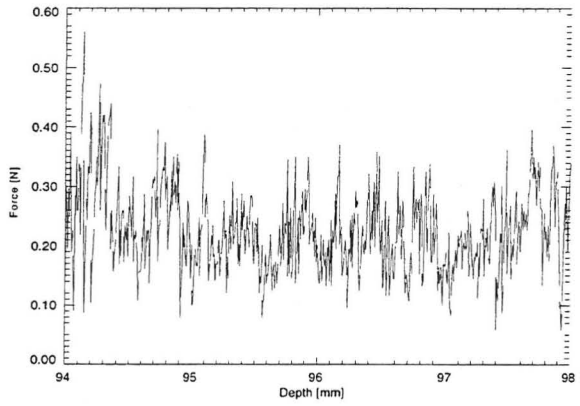

Fig. 3. Penetration measurement made in fine-grained snow shown in Fig. 2.

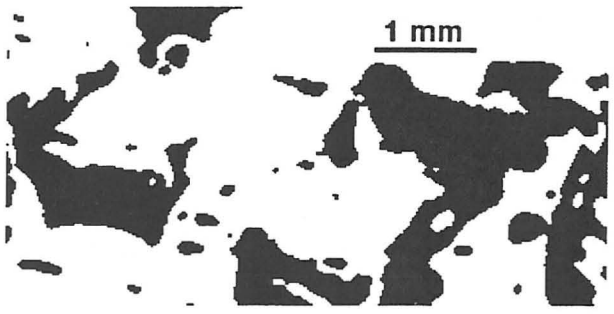

Fig. 4. Surface section of coarse-grained, temperature gradient metamorphosed snow.

Figures 2–5 compare serial sections and the corresponding penetration-resistance measurements. They show that length of the rising portion is dependent on the snow structure. We defined a structural index as grain size divided by the density of the snow. This structural index can be fitted over a wide range of snow with the coefficient of variation measured on a range of 4 mm (250 data points). More refined interpretations of the signal are currently underway.

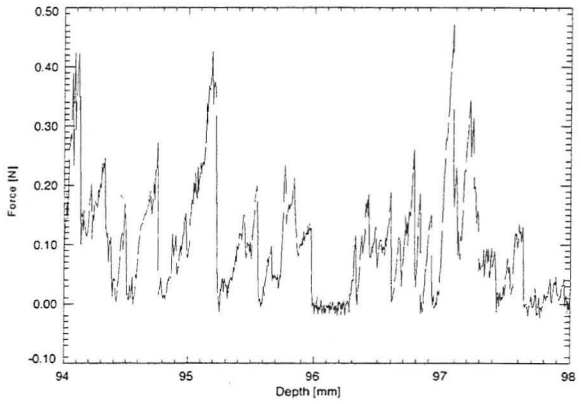

Fig. 5. Penetration measurement made in coarse-grained snow shown in Fig. 4.

References: [1] Johnson J. B. and Schneebeli M. (1997) *U.S. Patent Application 08/850,160.* [2] Schneebeli M. and Johnson J. B. (1998) *Ann. Glaciol., 26,* 107–111.

DOWNSLOPE WINDSTORMS IN THE MARTIAN POLAR REGIONS: A SENSITIVITY STUDY.

T. Siili, Finnish Meteorological Institute, Geophysical Research Division, P.O. Box 503, FIN-00101 Helsinki, Finland (Tero.Siili@fmi.fi).

Introduction: When large-scale flow takes place over and across an obstacle (e.g., a mountain range) or the flow over a plateau reaches a topographical (often steep) downward slope, strong downslope surface winds — attributed to the *shooting effect* or to *downslope windstorms* — are observed along the lee sides of the obstacles or topographical drops [see, e.g., 1]. On Earth these downslope storm events are known with a number of regional names, such as föhns, boras, and chinooks, depending on the region and whether the flow is typically colder or warmer than its surroundings.

The occurrence of a downslope windstorm is linked with a combination of subcriticality or criticality of a flow arriving at the obstacle or the slope edge, and subsequent supercriticality of the flow at the edge or further down the slope, and ensuing conversion of potential energy to kinetic energy [1]. In supercritical flow, the local Froude number is Fr > 1. The Froude number is defined as

$$\mathrm{Fr} = \frac{\bar{u}^2}{c^2} = \bar{u}^2 \frac{1}{gH} \frac{\rho_1}{\delta\rho}$$

where $\bar{u}$ is the mean flow speed, c the shallow-water wave speed, g the acceleration of gravity, H the mean height of the strongly stable near-surface layer, and $\delta\rho_1/\rho$ the fractional change in density across the interface between the lower stable layer and the weakly stable layer above it.

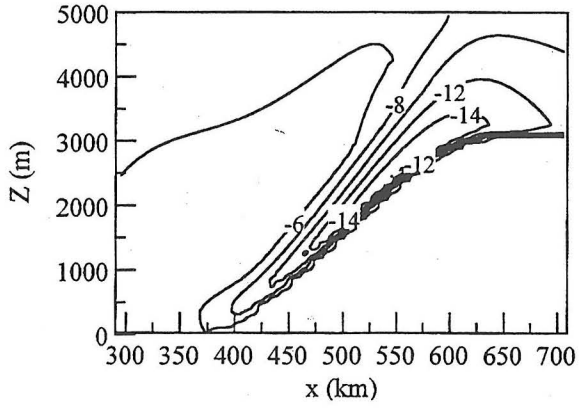

Fig. 1. The difference in the upslope/downslope wind component u at ~1600 local time between simulations with no large-scale wind and with southerly (from the right) 7 m/s large-scale wind. The slope angle is 0.6° and the plateau on the righthand side is fully covered with CO_2 ice with the coverage fraction gradually decreasing to zero by x = 350 km.

Plausibility and Indications of Martian Downslope Windstorms: Due to the spring and summer sublimation flows off the polar caps and due to the steeply sloped topographical features in, e.g., the Hellas and Argyre impact basins, the downslope windstorms are plausible especially in the southern polar regions of Mars. Recently this author and coworkers have used the Department of Meteorology/University of Helsinki (DMUH) two-dimensional Mars Mesoscale Circulation Model (MMCM; for model features see [2,3] and references therein) to simulate combined ice-cap edge and slope winds in idealized conditions corresponding to the martian late winter season and the southern slopes of the Hellas and Argyre impact basins [4]. Carbon dioxide ice coverage and subsequent low surface temperature on the plateau above the sloped region renders the near-surface flow arriving at the slope edge highly stable. The results of the simulations reported in [4] with southerly, downslope, large-scale flow (7 m/s, estimate derived from the NASA Ames Mars Global Circulation Model) indicate downslope wind component enhancement clearly exceeding the large-scale flow contribution and supercriticality of the flow above the sloped region (Fig. 1).

Maximum wind speeds in the simulations exceed 30 m/s and surface stresses are of the order of 20 mN/m^2, i.e., close to dust-lifting threshold estimates. The windstorms may hence play a significant role in lifting dust — at least in the impact basin regions — since these regions are also known areas of dust lifting and dust storm activity [5].

Sensitivity Study: In [4] the single, vertically constant large-scale wind of 7 m/s and fixed slope angle of 0.6° were used. In this work the sensitivity to large-scale flow and to slope angle have been investigated. The dust optical thickness has been set to $\tau = 0.3$, approximately corresponding to the martian dust background. The season(s) and latitude(s) are chosen to be in line with the locations of the seasonal ice cap edge(s) and plausible sloped terrains in the polar regions.

Sublimation flow. Since the Froude number increases as the square of the mean flow speed, even relatively small increases in the flow speed may induce significant changes in the windstorm spatial and temporal patterns and characteristics. In this work simulations have been made using a set of vertically constant wind fields with varying magnitudes.

Carbon dioxide sublimation flow off the polar caps is a particularly relevant special case of large-scale flow in the martian polar regions. Since the source of the mass flow is the surface ice, the flow tends to be concentrated close to the surface. To simulate the specific influence of the sublimation flow on the windstorms, the DMUH MMCM provision for use of vertically varying large-scale flow structure — previously used in study of the sensitivity of the southern polar cap edge winds to the sublimation flow [3] — has been used. The sublimation flow vertical structure may trigger downslope windstorms even in conditions of generally quiescent large-scale winds at higher altitudes.

Slope angle. The slope angle value of 0.6° used in [4] is a representative value derived from the DTM topography dataset. According to the DTM, even steeper slopes may occur in the Hellas Basin; also, the topographies and slopes of the polar regions are — until we obtain the results of surface mapping by the Mars Global Surveyor's altimeter — so far known to be less than satisfactory. To shed light on the correlation between the steepness of the slope and the characteristics of the windstorms, a number of simulations have been carried out using a set of reasonable slope angle values.

References: [1] Atkinson B. W. (1981) *Meso-scale Atmospheric Circulations,* Academic, London. [2] Savijärvi H. and Siili T. (1993) *J. Atmos. Sci., 50,* 77–88. [3] T. Siili et al. (1997) *Adv. Sp. Res., 19,* 1241-1244. [4] Siili T. et al. (1998) *Planet. Space Sci.,* submitted. [5] Kahn R. A. et al. (1992) in *Mars* (H. H. Kieffer et al., eds.), pp. 1017–1053, Univ. of Arizona, Tucson.

MICROBIAL EXPERIMENTS ON BASAL ICE FROM JOHN EVANS GLACIER, EASTERN ELLESMERE ISLAND, NORTHWEST TERRITORIES, CANADA. M. Skidmore[1], J. Foght[2], and M. Sharp[1], [1]Department of Earth and Atmospheric Sciences, University of Alberta, Edmonton, Alberta, T6G 2E3, Canada (Mark.Skidmore@ualberta.ca; Martin.Sharp@ualberta.ca), [2]Department of Biological Sciences, University of Alberta, Edmonton, Alberta, Canada, T6G 2E9 (Julia.Foght@ualberta.ca).

Recent research on permanent-ice associated microorganisms has focused on surficial ice environments [1,2]. We present evidence that, to the authors' knowledge, is the first example that aerobic and anaerobic bacteria can be cultured at 4°C from sediment-rich basal ice from a large polythermal Arctic glacier (John Evans Glacier) [3]. This builds on previous work [4] in which we demonstrated that both aerobic and anaerobic microbes exist in viable populations in subglacial meltwaters at the same glacier, and that the populations increase with sediment concentration. This high Arctic glacier (at 80°N) may be a reasonable terrestrial analog for martian polar environments, and hence the findings of this study may be important in assisting sampling program development for microbiology in the martian polar regions.

Sterile samples of both debris-rich basal ice and debris-poor (clean) glacier ice were taken aseptically from the glacier margin in the spring of 1997 prior to the onset of the melt season to examine whether any observed microbial activity was linked to sediment concentration. The samples were melted slowly in a sterile environment and then incubated at 4°C under nutrient-amended and nutrient-unamended conditions for three months. Parallel sterile and poisoned controls were included to account for abiotic processes. In all cases microbiological activity was recorded in the sediment-rich samples amended with growth medium. This indicates that viable

anaerobic and aerobic bacteria were present in the debris-rich basal ice.

The dissolved organic C (DOC) concentrations and $\delta^{13}C$ DOC of unamended ice samples were also analyzed [5]. DOC concentrations in the basal ice were 4× higher than in the clean ice. Furthermore, the $\delta^{13}C$ values of the DOC suggested different sources for the DOC in the two types of ice.

The higher DOC values in the unamended basal ice samples suggest that there is *in situ* microbial activity in the subglacial sediments. This is supported by the presence of viable microbial populations in the basal sediments. Hence, *in situ* oxidation/fermentation of organic C in basal sediments beneath the ice is a tenable process in high Arctic subglacial environments. This work shows that bacteria can function in anaerobic conditions at temperatures close to freezing. Similar conditions may exist or may have existed in the basal sediments and ice at the base or margins of the martian polar ice caps. Such environments should therefore be examined for evidence of life on Mars.

References: [1] Psenner R. and Sattler B. (1998) *Science, 280,* 2073–2074. [2] Priscu J. et al. (1998) *Science, 280,* 2095–2098. [3] Skidmore M. L. et al., in preparation. [4] Skidmore M. L. et al. (1997) *GSA Abstr. with Progr., 29(6),* 362. [5] DOC analyses performed by K. Leckrone.

AN OVERVIEW OF OBSERVATIONS OF MARS' NORTH POLAR REGION FROM THE MARS GLOBAL SURVEYOR LASER ALTIMETER.

D. E. Smith[1] and M. T. Zuber[1,2], [1]Mail Code 920, Laboratory for Terrestrial Physics, NASA Goddard Space Flight Center, Greenbelt MD 20771, USA (dsmith@tharsis.gsfc.nasa.gov), [2]Department of Earth, Atmospheric and Planetary Sciences, 54-518, Massachusetts Institute of Technology, Cambridge MA 02139, USA (zuber@tharsis.gsfc.nasa.gov).

Background: Since its arrival at Mars on September 15, 1997, the Mars Global Surveyor (MGS) [1] has been in a near-polar elliptical orbit, with the orbital eccentricity decreasing during orbital periapse passes where the spacecraft aerobrakes through the martian atmosphere. The Mars Orbiter Laser Altimeter (MOLA) [2], an instrument on the MGS, has the ability to range to the martian surface during nonaerobraking passes. MOLA can operate whenever the range from the spacecraft to the surface is <786 km, with the limit determined by the number of bits encoded for the range measurement [2].

During the capture orbit, aerobraking hiatus, and science phasing orbit (SPO) mission phases, MOLA acquired approximately 200 profiles across the northern hemisphere of Mars and provided more than 2,000,000 measurements of the radius of the planet. These observations cover the region from the north pole to ~10°S latitude with a precision of a few tens of centimeters and an accuracy (at present) of about 30 m. Absolute accuracy of the elevations is limited by the knowledge of the MGS orbits; these should improve later in the mission due to a more optimal tracking geometry, an improved gravitational field, and the use of the high-gain antenna once the spacecraft achieves its ~400-km-altitude circular mapping orbit. MOLA measurements so far show a planet with a low, flat high-latitude region in the north and a higher, topographically rougher terrain nearer the equator [3]. The north polar cap stands ~2–3 km above the surrounding terrain and displays deep chasms and complex structure. MOLA measurements of elevation, 1064-nm reflectivity, and backscattered pulse width indicate that the layered terrains are composed mainly of ice [3].

Radius and Flattening: The MOLA data have provided a new estimate for Mars' mean equatorial radius of 3396.0 ± 0.3 km and a north polar radius extrapolated to beneath the icecap of 3373.4 ± 0.5 km. The corresponding flattening of the northern hemisphere is 1/(150 ± 3), ignoring, for the present, the possible effect of flexural loading [4]. Allowing for the 3.1-km offset of the center of mass from the center of figure along the rotation axis [5], the geometric flattening of the full planet would be expected to be ~1/174, which is less than earlier estimates [5,6]. When the addition of the icecap topography is taken into account, the flattening will decrease even further with respect to previous values.

If uncompensated, the polar caps will contribute to the planet's mass distribution and affect the moment of inertia, which may ultimately have implications for the stability of Mars with respect to polar wander. Work is under way to combine observations of polar cap shape with gravity observations [7] and flexural models [4]. The objective is to assess the role of the present-day cap with regard to Mars' dynamics, and to consider implications of different contributions of the polar caps for the global mass distribution in Mars' past.

Polar Deposit Observations: Topographic profiles across the northern polar cap (e.g., Fig. 1) show the height of the martian surface to increase sharply by ~1 km above the surrounding terrain at the cap edge at a latitude of ~80°N. Slopes at the margin of the cap are generally 15°–20° and are indicative of active or recent ablation [3]. The elevation of the cap increases toward the pole and achieves heights above the surroundings of 2–2.5 km at the highest latitude sampled in the nadir-oriented observations (86.3°). The ratio of MOLA's return to output laser pulse energy, which provides a measure of the 1064-nm reflectiviy, is a factor of 3 greater over the polar deposits than it is over the surroundings. This indicates an ice composition for the polar deposits [3].

The topographic profiles reveal striking surface topology of canyons and spiral troughs, which cut through the upper portions of the northern polar cap to depths as great as 300 m below the ice surface. Some chasms penetrate to nearly the level of surrounding terrain. The interiors of chasms exhibit significantly lower values of 1064 nm reflectivity than the nearby terrain, which verifies that these structures are sinks for windblown dust [8]. Chasm cross sections can be successfully explained by a radiative model based on preferential ablation of deposited dust [8].

MOLA observations have revealed that large areas of the ice cap are extremely smooth, with constant regional slopes over many tens of kilometers on the order of 0.2°. Regional slopes are comparable to those that have been observed on terrestrial ice sheets when scaled for the difference in gravity between Mars and Earth [9]. Topography on spatial scales of kilometers in several areas has been observed to be smooth at the resolution of the instrument (~30 cm). These surfaces also appear smooth at the spatial scale of the MOLA laser footprint (~100 m), as evidenced by the instrument's returned pulse width. Deposits outward of the main cap (Fig. 2) show regional slopes that are comparable to those observed in association with the central cap deposits, but the outer terrains exhibit less amplitude variation than the central cap deposits, even in areas where no dunes have been imaged. Such topographic variance may be indicative of stagnant ice in the outlying deposits [9].

The broadscale planform of the MOLA polar profiles shows evidence for viscous flow [10], which would be predicted by experimental data on H_2O ice rheology [11]. Simple radiative models can

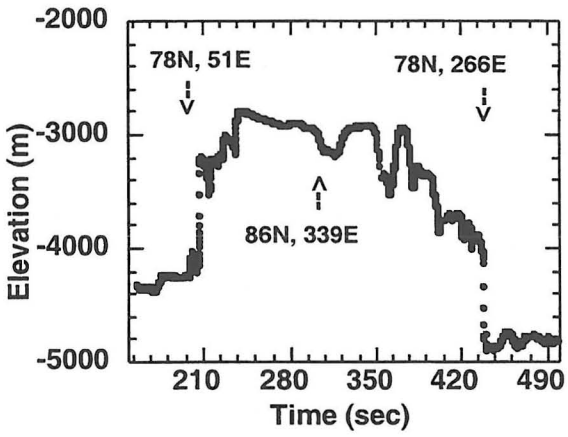

Fig. 1. MOLA Pass 210 across the north polar cap. The length of the profile is approximately 1200 km. Slopes at the icecap periphery are ~15°.

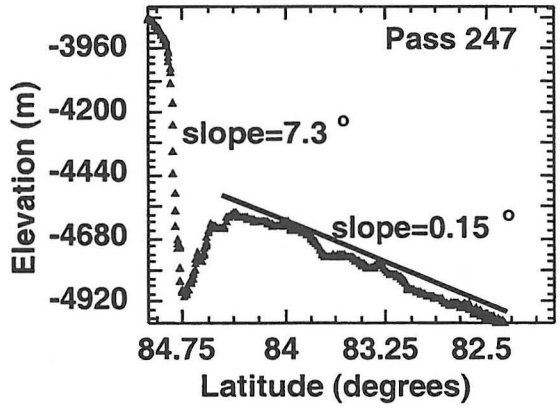

Fig. 2. MOLA Pass 247 shows the edge of the main cap deposit (Api) [13] at the far left and provides details of the regional and local slope distribution of outer cap deposits (Apl, Adl). Observed variations in measured topographic roughness do not correlate directly with mapped geologic units. The approximate longitude of the profile is 200°E.

also explain salient details of the cap shape (D. Muhleman, personal communication). Work is in progress to understand the contributions of each mechanism to the current macroscale morphology of the cap.

Polar Gap Observations: The inclination of the MGS orbit (~93.7°) results in an ~450-km-diameter gap in MOLA observations, centered on the pole. As a consequence, during a two-week period in June–July 1998 the MGS spacecraft was pointed off-nadir by ~50° on alternate passes to obtain data across the top of the icecap. A total of 10 passes were collected in this mode, which enabled the top of the icecap to be observed and its maximum height estimated. These observations were obtained at the peak of the expected maximum ice load in the northern hemisphere winter based on general circulation model simulations (R. Haberle, personal communication).

Dune Fields: MOLA profiled the vast dune fields that surround the polar cap. The dunes are typically ~15–50 m in height with crest-to-crest spacings of ~1 km in most cases, although the MOLA shot spacing of 330 m dictates that the along-track sampling is aliased. The geometric and topographic properties of the polar dunes are similar to some forms of terrestrial dunes, especially those that form sand seas or ergs in North Africa deserts (J. B. Garvin, personal communication).

Clouds: Over half the MOLA profiles collected in the SPO revealed the presence of clouds. Reflections from the atmosphere were obtained at altitudes from just above the surface to 15 km, but most were in the 5–10 km range. Most cloud detections were made at high latitudes, at the boundary of the icecap and surrounding terrain. The cloud detections were all made in the dark, but the distribution may be biased by the MOLA observation geometry (G. H. Pettengill, personal communication). Cloud returns were also obtained over some craters and other structures surrounding the polar region, and these also appear to have been in the dark [12].

References: [1] Albee A. A. et al. (1998) *Science, 279,* 1671–1672. [2] Zuber M. T. et al. (1992) *JGR, 97,* 7781–7797. [3] Smith D. E. et al. (1998) *Science, 279,* 1686–1692. [4] Solomon S. C. et al. (1998) *LPS XIX,* 1389–1390. [5] Smith D. E. and Zuber M. T. (1996) *Science, 271,* 184–188. [6] Bills B. G. and Ferrari A. J. (1983) *JGR, 83,* 3497–3508. [7] Tyler G. L. et al. (1998) *EOS Trans. AGU, 7.* [8] Ivanov A. B. et al. (1998) *LPS XXIX,* 1911–1912. [9] Zwally H. J. et al., in preparation. [10] Zuber M. T. et al., this volume. [11] Durham W. B. et al. (1997) *JGR, 97,* 16293–16302. [12] Ivanov A. B. and Muhleman D. O. (1998) *LPS XXIX,* 1784–1785. [13] Tanaka D. L. and Scott D. H. (1987) *U.S. Geol. Surv. Misc. Inv. Series Map, I-1802-C.*

DEEP SPACE 2: THE MARS MICROPROBE PROJECT AND BEYOND.

S. E. Smrekar and S. A. Gavit, Mail Stop 183-501, Jet Propulsion Laboratory, California Institute of Technology, 4800 Oak Grove Drive, Pasadena CA 91109, USA (ssmrekar@cythera.jpl.nasa.gov).

Mission Overview: The Mars Microprobe Project, or Deep Space 2 (DS2), is the second of the New Millennium Program planetary missions and is designed to enable future space science network missions through flight validation of new technologies. A secondary goal is the collection of meaningful science data. Two micropenetrators will be deployed to carry out surface and subsurface science.

The penetrators are being carried as a piggyback payload on the Mars Polar Lander cruise ring and will be launched in January 1999. The microprobe has no active control, attitude determination, or propulsive systems. It is a single stage from separation until landing and will passively orient itself due to its aerodynamic design (Fig. 1). The aeroshell will be made of a nonerosive heat shield material, Silicon

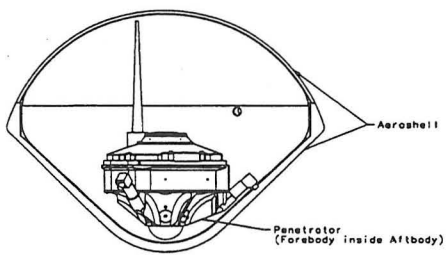

Fig. 1. Penetrator stowed within aeroshell.

Impregnated Reusable Ceramic Ablator (SIRCA), developed at Ames Research Center. The aeroshell shatters on impact, at which time the probe separates into an aftbody that remains at the surface and a forebody that penetrates into the subsurface (see Fig. 2). Each probe has a total mass of up to 3 kg, including the aeroshell. The impact velocity will be ~180 m/s. The forebody will experience up to 30,000 *g*'s and penetrate between 0.3 and 2 m, depending on the ice content of the soil. The aftbody deceleration will be up to 80,000 *g*.

The penetrators arrive in December 1999. The landing ellipse latitude range is 73°–77°S. The longitude will be selected by the Mars Surveyor Project to place the lander on the polar layered deposits in the range of 180°–230°W. The two micropenetrators are likely to land within 100 km of the Mars Surveyor Lander, on the polar deposits. The likely arrival date is L_s = 256, late southern spring. The nominal mission lasts 2 days. A science team was selected in April 1998.

System Design, Technologies, and Instruments: *Telecommunications.* The DS2 telecom system, which is mounted on the aftbody electronics plate, relays data back to Earth via the Mars Global Surveyor spacecraft, which passes overhead approximately once every 2 hr. The receiver and transmitter operate in the Ultraviolet Frequency Range (UHF) and data is returned at a rate of 7 Kbits/s.

Ultra-low-temperature lithium primary battery. One challenging aspect of the microprobe design is the thermal environment. The batteries are likely to stay no warmer than –78° C. A lithium-thionyl primary battery was developed to survive the extreme temperature, with a 6–14 V range and a 3-yr shelf life. The battery is also designed to withstand a worst case 80,000 *g* rigid body shock environment.

Advanced microcontroller. The microprobes will include an 8051-based data acquisition and control system with modest data processing capability. This microcontroller is an 8-bit processor with 64K RAM and 128K EEPROM. The system is designed for both very low power (<50 mW at 1 MHz, 1 mW sleep mode) and small volume and mass (<8 cc, 30–90 g). The microcontroller system will also include an internal 12-bit 16-channel analog-to-digital converter (ADC).

Flexible interconnects for system cabling. One packaging approach for the high-shock environment that will be demonstrated is flexible interconnects for system-level cabling. Flex is Kapton-based multilayer circuit carrier and interconnect technology. The flex circuits will include electrical interconnect layers formed with a patented anisotropic bonding material made of thermal glue matrix with embedded solder balls. This bonding technique can withstand temperature extremes and can be used to attach surface mount parts using reflow solder.

Instruments. The instrument package is designed to demonstrate that valid scientific measurements of both Mars atmospheric conditions and the subsurface soil characteristics can be obtained using micropenetrators. The primary experiment is the subsurface soil sampling/water experiment. An auger drill will extend out from the side of the forebody to approximately 1 cm (Fig. 2), collecting up to 100 ml of soil. After the sample is collected, the chamber is sealed and the sample is heated to release water vapor. The vapor will flow from the sample chamber through a vented analysis chamber. While in the analysis chamber, the vapor is illuminated by a tunable diode laser (TDL), and the transmitted power signal is measured to observe the 1.37-μm water absorption line.

The forebody also contains an impact accelerometer to determine the depth of penetration and presence of layering and temperature sensors to estimate soil conductivity. The single axis accelerometer has a range of –10 to 30,000 *g*, a precision of 10 *g*, and a sampling rate of 25 kHz. The instrument and expected science return are described more fully in [1]. The conductivity of the soil will be estimated using the cooldown rate of the forebody as recorded by two temperature sensors mounted near the outer wall of the forebody (Fig. 2). The soil conductivity is primarily a function of the grain size and the presence of frozen volatiles [2].

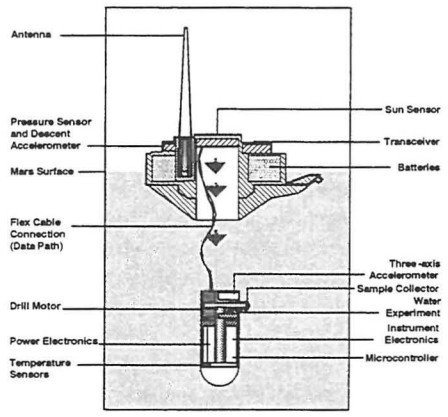

Fig. 2. Penetrator in deployed configuration.

The aftbody houses a surface atmospheric pressure sensor and a descent accelerometer to measure atmospheric drag on the microprobe. The atmospheric pressure sensor has a range of 0 to 25 mbar, a precision of 0.01 mbar and an accuracy of 0.03 mbar. The single axis descent accelerometer has a range of 1 to 40 *g*, a precision of 25 mg, and a sampling rate of 20 Hz. Measurement of the atmospheric density can be translated into pressure and temperature using the hydrostatic equation and the equation of state.

Beyond DS2: The technologies developed by DS2 have much to offer future missions in general and Mars polar missions in particular. The design objective of allowing multiple small landers for network science enables multiple measurements of any kind. The low mass of this type of lander and thus its lower ballistic coefficient allow it to reach any latitude on Mars at any opportunity. It is also capable of landing at elevations up to 6 km, and is robust with respect to the type of terrain. The current probe is intended to survive impact into solid ice and penetrate up to 20 cm. If it hits a rock approximately 10 cm or greater in diameter the probe is likely to fail. However, it can survive an incidence angle (the angle between the trajectory and the surface slope) of up to 27°. As the entry trajectory becomes more vertical as it reaches lower elevations, the incidence angle is a function of both elevation and local surface slope. Additionally, the forebody electronics are designed to function at –120°C and the battery operates efficiently down to –80°C.

The depth of penetration is a function of the diameter of the forebody, the velocity, and the mass. Increasing the mass does not severely increase the *g* loads, but for a given diameter is limited by a length-to-width ratio of approximately 5. An additional constraint is the position of the center of mass relative to the center of pressure. The center of mass must be very far forward in the aeroshell to obtain stability during entry. The size of the aeroshell and overall mass of the system is approximately linearly proportional to the mass of the penetrator. As a rough approximation, a 20-kg system (aeroshell + probe) might attain a depth of penetration of 2 m in a region with a high ice content.

Changing the instrument package would result in redesign of the electronics. The telecom system would likely have to be redesigned as well, depending on future relay options. However, packaging techniques for surviving high *g* loads permit a wide range of instruments. The primary techniques used to withstand high loads are the use of flex interconnect material rather than wire bonds, the smallest possible components, and either rigid or compliant mounting. The mission duration could be increased by adding solar power or increasing the battery mass.

The possibility for future joint U.S.-French "micromissions" to Mars was recently explored in a workshop at JPL on May 21–22. Spacecraft of up to 50 kg can be launched to Mars as piggyback payloads on the French Ariane carrier. These payloads are called ASAPs (Ariane Special Auxiliary Payloads). Many innovative instrument concepts were presented at the workshop for looking at oxidants, organics, the depth to the water or ice interface, and mineralogy or geochemistry based on the DS2 design.

References: [1] Moersch J. E. and Lorenz R. D., this volume. [2] Presley M. A. and Christensen P. R. (1997) *JGR-P, 102,* 9221–9229.

ROVERS FOR MARS POLAR EXPLORATION. C. Stoker, NASA Ames Research Center, Moffett Field CA 94035, USA.

Mobility is a generic capability needed for Mars exploration. Requirements for mobility range from those needed to get observations of individual rocks all the way to those for getting high-resolution observations of regional areas. Table 1 shows the required range of mobility to achieve various tasks.

The Pathfinder mission and field experiments simulating rover missions [1–5] provide guidance as to rover capabilities that can reasonably be expected in the next decade.

Rover mobility can be accomplished in a variety of ways, the most common being wheels or tracks and legged walkers. Wheeled vehicles can traverse over rocks smaller than 1/2 wheel diameter, and, with path planning to avoid larger rocks, can traverse terrains comparable to those seen on Mars in the Viking and Pathfinder landing sites. Slopes of 45° can be easily negotiated by wheeled rovers. Walking vehicles can negotiate even more complex terrain but require computation capability for leg placement. Extremely complex terrain was traversed by the Nomad II walker, which descended into (and most of the way out of) an active volcanic caldera (Mount Spur, AK) in 1995, although a slope failure eventually resulted in broken legs.

TABLE 1.

Requirement for Mobility	Range of Mobility
Traverse from landing site to target of interest	Size of landing error ellipse (~50 km) with current entry technology
Examine a specific science target	1–10 m (assuming the target is small)
Traverse from study target to study target	10–100 m (depends on spacing of targets)
Examine several different geologic processes	100s of m to few km (depends on proximity of different processes)
Examine geologic province	100s to 1000s km

The traverse range of a rover is limited by its science objectives, performance capabilities, and operational lifetime. The speed of rover traverse is a relatively minor factor. With a different communication system, and no stops for science experiments, Sojourner could probably have traveled a kilometer. But achieving land speed records is not a major objective of a science mission. Achieving science objectives requires targeting particular objects and studying them in detail, and the associated operational requirements will likely limit rover traverse range significantly. Traversing from target to target requires relatively few command cycles provided the traverse is over a short enough distance that it can be adequately planned. An operational goal of 100 m traverse per command cycle, arriving at a predetermined target, seems achievable. Investigating science targets requiring manipulator or instrument placement and sample collection will likely take several command cycles per target. Mission simulations [6] have demonstrated that traverse distances of 100–300 m, with detailed investigation of 5–10 targets, take 50–100 command cycles, (not unlike the Pathfinder experience, in spite of the use of larger, faster, more capable rovers). Significant advances in rover autonomy will be needed to improve this situation, and it is not clear how much improvement will be brought to flight programs in the next decade. Dust accumulation on solar panels degrades power over time; without dust removal, rover operational lifetimes may be limited to 90 sols. The lifetime of any system on Mars is limited by the stress of thermal cycling. For polar missions in summer, stresses due to thermal cycling and power outage at night are minimized. Therefore, polar missions represent fewer design challenges than low latitudes.

Rover payload is limited by the total mass that can be delivered to the martian surface and the design strategy for the overall mission. In the Mars Surveyor 2001 mission, as orignally described in the NASA Announcement of Opportunity, a rover of 40 kg, including a 15-kg payload, was to be delivered to the martian surface, riding "piggy-back" on a lander. The lander would have its own science payload as well as power and communication subsystems. Alternatively, the entire payload could be mobilized by landing on the legs or wheels, thereby increasing the mass available for a mobile science payload. An attractive concept for polar exploration would be to incorporate a walking mobility system on a lander and payload system similar to the Mars Surveyor '98 package.

Field experiments [6] have provided insight into the science capabilities of rover missions by comparing them with "ground truth." Science teams have been able to interpret rover observations correctly, but a consistent finding is that important things are missed. In one case [6], two out of three science teams missed clear evidence of aqueous sediments (an objective of the mission) within 30 m of the landing site, while a third team found this evidence. In another case [4], a suspected fossil structure was identied from imaging observations, and a sample was collected and returned. Detailed sample analysis performed in the laboratory failed to verify the fossil interpretation. However, other fossil structures (positively identified in the field) occurred nearby that were missed by the rover. Not surprisingly, science accomplishment correlates with imaging quality and data volume. The limitations of data transmission rate and the trade between image resolution and data volume are significant constraints for the operation of rovers.

Success of rover missions in achieving science goals depends on having adequate support imaging to enable traverses to targets of high science interest. Rover field experiments to date have used

aerial photographs to provide support imaging. Pathfinder Sojourner operated in the field of view of the IMP camera. Plans for the future involve the use of descent imagers. However, the descent imager planned for the 2001 mission achieves resolution adequate to plan rover traverses only in the near vicinity of the lander (within a few hundred meters). Aircraft could provide aerial support imaging with a resolution of 10 cm over the entire area accessible to a rover. Aircraft could also provide the mobility needed to explore regional scale areas (Table 1).

References: [1] Rover Team (1997) *Science, 278,* 1765–1768. [2] Greeley R. et al. (1994) *Proceedings of International Planetary Rover Symposium,* Russia. [3] Stoker C. (1998) *JGR,* in press. [4] Cabrol N. et al. (1998) *LPS XXIX,* Abstract #1013. [5] Arvidson R. et al. (1998) *JGR,* submitted. [6] Marsokhod, field experiment reports on http://cmex.arc.nasa.gov.

MARTIAN PALEOPOLAR DEPOSITS: EVIDENCE FOR A STABLE POLE AND PERIODS OF CLIMATE CHANGE.

K. L. Tanaka and G. J. Leonard, U. S. Geological Survey, 2255 North Gemini Drive, Flagstaff AZ 86001, USA (ktanaka@flagmail.wr.usgs.gov).

Introduction: The current polar deposits on Mars are sparsely cratered and indicate a total age of perhaps hundreds of millions of years [1], which corresponds to the late and possibly middle Amazonian epochs [2]. An investigation of possible earlier polar deposits may give significant insight into global climate and volatile history, polar wandering, and the development of the present polar deposits.

Candidate Polar Deposits: Here, we define polar deposits as material emplaced in similar fashion to that of present polar material, through condensation of ice and accumulation of dust coated with water and CO_2 ice during the winter. Although such deposits should be favored at near-polar latitudes, lower-latitude deposits may occur during periods of high obliquity or may have been at polar latitudes prior to polar wandering. Possible dust and ice deposits occur around the planet, and some have been proposed as paleopolar deposits or other ice and dust mantles formed during widespread depositional episodes. However, some of these deposits have been interpreted as other types of materials, including volcanic airfall deposits, ignimbrites, fluvial and lacustrine detritus, and evaporites. Thus the polar interpretation may not stick in each case.

Dimensions, location, relative ages, and morphologic characteristics of the largest of these deposits (>10^6 km^2) are summarized in Table 1, based on data from a variety of sources [3–8]. For the north polar deposits, mantle and dune material are included in the area estimate. We have also included unspecified Noachian terrains as possible major storehouses of eolian deposits; gradation and bombardment of the surface occurred at the highest rates planetwide during that period. However, discrete Noachian deposits are generally difficult to characterize and distinguish because of impact mixing and fluvial and eolian modification. These statistics indicate that polar and polar-type deposition of dust and ice deposits have played a significant role in sedimentation of large regions of Mars over virtually all major geologic periods.

Did Paleowander Occur?: In the scenario for polar wandering proposed by Schultz and Lutz [5], the Medusae Fossae Formation (MFF) and western Arabia deposits are proposed antipodal polar deposits. However, this scenario seems to have difficulties when considering the MFF's middle to late amazonian age [2]: (1) MFF likely overlaps in age with present polar deposits (Table 1); (2) the western Arabia deposits appear to be older than MFF; and (3) MFF postdates the majority of the development of the Tharsis rise, which has been suggested as a driving mechanism for polar wander on Mars [5] and which began in earnest by late Noachian and continued highly active throughout the Hesperian and early Amazonian [4].

Even if that particular scenario is unworkable, polar wander may have occurred through the growth of Tharsis. This volcanotectonic rise forms a large, equatorial topographic bulge that dominates the nonhydrostatic component to the planet's moment of inertia [9]. However, a calculation of the amount of polar wander that the Tharsis load may have induced resulted in a maximum estimate of only 9° [10]. Also, if large amounts of polar wander had occurred, sufficient surface stresses should have been imposed for the generation of distinctive fault patterns, which have not been observed for Mars [10].

Implications for Past Climate: If polar wandering has not occurred at least since the end of the Noachian, then the candidate Hesperian and Amazonian paleopolar deposits were emplaced at their current latitudes. Of these deposits, the south polar pitted plains material makes up the only paleopolar deposit at polar latitudes. The material's pitted character distinguishes it morphologically from the present polar layered terrains, which may indicate that its makeup is different. One possibility is that the pits represent thermokarst in which pockets of subsurface ice have been removed by melting or sublimation; loosened material may also have been removed by eolian erosion [12]. Suspect thermokarst of similar appearance also occurs in northern plains deposits, which are thought to be water-laid in a freezing climate [13]. Flow deposits of Hesperian age surround parts of the south polar pitted terrain [14]; these may represent debris flows formed by melting of an earlier polar deposit [15]. At Planum Boreale at the north pole, possible remnants of an early polar plateau form grooved terrain at the mouth of the large spiral trough, Chasma Boreale [14]. The plains material of the Vastitas Borealis Formation, surrounding Planum Boreale and partly overlaid by younger mantle and dune material, has a Late Hesperian age. A pair of studies indicate that these materials may have originated from a proto-Planum Boreale [15-16], perhaps similar in time to the formation of the outflow channels of Chryse Planitia. These observations at the north and south pole suggest the possibility of the melting of the polar ice caps and layered terrains during the Hesperian, in conjunction with outflow channeling. Climate changes like these may be driven by periods of high obliquity or by the introduction of large amounts of volatiles into the atmosphere by outflow channeling and or volcanism [17].

The Hellas interior deposits, like the Medusae Fossae Formation, show striking morphologic similarities to present polar deposits. Hellas basin, because of its low elevations, presents a cold trap for wintertime frost accumulation. The interior deposit may be an accumulation of transient dust that had been circulating about the planet during the Noachian, after which the atmosphere likely decreased in density and dust-moving capacity. If sufficient warming to melt polar deposits did occur later in the Hesperian, then the Hellas interior deposits must not have included a high proportion of ice, because they show no substantial evidence for meltdown.

Conclusions: The polar deposits on Mars provide an excellent laboratory not only for recent climate studies, but also the assessment of paleoclimate. Regional geologic considerations yield possible

TABLE 1. Characteristics of present and possible past polar deposits on Mars.

Feature	Location	Area (10^6 km^2)	Maximum Thickness (km)	Age*
Planum Boreale	66°–90°N	3.3	4–6	LA, present
Planum Australe	70°–90°S	1.5	3	MA-LA, present
Medusae Fossae Fm	0 ± 13°N, 126–221°W	2.5	5	MA-LA
Western Arabia	7°S–20°N, 332°–13°W	2–3	>1	LH?
Electris	31°–57°S, 165°–200°W	1.8	0.3–0.7	LH
South polar pitted plains	65°–84°S, 333°–110°W	~1	<1	EH-LH
Hellas interior	31°–51°S, 270°–312°W	1.3	1–2	EH
Noachin terrains?	planet wide	?	?	N

Feature	Morphologies	References
Planum Boreale	Layered, swirled troughs, surrounding dunes, mantle	[3,4]
Planum Australe	Layered, swirled troughs, etched surfaces	[3,4]
Medusae Fossae Fm	Layered, local troughs, lineated etched	[4,5]
Western Arabia	Smooth, etched margins, layered?	[5]
Electris	Dissected, knobby, chaotic	[6]
South polar pitted plains	Smooth, deeply pitted	[1,4,7]
Hellas interior	Deeply etched, hummocky, knobby plateaus	[4,8]
Noachin terrains?	Cratered plains and plateaus	

* Stratigraphic units: N = Noachian, H = Hesperian, A = Amazonian, E = Early, M = Middle, L = Late; see [2].

scenarios for climate change and emplacement of voluminous mantle deposits, which can be tested by further analysis and new Mars Surveyor datasets.

References: [1] Plaut J. J. et al. (1988) *Icarus, 75,* 357–277. [2] Tanaka K. L. (1986) *Proc. LPSC 17th,* in *JGR, 91,* E139–E158. [3] Dzurisin D. and Blasius K. R. (1975) *JGR, 80,* 3286–3306. [4] Tanaka K. L. et al. (1988) *Proc. LPSC 18th,* 665–678. [5] Schultz P. H. and Lutz A. B. (1988) *Icarus, 73,* 91–41. [6] Grant J. A. and Schultz P. H. (1990) *Icarus, 84,* 166–195. [7] Grizzaffi P. and Schultz P. H. (1989) *Icarus, 77,* 358–381. [8] Tanaka K. L. and Leonard G. J. (1995) *JGR, 100,* 5407–5432. [9] Esposito P. B. et al. (1992) in *Mars,* pp. 209–248, Univ. of Arizona, Tucson. [10] Willeman R. J. (1984) *Icarus, 60,* 701–709. [11] Banerdt W. B. et al. (1992) in *Mars,* pp. 249–297, Univ. of Arizona, Tucson. [12] Sharp R. P. (1973) *JGR, 78,* 4222–4230. [13] Costard F. M. and Kargel J. S. (1995) *Icarus, 114,* 93–112. [14] Tanaka K. L. and Scott D. H. (1987) *USGS Map I-1802-C.* [15] Jöns H.-P. (1991) *The Planet Mars (map),* Lithograph. Inst. Berlin. [16] Tanaka K. L. (1997) *JGR, 102,* 4131–4149. [17] Baker V. R. et al. (1991) *Nature, 359,* 589–594.

TERRESTRIAL ICE SHEETS: STUDIES OF CLIMATE HISTORY, INTERNAL STRUCTURE, SURFACE, AND BEDROCK.

Th. Thorsteinsson, J. Kipfstuhl, U. Nixdorf, H. Oerter, H. Miller, D. Fritsche, F. Jung-Rothenhaeusler, C. Mayer, M. Schwager, F. Wilhelms, D. Steinhage, and F. Goektas, Department of Glaciology, Alfred Wegener Institute for Polar and Marine Research, P.O. Box 120161, D-27515 Bremerhaven, Germany (tthorste@awi-bremerhaven.de).

Deep Ice Core Studies: Recently drilled deep ice cores from Central Greenland (GRIP and GISP2) provide the most detailed results available on climatic variation in the northern hemisphere during the last 100,000 years [1–3], a period that includes the Holocene (0–11.5 ka) and most of the Wisconsin glacial period. Summer-winter variation in various physical and chemical properties of polar ice allows dating of ice cores by annual layer counting. Several such methods are currently being employed on an ice core drilled by the new North Greenland Ice Core Project (NGRIP), which is aimed at extending the Greenland ice palaeoclimatic record through the last interglacial, the Eemian. Two examples will be presented: (1) visual and photographic studies of seasonal variation in stratigraphic layering, crystal size, air bubble and clathrate concentration [4,5], and (2) studies of electric stratigraphy, using the method of dielectric profiling (DEP) [6]. This method records the AC conductivity of ice cores, which is negatively correlated with the concentration of airborne dust in the ice but positively correlated with volcanic and marine aerosols.

Surface Traverses: Comprehensive surface traverse programs, which include shallow coring and ice velocity measurements, have recently been carried out by the Alfred Wegener Institute in previously little-investigated regions of Greenland and Antarctica. Serving partly as reconnaissance prior to deep drilling projects, such studies also help to reduce considerable uncertainties in the mass balance of the two large polar ice sheets and thus in their estimated response to climate change. Main results of a recent traverse in North Greenland include the following: (1) A new map of the accumulation distribution on the ice sheet indicates a large low-accumulation region in Northeast-Greenland [7]; (2) North Greenland records show significantly greater climatic variability during the last 500 yr than corresponding records from the southern part of the ice sheet [8]; and (3) data on variation in accumulation rates do not indicate a definite trend in the region during this century [9].

Radio Echo Sounding: The Alfred Wegener Institute has in recent years employed both airborne and ground-penetrating ice radar systems to map the bedrock around deep drilling sites in Central and North Greenland, as well as in a planned Antarctic site in Dronning Maud Land [10,11]. The radar also records shallow and deep internal echoes, caused by rapid variation in density and ice acidity in layers of certain ages, allowing isochrones to be traced over wide reaches of the ice sheet. Disturbances in regular stratigraphic layering, due to ice flow over an irregular bed, were observed in the lowest 200–300 m of the GRIP and GISP2 ice cores [12,13]. Since the aim of the new NGRIP coring program is to obtain an ice core reaching further back in time than the Central Greenland cores, this site was chosen in a region where the bedrock is relatively flat. Echo-sounding surveys between GRIP and NGRIP show that the isochrones lie 100–200 m higher above the bed at NGRIP, indicating that the Eemian layer is unlikely to have been disturbed by ice flow at this location.

Ice Margin Studies: Due to the flow pattern of ice sheets, layers forming a vertical sequence in the interior regions of an ice

sheet can, under favorable conditions, be traced on horizontal profiles at the margins. Some meaningful correlations have already been established between Greenland deep ice core climatic records and corresponding records from ice margins [14]. In these regions, a clear contrast is observed between ice of Holocene origin and significantly darker-looking ice dating from the Wisconsin glacial period, which displays summertime ablation rates 2–4× higher than the Holocene ice. This difference is due to higher concentrations of dust and other impurities in the Wisconsin ice, by 1–2 orders of magnitude, leading to reduced albedo [15]. Furthermore, smaller crystal sizes in the Wisconsin ice lead to a more homogeneous distribution of impurities on the surface, which probably contributes to lowering the albedo.

Recrystallization and Rheology: Comprehensive studies of ice crystal size and c-axis orientations on the GRIP and NGRIP deep cores provide detailed information on recrystallization processes in polar ice sheets [16]. Based on the GRIP results, the Central-Greenland ice sheet can be vertically divided into three different recrystallization regimes: (1) normal grain growth regime (0–700 m), in which the average crystal size increases steadily to 4 mm diameter; (2) polygonization regime (700–2800 m), in which crystals are subdivided due to increasing strain and no further increase in crystal size is observed; and (3) migration recrystallization regime (2800–3050 m), where higher temperatures (–10°C) cause rapid crystal growth with average diameters increasing to 30 mm in the bottom layers. Higher impurity content in ice dating from glacial periods is seen to exert a strong inhibitive effect on crystal growth. The data on c-axis fabrics demonstrate the development of crystalline anisotropy with depth, leading to significant variation in flow properties. In particular, strong rheological contrasts are observed between glacial and interglacial ice, with fine-grained ice dating from glacial periods deforming more rapidly under conditions of simple shear than more coarse-grained interglacial ice [17].

Lake Vostok Modeling: When the dynamics of ice masses are addressed by modeling, special attention must be given to the transition zone between ice resting on bedrock and floating ice shelves. One application for numerical ice-dynamics models that deal with such transition zones is the investigation of areas with special mass balance characteristics, like ice streams entering ice shelves or ice sheet areas over subglacial lakes. Recent results from a model applied to the ice above Lake Vostok in East Antarctica indicate that comparatively strong basal melting and adjacent refreezing occur close to the western shore of the lake [18]. This might have implications for the study of the deepest part of the Vostok deep ice core drilled down to 50 m above the lake, as well as on the history of the lake water itself.

References: [1] Dansgaard W. D. et al. (1993) *Nature, 364,* 218–220. [2] Johnsen S. J. et al. (1997) *JGR, 102,* 26397–26410. [3] Mayewski P. A. et al. (1997) *JGR, 102,* 26345–26366. [4] Wilhelms F. et al. (1997) *Eos Trans. AGU, 78.* [5] Kipfstuhl J. et al. (1997) *Eos Trans. Nav., 78.* [6] Wilhelms F. et al. (1998) *J. Glaciol,* in press. [7] Jung-Rothenhaeusler F. et al., *J. Glaciol.,* submitted. [8] Fischer H. et al. (1998) *GRL, 25,* 1749–1752. [9] Schwager M. (1998) *Ber. Polarforsch.,* in press. [10] Nixdorf U. et al., *Ann. Glaciol.,* submitted. [11] Steinhage D. et al., *Ann. Glaciol.,* submitted. [12] Kipfstuhl J. and Thorsteinsson Th. (1993) *Eos Trans. AGU, 74.* [13] Alley R. B. et al. (1995) *Nature, 373,* 393–394. [14] Reeh N. et al. (1993) *NATO ASI Ser., I12,* 481–497. [15] Boeggild C. et al. (1996) *Ann. Glaciol., 23,* 144–148. [16] Thorsteinsson Th. et al. (1997) *JGR, 102,* 26583–26599. [17] Dahl-Jensen D. and Gundestrup N. (1987) *IAHS Publ.170,* 31–43. [18] Mayer C. and Siegert M., *J. Glaciol.,* submitted.

DENSIFICATION OF SURFACE DEPOSITS ON TERRESTRIAL AND MARTIAN ICE SHEETS. E. D. Waddington[1], G. D. Clow[2], and D. P. Winebrenner[3], [1]Geophysics Program, University of Washington, Seattle WA 98195-1650, USA (edw@geophys.washington.edu), [2]Climate History Program, U.S. Geological Survey, Denver CO 80223, USA, [3]Polar Science Center, University of Washington, Seattle WA 98195, USA.

Earth and Mars both have polar water ice caps with thicknesses on the order of a kilometer and spatial scales on the order of hundreds of kilometers. These ice caps on both planets must flow under the influence of gravity; maintenance of a steady state then requires accumulation of mass at high elevations and loss of mass at low elevations. The ice sheet thickness divided by the "typical" mass accumulation rate (meters of ice per year) gives a characteristic response time for ice sheets on both planets. Values of tens of kiloyears are typical on Earth; characteristic times measured in megayears are expected on Mars.

At shorter spatial and temporal scales, these ice sheets may be more qualitatively dissimilar, in that ice-sheet surface processes may be controlled by quite different physical considerations on the two planets. On Earth, snow forms as a result of thermodynamic processes in the atmosphere and falls to the ice sheet surfaces, making layered deposits with relatively low density compared to ice. Gravitational settling dominates the subsequent transformation from snow through firn to glacial ice. The ice density is typically reached at depths on the order of 100 m. A characteristic compaction time can be derived from the strength of gravity, the density and viscosity of ice at the appropriate temperature, and the snow accumulation rate. On Mars, accumulation of water ice is probably dominated by direct deposition to the surface from the vapor phase, complicated by simultaneous deposition of CO_2 ice that later sublimates. As a result, the physical character of the surface deposits may depend more on local conditions than on regional atmospheric dynamics. If new ice deposits are not already at the ice density, post-depositional alterations may be dominated by vapor transport resulting from radiation, grain-scale physical properties, temperature gradients, and impurities, rather than by gravitational settling.

Starting from processes known to operate on Earth, we will summarize characteristic scaling parameters that can affect rates of deposition, the form of the deposition, and its subsequent density evolution. We then investigate the comparable scaling parameters in the martian environment to formulate order-of-magnitude expectations about the mass accumulation and density-depth variation on martian polar caps.

Finally we consider satellite and groundbased experiments whose measurements could be relevant both to understanding the evolution of new deposits and to the inverse problem of inferring accumulation rate from geophysical observations of the ice caps.

MASS BALANCE OF MARTIAN ICE CAPS: IS THERE ANOTHER TYPE OF POLAR GLACIER? A. T. Wilson, Department of Geosciences, University of Arizona, Tucson AZ 85721, USA (atwilson@u.arizona.edu).

Introduction: The recent discovery of water ice exposed to the atmosphere in the polar regions of Mars raises some interesting questions. It implies that at least some water vapor is being lost to the

atmosphere by these exposed ice surfaces. If one assumes steady state, the question immediately arises as to how this ice is being replaced. It is proposed that a new type of polar glacier is possible in very cold regions with large annual temperature cycles and with relatively low annual ablation. It is also suggested that terrestrial analogues exist, but they have never been described because they are relatively unspectacular and exist in remote regions seldom visited by glaciologists.

Background: All glaciers and ice sheets have a zone of accumulation (where the mass balance is positive) and a zone of ablation (where the mass balance is negative). The line separating these two zones is called the snow or equilibrium line. The mass balance of the ice body is maintained by the flow of ice across the snow line.

On Earth there are basically two kinds of glaciers/ice sheets — temperate and polar: (1) The temperate glaciers and ice sheets of the world are composed of ice that is everywhere at the melting point. Unlike polar glaciers, described below, temperate glaciers can utilize a freeze/thaw mechanism in order to flow, and temperate glaciers can move as much as a meter a day. (2) Polar glaciers and ice sheets are composed of ice that is everywhere below the pressure melting point. Movement can only take place by plastic deformation, which means that they can only move a few tens of meters per year. The colder the ice, the slower it can flow. In cold and arid regions, e.g., the Dry Valleys of Antarctica, the ablation zone is surrounded by vertical walls of ice 20 m high. Polar glaciers are frozen to their bed and do no cutting. The movement is within the ice itself, with the top of the frontal ice cliff (of a glacier at 20°C) moving 20 m a year and lower levels moving progressively more slowly, until at the bottom there is little movement with respect to the base. This often leads to the ice from the glacier frontal cliff calving in great slabs of broken ice that lie in front of the glacier until they ablate away.

Is It Possible to Have a Second Type of Polar Glacier?: Because ice can deform when subjected to stress, it does not form stress cracks as a result of the annual temperature cycles. This is not the case for frozen ice-impregnated ground. In polar regions, frozen ground can form very spectacular "polygons." These are polygon patterns of cracks that open in winter, and close in summer. During winter, sand and snow can blow into the open cracks to be compressed as the ground warms in the summer. The following winter, the system cracks again and the process repeats itself. As years pass, the sand wedge gets wider and wider. This results in heaving along the sides of the cracks, which leave a permanent record as "patterned" ground.

In the very high, cold regions of the McMurdo Dry Valleys (Antarctica), the author has observed that the small ice bodies have large stress cracks, often filled with snow. This is presumably due to the extremely cold ice in these ice bodies not being able to accommodate the thermal stresses imposed by the annual temperature changes. It is proposed here that as one goes to colder and colder arid areas there is a natural progression from the "normal" polar glaciers to the new (as yet unrecognized) type of ice body described here. The change from one type of polar glacier to the other is determined by the strain rate (controlled by the temperature of the ice) being unable to accommodate the rate of contraction of the ice body during the winter cooling. This latter is controlled by the summer-to-winter temperature change and the speed at which it occurs. During winter, dry powder snow (or the very fine "diamond dust" that falls in the very cold and arid polar regions) falls or is blown into these cracks. With the onset of summer the ice expands, and the snow trapped in the cracks is compressed into ice. This is a process analogous to the firn/ice transition of normal ice sheets and glaciers. This new type of ice body has a mechanism for acquiring ice that enables it to make up for ice that is lost by sublimation from the ice sheet surface. An important point is that this method of acquiring ice can take place below the snow line. Hybrid glaciers can exist, but in the extreme case, an ice body could exist completely below the snow line and have no snow-covered accumulation zone.

Are the ice bodies on Mars this third type of glacier? Such an ice body does not require an accumulation zone but does require: (1) a low mean annual temperature, with the consequent low annual ablation rate and low strain rate; (2) a large annual temperature cycle; and (3) some wind-blown dry power snow or diamond dust.

Proposed New Type Of Ice Body: (1) The ice body could be below the snow line. This means that it could be bare solid ice with no large snow fields. (2) Because of the very low temperatures in the ice body, there would be very little lateral movement, and hence no deep crevasses. (3) Since all the "action" takes place in the top few meters, the ice below the level to which the thermal stress cracks can penetrate could be extremely old and contain a record of the atmosphere and composition of precipitation from times long in the past. (4) A glacial "advance" may be manifested in a completely different way to normal terrestrial glaciers. For example, it may put a layer on the surface of the ice cap, like icing on a cake. (5) How would such an ice cap originate? Unlike most terrestrial ice sheets, which can start out as a patch of perennial snow, these "Wilsonian" ice caps would probably have to have evolved from a terrestrial-type ice cap that, as a result of a climatic change, became colder and colder until they could form annual stress cracks. If this is true, then the present ice caps on Mars must be very old, and contain ice at their base that is very old indeed.

Implications for Martian Exploration and Establishment of a Martian Base: If the hypothesis proposed above proves to be correct, then a martian ice sheet may be a very suitable place to establish a scientific base. The ice should provide a very stable platform. One could "mine" into the ice cap to below a level penetrated by the annual stress cracks and construct a base in the resulting ice cave. Such a situation has a number of important advantages: (1) The temperature would be the mean annual temperature; (2) there would be no wind which means the buildings can be of much lighter construction and the wind chill factor would be eliminated; (3) pure water in large quantities would be readily available, free of cosmogenic isotopes; (4) the overlying ice would protect personnel from cosmic-ray radiation and solar flares, which with the thin atmosphere of Mars might otherwise be a problem; and (5) it would be relatively simple to seal the ice cave and control the atmosphere to a suitable O pressure for human habitation. Lightly constructed but extremely well-insulated buildings would be constructed within the ice cave. Because of the extremely low temperatures involved it may prove worthwhile to construct one or more concentric hemi-cylindrical "igloos" over a line of buildings. This would be done using blocks of ice mined from the ice cave walls and cemented together with frozen water. This would provide an ice "building" at a temperature intermediate between the ice sheet and the living quarters, a place to perform "outside" work. It would also make the whole system more thermally efficient. It is very important not to significantly warm the ice forming the walls of the ice cave. Any significant warming would lead to the closing-in of the ice cave. Much of the technology needed

has already been developed for the construction of the Cold War military base at Camp Century (Greenland). Such a plan would greatly reduce the amount of building materials that would have to be transported from Earth.

Work to be Undertaken as a Result of the Above Discussion: *Satellite Photography.* Good satellite photographs of the martian polar ice sheets would resolve many of the following questions: (1) Do the ice fronts have vertical sides? (2) Is there a snow-covered accumulation zone in the center of the ice caps or is it bare ice? (3) Are the surfaces of the martian ice sheets covered with a pattern of cracks? (4) Is there snow in these cracks? and (5) Do the surface of the ice sheets have smoothly rising profile as do terrestrial ice sheets? (This is a "Nye" profile, where the slope of the ice sheet surface is inversely proportional to its thickness.)

Study of terrestrial analogs. An expedition should be sent to the McMurdo Dry Valleys in Antarctica to study in detail the terrestrial analogues of the martian ice sheets. The aim of this project would be to study in detail the proposed "snow infilled polygon crack" mechanism for adding new ice to an ice body lying below the snow line. This work would include: (1) The hand-drilling of many ice cores for examination and ^{14}C dating. This should confirm that the upper "shell" of the ice body is young and the ice below the thermal stress cracks is very old. (2) Confirmation that the ice in the center of the polygon is older than the ice adjacent to the crack. (3) Measurement of the chemistry of the "shell" vs the "core" ice. Since snow is being added to the shell and water is being lost from the shell, the chloride and other anions and cations should be enriched as compared to the core. The chloride concentrations would be measured in the field. (4) Measurement of the isotope composition of the H and O of the ice would be measured; this would indicate if any of the ice was of glacial age. (5) Measurement of the total air and CO_2 content of the ice. This would confirm that the snow in the closing cracks was being compacted into ice in a "dry" process, similar to the firnification process in a normal ice sheet, as opposed to melt water (high CO_2 low air content). (6) Measurement of the the isotopic composition of the O gas obtained in "4" above. This would also be an indication of the deep "core" ice being of glacial age.

WHERE DO WE LOOK FOR LIFE IN THE POLAR REGIONS OF MARS?

A. T. Wilson, Department of Geosciences, University of Arizona, Tucson AZ 85721, USA (atwilson@u.arizona.edu).

Introduction and Analysis of Problem: The problem is initially to decide where, in the polar regions of Mars, "ecological niches" might exist in which life forms may currently be present. To find "C-based" life (similar to our own) in other parts of the solar system, one must find places where liquid water in some form might exist. To locate currently living C-based life forms, the liquid water must have existed continuously on a geological (as opposed to a biological) timescale. The energy source for these organisms would, in the absence of photosynthesis, have to be chemical. For example, one such energy source is the reaction of atmospheric oxygen with ferrous iron to produce ferric iron. The ferric iron would interact with rock minerals and be converted back to ferrous iron. This is the case with iron bacteria on the Earth today. The life forms would take part in the weathering of the rock and derive their energy from it.

Approach Suggested: As will be discussed below, we favor looking for current life forms on Mars in very saline water. This is because such a system has a very low freezing point, and under cold conditions, can be in dynamic equilibrium with very low partial pressures of water vapor. Both these conditions are likely to exist or have existed on a planet such as Mars. In practice, this would mean a very concentrated Mg/CaCl solution produced by the weathering of rock. Such solutions can exist in a liquid state down to below –30°C at as low as 0.1 torr water vapor pressure.

Such a system has the advantage of being a "steady-state" system, able to exist for long times on a geological timescale. The problem for life forms in an intermittent non-steady-state system is how to survive the quiescent periods (with no energy source).

Terrestrial Model for Such a System: This proposal suggests that the geochemical system found in the cold rainless deserts of the Antarctic might be studied as models for similar, but probably more extreme, systems that probably exist or have existed in the past on Mars.

Dry Ice-Free Areas of High-Latitude Southern Hemisphere: Although much of the Antarctic continent is covered with ice and snow, some areas are ice-free. These so-called "dry areas" are extreme deserts, characterized by extreme cold and aridity. They are also unique among terrestrial deserts in being completely rainless. All precipitation falls as snow, which is lost by sublimation. If one digs into the loose "soil" of a dry area in this cold and arid region, one passes through loose dry debris and can suddenly strike a very hard and impenetrable layer, which on examination proves to be debris as above but cemented with ice crystals. Sometimes in late summer, saline water can be detected moving downslope along the surface of what Wilson [1] called the "frozen water table."

In the lowest points of dry enclosed drainage basins, one can sometimes sink into a subsurface shallow pond of very saline water. One of these, in the south fork of the Wright Valley, had a composition of 60,000 ppm chloride, 18,000 ppm Ca, 7000 ppm Mg, and 9900 ppm Na.

In an even more arid situation such as the surface of Mars, one would predict that the concentration of chloride would be higher, as would the Mg; this would be followed by the Ca, and the Na would be lower.

It is clear that in a cold rainless desert different phenomena exist that can produce subsurface shallow ponds of very saline water. On Earth we only just reach the beginning of this rainless desert ecosystem, but as Wilson [1] suggested two decades ago, Mars is also a rainless desert, and is probably even more arid. It would be a natural progression from the Antarctic systems, and may have similar subsurface pools of even more saline brine. It is suggested that these pools might be a place to look for "extraterrestrial" life.

The aim of the earlier work [1] was to understand the geochemistry of the Antarctic rainless deserts. How the salts were separated, and why some remained in the "soil" while others moved down-slope were areas of study.

Work to be Undertaken as a Result of Above Discussion: *Long term.* The above discussion suggests that we should put an infrared sensing satellite in polar orbit around Mars and look for halos of water vapor in topological depressions, particularly those in the front of glaciers. The very existence of bare ice suggests that the ice must be losing water by sublimation. If a steady-state situation is assumed, then there must be some form of snowfall that represents an

infall of salts to the drainage basin. These, over time, must end up as a subsurface saline pond in depressions in front of the ice sheets. This might ultimately be a prime area to look for life on Mars.

Short term. We should do research on Earth to answer the following questions: (1) Can we locate subsurface pools of saline brine in the Antarctic "Dry Valleys" using infrared sensing from an orbiting satellite? (2) Is the summertime water vapor higher over subsurface brine pools than their surroundings? Is it high enough to detect with infrared sensing from an orbiting satellite? The relative humidity over the brine is a constant under equilibrium conditions. It is a function of its concentration (strictly the fugacity of the water in the brine). It changes only slightly with temperature. The relative humidity of a sample of air of fixed water vapor pressure changes rapidly as the air warms. (Relative humidity is defined as the partial pressure of water vapor in the air, divided by the partial pressure of water vapor in the air if it were in equilibrium with pure liquid water at that temperature, expressed as a percent.) For this reason, one would expect water to be given up by the brine under warm conditions and to be adsorbed under cold conditions. Thus in "summer" under calm conditions, one might expect our brine pools to have a halo of water vapor above them.

The geomorphology on Mars is very similar to that of the older parts of the Antarctic dry areas. The weathering that creates these landforms on Mars is caused by the repeated recrystallization of salts made possible by the cycling of the relative humidity [2–4]. This lends strong support to the possibility that salts have been absorbing water from the atmosphere and going into solution. If this is occuring now, then it is possible that microorganisms may still be living in subsurface liquid brine ponds on Mars. If this happened in the past, then these subsurface ponds will have frozen or dried up. On a planet without life, the bodies/spores of these organisms would have a good chance of surviving millions of years in frozen brine or salt crystals. It would be a relatively simple matter to recover fossil microorganisms or spores from samples of frozen brine or salt crystals. There would be fewer problems with other objects that may look like microorganisms, since the matrix would be expected to be water soluble.

References: [1] Wilson A. T. (1979) *Nature, 280,* 205–208. [2] Wellman H. W. and Wilson A. T. (1965) *Nature, 205,* 1097. [3] Cotton A. and Wilson A. T. (1971) *Earth Sci. J., 5,* 1–15. [4] Cotton A. and Wilson A. T. (1971) *Z. Geomorph., 15,* 199–211.

THE INITIATION AND MAINTENANCE OF AN ICE SHEET AT THE MARTIAN SOUTH POLE. T. M. H. Wohlleben, Department of Earth and Atmospheric Sciences, University of Alberta, Edmonton, Alberta T6G 2E3, Canada (tmw2@gpu.srv.ualberta.ca).

During winter at the south pole of Mars, atmospheric CO_2 condenses out of the atmosphere and precipitates to the ground. Internal mass and energy feedbacks resulting from this process amplify the seasonal cycle, with ramifications for long-term climate.

A simplified model that incoporates balanced budgets for energy, moisture, and CO_2 is developed to investigate the factors responsible for the initiation and maintenance of an ice sheet at the martian south pole. Surface albedo and atmospheric absorption of longwave radiation are shown to be extremely important to the process.

RAMAN SPECTROSCOPY OF MARTIAN ANALOGS. D. D. Wynn-Williams[1] and H. G. M. Edwards[2], [1]British Antarctic Survey, High Cross Madingley Road, Cambridge, CB3 0ET, UK (ddww@ bas.ac.uk), [2]Chemical and Forensic Sciences, University of Bradford, Bradford BD7 1DP, UK.

The potential of Raman spectroscopic techniques for the characterization of molecular compounds of geological and biological relevance is well established. Spectroscopic techniques have been used extensively in space exploration to obtain information about the surfaces of planets. The *in situ* mineral identification is a challenge for planetary scientists and spectroscopists, and, for this, Raman spectroscopy is attractive since it can provide unique information on the structure and composition of oxyanion minerals and phase identification in mixtures [1]. In addition, the technical application of miniaturized, robust Raman spectrometers with remote-sensing heads for the robotic exploration of planetary surfaces and Antarctic analogues is receiving attention [2]. Martian soil simulates have been successfully studied as finely divided powders using such a system with a 25-μm sampling "footprint" [3].

We have compared near-IR and visible laser Raman spectroscopic techniques for the analysis of living organic material in rocks from the Antarctic Dry Valleys, analogous to those found on Mars [4, 5]. Cryptoendolithic microbes survive within rocks, chilled and desiccated by katabatic winds from the polar plateau and exposed to enhanced UVB radiation within the ozone "hole" [6].

Using an FT-Raman microscope system operating with 1064-nm excitation [5], we have studied the Raman spectra of cryptoendolithic communities in Beacon Sandstone. We have identified vibrational features characteristic of key markers such as hydrated Ca oxalate, chlorophyll, and carotenoids, as well as mineral deposits such as haematite and quartz. In this way, we now have a better understanding of the strategies employed by living organisms for survival under hostile, stressed environments.

We have also studied a martian meteorite, Nakhla (classified as an SNC meteorite), using different Raman techniques [7] to test their viability for the detection of organic and inorganic material at the micrometer level. Visible excitation in the red part of the spectrum (780 nm) proved superior for geological prospecting of nonfluorescent minerals (plagioclase, olivine, and clinopyroxene were evident). However, the near-IR equipment was definitely superior for the organic constituents of primitive photosynthetic organisms such as cyanobacteria, which autofluoresced strongly with visible excitation. These organisms were fundamental in the evolution of life on Earth and may be expected to have had a similar role on early Mars. An FT-Raman system probing the subsurface polar permafrost of Mars could send us the first fossil organic fingerprints of any previous martian microbial life.

References: [1] Cooney T. F. et al., Abstract #1332; El Goresy et al., Abstract #1707; Treiman A. and Treado P., Abstract #1196; Wang A. et al., Abstract #1523; Wang A. et al., Abstract #1819; all in (1998) *LPS XXIX.* [2] Edwards H. G. M. and Wynn-Williams D. D. (1998) *JBIS,* forthcoming. [3] Jolliff B. L. and Haskin L. A. (1995) *JGR, 100,* 21189–21199. [4] Russell N. C. et al. (1998) *Antarctic Science, 10,* 63–74. [5] Edwards H. G. M. et al. (1997) *J. Raman Spectroscopy, 28,* 685–690. [6] Bodeker G. (1997) in *Ecosystem Processes in Antarctic Ice-Free Landscapes,* (C. Howard-Williams et al., eds.) pp. 23–42, Balkema, Amsterdam. [7] Edwards H. G. M., forthcoming.

THE ROLE OF VISCOUS DEFORMATION IN THE MORPHOLOGY OF THE MARTIAN NORTH POLAR CAP.
M. T. Zuber[1,2], L. Lim[1,3], and H. J. Zwally[2], [1]Mail Stop 54-518, Department of Earth, Atmospheric and Planetary Sciences, Massachusetts Institute of Technology, Cambridge MA 02139, USA (zuber@tharsis. gsfc.nasa.gov), [2]Earth Sciences Directorate, Mail Code 900, NASA God-dard Space Flight Center, Greenbelt MD 20771, USA (zwally@ intrepid.gsfc.nasa.gov), [3]Center for Radiophysics and Space Research, Cornell University, Ithaca NY 14853, USA.

Background: The first detailed topographic measurements of Mars' north polar cap have recently been collected by the Mars Orbiter Laser Altimeter (MOLA) [1], an instrument on Mars Global Surveyor (MGS) [2]. These new data provide the opportunity to address in a quantitative way the processes responsible for the origin and evolution of the martian polar caps. On the basis of imaging and spectral observations from the Mariner 9 and Viking orbiters (see review in [3]), it was recognized that a number of physical mechanisms, including radiative transfer, wind erosion, and viscous flow, represent possible or probable contributors to the morphology of the polar cap. Here we review rheological data for H_2O and CO_2 at conditions relevant to the martian polar regions. We then use MOLA topographic profiles to perform a preliminary assessment of the role of power law flow in contributing to the regional-scale planform of the north polar cap.

MOLA Observations of North Polar Cap: During the capture orbit, aerobraking hiatus and Science Phasing Orbit (SPO) mission phases, the MOLA instrument acquired approximately 200 profiles across the northern hemisphere of Mars. At the time of the SPO orbits, the spacecraft periapsis was at high northern latitudes, which enabled detailed mapping of the north polar region. In its nominal nadir-viewing configuration, the instrument collected elevation data up to latitude 86.3°. The 93.7° inclination of the MGS orbit results in an ~450-km diameter gap in MOLA observations, centered on the pole. As a consequence, the MGS spacecraft was pointed off-nadir by ~50° on alternate passes during summer 1998 to obtain data across the top of the icecap. After correction for significant off-nadir pointing errors, these data will provide a measure of the maximum elevation of the northern cap.

In the MGS elliptical orbit, MOLA profiles have a surface spot size of ~70–300 m and a footprint-to-footprint spacing of ~300–400 m. The shot-to-shot precision of the instrument is a few tens of centimeters and measurements have an absolute accuracy of ~30 m [4]. Across-track accuracy varies with latitude and spacecraft groundtrack coverage.

H_2O Ice Rheology: To first order, the deformation of polycrystalline water ice under stress follows a power law rheology [6] that includes an Arrhenius temperature dependence

$$\varepsilon = A\sigma^n \exp[(-E^* - PV^*)/RT]$$

where ε is strain rate, σ is stress, n is an empirical stress exponent, R is the gas constant, and A, E*, and V* are empirical constants with units of stress^{-n}, energy and volume, respectively. Recent work motivated by structure and tectonic studies of icy satellites of the outer solar system has led to detailed characterization of the flow properties of H_2O ice at low temperatures [7]. For example, the relationship between strain rate and temperature is shown in Fig. 1. This experimental data is also relevant to studies of the martian ice caps. For environmental conditions relevant to Mars, the temperature dependence of creep is much stronger than the pressure dependence ($E^* \gg P^*$).

Estimates from Viking Orbiter observations place the surface temperature of the martian polar regions in the range 150°–220°K [8,9]. Depending on the level of differential stress, water ice in this temperature range may deform in either regime B (T < 240°K) or regime C (T < 195°K) of [7]. The threshold between the two mechanisms increases with strain rate. At 3.5×10^{-4} s^{-1}, the maximum strain rate tested in the experiments, the temperature threshold is higher than 200°K. This strain rate corresponds to a differential stress of 50 MPa. However, typical deviatoric stresses in the martian polar cap estimated from surface profile slopes are much lower — on the order of 10^4 Pa. We thus expect regime B to dominate but have tested models for regime C as well.

Role of Particulates: Given the nature of global dust transport on Mars [cf. 10] it is possible that polar cap material could contain a significant dust component. The presence of a significant amount of dispersed particulates inhibits the flow of ice [11]. A modified flow law that takes into account the influence of particulates can be written [11]

$$\varepsilon = A\sigma^n \exp[-nb\phi]\exp[-(E^* - PV^*)/RT]$$

where b is a constant and ϕ is the volume fraction of particulate material. Note that the influence of temperature and particulate fraction exhibit the same functional form. Thus ice containing particulate material will deform in the same manner as a mass of pure ice at a lower temperature. Given this behavior, it is unlikely that profiles of topography can be used in conjunction with flow models to reliably estimate the dust content of the caps.

Carbon Dioxide Ice Rheology: Unlike H_2O, data on the flow behavior of CO_2 at the appropriate temperature-pressure conditions are extremely limited. The most precise data available were based on experiments on two samples at 180°K and another at 77°K [12]. All experiments were performed at a confining pressure of 0.7 MPa and steady-state stresses of 10 MPa. At the lower temperature experiment, the CO_2 exhibited brittle behavior. At the higher temperature, the CO_2 displayed viscous properties, although at a higher pressure than is relevant for polar processes at Mars (~6 mbar at the surface; g = 3.3.7 ms^{-2}).

Flow Models: As a first step toward understanding the potential role of power law flow in the martian cap, we consider a mass balance model that will enable us to match surface profiles. We assume a steady-state system in which the loss of material from the circumference of the cap balances the accumulation on its upper surface [13]. We apply the model of Haefeli [14], in which differential stress at any point is approximated as being proportional to the surface slope, and then use ice-flow relations to find the profile of the horizontal velocity component. The mean horizontal velocity is found by integrating over height. We assume a cylindrical ice sheet and invoke the continuity condition such that the integrated horizontal velocity balances the accumulation. We assume a no-slip base, which is likely relevant for Mars. We obtain a single differential equation for a surface profile that can be integrated to yield ice thickness as a function of radius from the cap central axis. A typical model fit is shown in Fig. 2 for both H_2O and CO_2 ice. These preliminary models do not distinguish between the two composi

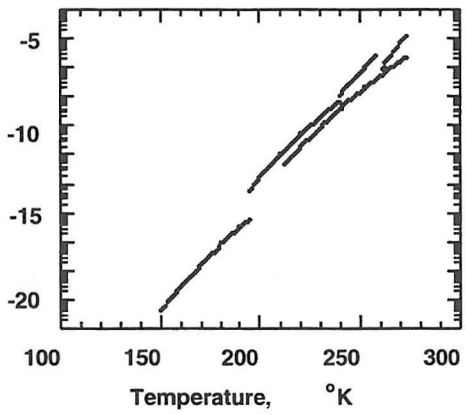

Fig. 1. Relationship between strain rate and temperature for H_2O ice. Data taken from [7] and references therein.

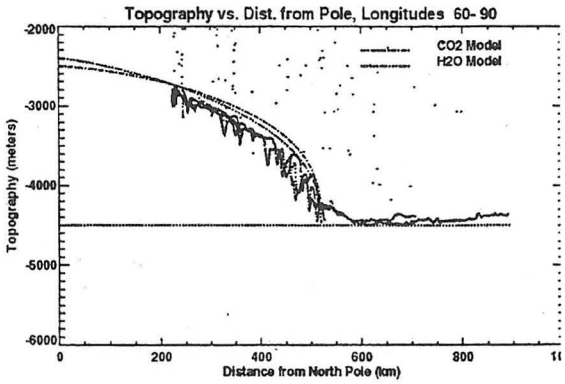

Fig. 2. Fit of Haefeli model [14] to MOLA profiles for H_2O (regime B) and CO_2 ice. For both models the best fit is for a cap with a negligible accumulation rate.

tions, perhaps in part because we have not yet fit profiles all the way to the pole, where the two rheologies predict different behavior. But for various profiles the general shape of the cap can be fit by models that invoke power-law flow. All models are best fit for negligible ice sheet accumulation rates. If this result holds up with more detailed modeling, then it would suggest that the current Mars north polar cap is either static or shrinking over the timescales longer than the oscillatory seasonal cycle.

Other Effects: Important details of the cap, such as the chasms, are not explainable by viscous flow and represent clear evidence that other dynamic processes are at work. Radiative models can also explain salient details of the cap shape [15]. Analysis is under way to understand the contributions of each mechanism to the macroscale morphology of the northern cap. In addition, we note that more experimental data on CO_2 ice at appropriate P/T conditions would be invaluable to the analysis.

References: [1] Zuber M. T. et al. (1992) *JGR, 97,* 7781–7797. [2] Albee A. A. et al. (1998) *Science, 279,* 1671–1672. [3] Thomas P. (1992) in *Mars,* pp. 767–795, Univ. of Arizona, Tucson. [5] Smith D. E. et al., *Science, 279,* 1686–1692. [6] Glen J. W. (1952) *J. Glaciol., 2,* 111–114. [7] Durham W. B. (1997) *JGR, 97,* 16293–16302. [8] Kieffer H. H. et al. (1976) *Science, 194,* 1341–1343. [9] Paige D. A. et al. (1994) *JGR, 99,* 25959–25991. [10] Greeley R. et al. (1992) in *Mars,* pp. 730–766, Univ. of Arizona, Tucson. [11] Durham W. B. et al. (1992) *JGR, 97,* 20883–20897. [12] Yamashita Y. and Kato M. (1997) *GRL., 24,* 1327–1330. [13] Budd W. F. et al. (1986) *Polarforsch., 56,* 43–63. [14] Haefeli R. (1961) *J. Glaciol., 3,* 1133–1150. [15] Ivanov A. B. et al. (1998) *LPS XXIX,* 1911–1912.